AD NUMBER

AD475369

LIMITATION CHANGES

TO:

Approved for public release; distribution is unlimited.

FROM:

**Distribution authorized to U.S. Gov't. agencies and their contractors;
Administrative/Operational Use; NOV 1965. Other requests shall be referred to Air Force Weapons Lab., Kirtland AFB, NM.**

AUTHORITY

AFWL ltr 21 Jun 1971

AFWL-TR
65-21

DESIGN STUDIES FOR ULTRA-FAST, LOW-IMPEDANCE HIGH-PEAK-POWER PULSED SYSTEMS

J. L. Brewster, F. M. Carbonnier
L. F. Garrett, K. W. Riegelmann
and J. K. Trolan

Field Emission Corporation
McMinnville, Oregon

Contract AF29(601)-5380

TECHNICAL REPORT NO. AFWL-TR-65-21
November 1965

AIR FORCE WEAPONS LABORATORY
Research and Technology Division
Air Force Systems Command
Kirtland Air Force Base
New Mexico

DISCLAIMER NOTICE

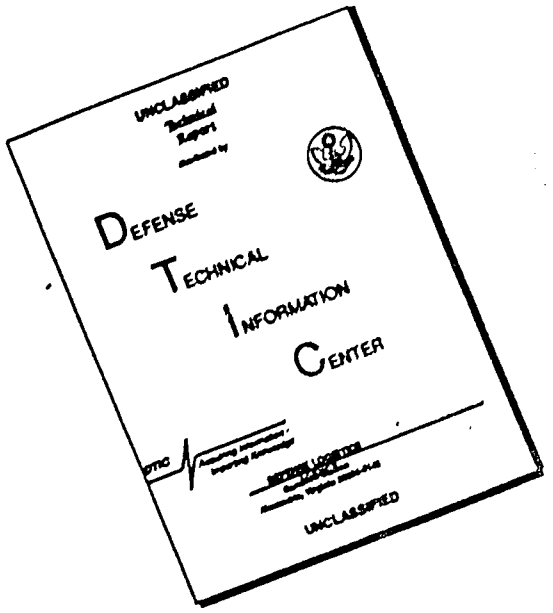

THIS DOCUMENT IS BEST QUALITY AVAILABLE. THE COPY FURNISHED TO DTIC CONTAINED A SIGNIFICANT NUMBER OF PAGES WHICH DO NOT REPRODUCE LEGIBLY.

AFWL-TR-65-21

Research and Technology Division
AIR FORCE WEAPONS LABORATORY
Air Force Systems Command
Kirtland Air Force Base
New Mexico

AFWL-TR-65-21

DESIGN STUDIES FOR ULTRA-FAST, LOW-IMPEDANCE HIGH-PEAK-POWER PULSED SYSTEMS

J. L. Brewster F. M. Charbonnier

L. F. Garrett K. W. Riegelmann

J. K. Trolan

Field Emission Corporation
McMinnville, Oregon
Contract AF29(601)-5380

TECHNICAL REPORT NO. AFWL-TR-65-21

FOREWORD

This report was prepared by the Field Emission Corporation, McMinnville, Oregon, under Contract AF29(601)-5380. The research was performed under Program Element 7.60.06.01.D, Project 5710, Subtask 07.002, and was funded by the Defense Atomic Support Agency (DASA).

Inclusive dates of research were April 1962 through August 1965. The report was submitted 20 October 1965 by the AFWL Project Officer, Dr. Arthur H. Guenther (WLRE).

This report has been reviewed and is approved.

DR. ARTHUR H. GUENTHER
Project Officer
Effects Branch

EDGAR M. MUNYON
Lt Colonel USAF
Chief, Effects Branch

WILLIAM H. STEPHENS
Colonel USAF
Chief, Research Division

ABSTRACT

Ultrafast pulsed power systems have proved to be effective energy sources for transducers to produce intense X rays, dense electron beams, and very high temperature plasmas. The principal function of a single shot or low repetition rate pulsed power system is to accept energy at low power levels and subsequently to deliver such energy at extremely high power levels, with maximum efficiency, to a suitable transducer. This objective can best be met by use of either distributed or lumped-constant pulse forming networks where optimum performance is realized by maintaining the proper impedance match between the power source and transducer throughout the energy delivery process. Attainment of the proper impedance match can impose stringent and sometimes contra-indicating requirements upon the dielectric storage media, the switching mechanism, and the transducer chamber.

The most promising approach to such power sources appears to be a pulse-charged two-stage coaxial Blumlein system. Such a system can deliver 25 kiloamperes at 2 megavolts in a pulse width of 40 nanoseconds to a suitably matched flash X-ray tube to produce relatively high dose rates with long tube life and minimal maintenance. The performance of a Blumlein exploding wire system, with respect to the rate of energy transfer, is primarily limited by the uncancelled transducer chamber inductance--a function of the insulation spacing needed for voltage hold-off. High dielectric-constant liquids may allow reduction of the transducer chamber impedance to the extent required to give di/dt values close to 10^{14} amp/sec for wires a few mils in diameter. Attainment of transducer chamber voltage gradients of 300 kv/cm or better in vacuum will result in di/dt values of 1 to 2 x 10^{13} amp/sec.

CONTENTS

ILLUSTRATIONS

TABLES

ABBREVIATIONS AND SYMBOLS

A	Area
a	Ratio of load resistance to output impedance RL/Z_o
C	Capacitance
c	Velocity of EM wave in vacuum
c	(subscript) Charging
D	Diameter
d	Diameter, distance
E	Electric field
h	Height
I	Current
i	Current
I_o	Intensity, X ray, on axis ($\theta = 0$
$I(\theta)$	Intensity as a function of θ
J	Electron current density
L	Inductance
L	(Subscript) Load
ℓ	Length
m	(Subscript) Matched $^{R}L/Z_o = 1$
max	(Subscript) Maximum
Mv	Million volts
N	Number of turns, or Neutron flux

n	Neutron
o	(Subscript) Output, or initial
P	Power
p	Pressure
Q	Reaction threshold
R	Resistance
R_c	Resistance, charging
R_L	Resistance, load
r	Roentgen
S	Switch, or Spark gap
T	Temperature
T_o	Temperature, initial
t_o	Time, initial
U	Voltage, gap breakdown
V	Voltage
V_c	Voltage, charging
V_o	Voltage, output
W	Energy
w	Width
$\dot{x}$	Dose rate
Z_o	Impedance, characteristic
Z_G	Impedance, generator
Z_{out}	Impedance, output

v	Velocity of an EM wave in a dielectric
V_{oc}	Voltage, open circuit
a	Factor dependent on X-ray source
γ	Propigation constant
δ	Skin depth
ΔV	Incremental volume
ϵ_r	Dielectric constant, relative
ϵ_o	Permitivity of free space
η	Energy transfer ratio
$\eta_o = \sqrt{\mu_o/\epsilon_o}$	Intrinsic impedance of free space
θ	Cone angle
λ	Free space wave length
μ	Permeability
μ_o	Permeability of free space
ρ	Resistivity
ρ_v	Voltage transfer ratio
$\sum$	Maximum relative variation of dose
$\sigma(\theta)$	Angular Distance as a function of θ
σ_o	Transit time
$2\tau_o$	Pulse length
τ_w	Transit time, in w direction

SECTION I

INTRODUCTION

Ultra-fast, low-impedance, high-peak-power pulsed systems have proved to be effective energy sources for driving various types of transducers to produce intense X rays, high-density electron beams, extremely high-temperature plasmas, etc.

As an example, fifteen 320 kv, 70 ohm, 50 ns pulsers were successfully, simultaneously discharged in parallel into a common load in a 20-billion watt exploding wire system developed by Field Emission Corporation (Ref. 1) for the Air Force Weapons Laboratory, Kirtland Air Force Base. This specially designed apparatus, complete with extensive instrumentation, is being used by AFWL for the simulation of nuclear weapons effects by the generation of plasmas, shock waves, electromagnetic radiation, etc., by exploding wires of various types and geometries.

While the foregoing example represents a significant accomplishment it appeared possible to achieve significantly higher peak-power capabilities in these areas. Therefore, the investigation described in this report was initiated for the purpose of identifying promising approaches to new and better pulsers, to determine certain areas of difficulty, to evaluate performance capabilities and to weigh the relative merits of the various pulser systems with respect to their estimated complexity and cost of development, and manufacture. This study furthermore calls attention to certain areas where insufficient engineering information is presently available and further studies necessary.

As background for this study, Section II of this report is concerned with some general aspects of energy storage and delivery. Specific attention is given to the principles of operation of field reversal generators, which are

proposed as the most promising general design approach. This is followed by discussion of a number of general pulser designs and related circuitry. Attention is then devoted to the specific areas of interest, namely a modest energy and voltage ultra-fast exploding wire system, and a higher voltage system design for radiation effects application. Section III presents certain design support data which are pertinent to the systems discussed. Section IV presents detailed designs proposed for achieving a number of specific outputs. Finally, Section V summarizes and evaluates the main results of the study and reviews certain problem areas where further work is currently needed.

SECTION II

GENERAL DISCUSSION

1. General Principles of Operation

The principal function of a single-shot or low-repetition-rate pulsed power system is to accept energy from a low voltage source, over a relatively long period of time and at modest current level, and subsequently to deliver such energy with maximum efficiency, at high voltage and current levels and within an extremely short time. This energy is usually delivered to some kind of transducer, such as an exploding wire or an electron tube, which may in turn generate X rays or neutrons or extract the electrons into an accessible region. The basic energy conversion efficiency in these processes is usually quite low and it becomes important to maintain maximum efficiency in the transfer and conversion of stored energy from the pulser to the transducer.

Maximum energy can be transferred to the transducer in minimum time when an impedance match is maintained between the power source and the transducer throughout the energy delivery process. The sensitive voltage dependence of X ray and neutron yields suggests the possibility of increasing radiation output by intentional high-impedance mismatch of the transducer - - however, as discussed later in this report, consideration of all factors involved may still show a net advantage for matched load operation.

For many applications it is desirable to supply the transducer with a short pulse delivered from a constant impedance source. These objectives can be met by use of either distributed or lumped-constant pulse-forming networks, provided certain requirements can be satisfied: namely, the dielectric storage media should exhibit low volume and surface leakage

(creep) during the time of charge, and should withstand very high fields before the onset of the output discharge; high energy density storage may be important (this in turn may dictate the use of high dielectric constant materials for energy storage); the geometry of the pulse power package should be suitable for efficient energy storage; there should be ready access to the storage elements from the charging source; the design should permit effective coupling at the proper impedance level either directly to the transducer chamber or to a transmission system capable of delivering the energy undistorted to a transducer; there needs to be a reliable, convenient, efficient method of switching the energy from the stressed dielectric to the load.

It has long been recognized that switching problems are among the most severe encountered in the design and development of a suitable low-impedance fast-pulse power source. Switching energy from the pulser to the transducer chamber should introduce a minimum of resistive loss, inductance and distortion. Switches should exhibit long life, or at least have readily changeable electrodes and/or dielectric.

Furthermore, the energy delivered by the pulse generator must be coupled to the transducer by means of a transducer chamber. As discussed later in this report, this frequently poses serious design problems because of conflicting requirements for impedance matching, voltage breakdown, instrumentation requirements, etc., depending on the specific transducer employed.

2. Basic Characteristics of Pulse-Forming Lines

Energy storage pulse-forming lines are of a distributed or lumped-constant nature. As pulse lengths become shorter, storage networks become preponderantly of the distributed type. A distributed line is constituted of two electrodes separated by a dielectric having geometric and dielectric characteristics such that a constant impedance is found at every point of the line at any point along its length. Formulas relating line impedance to certain line geometries are given in Figure 1.

To illustrate the interrelationships of various parameters, consider the elementary strip-line-network pulser of Figure 2, where V_c is the charging potential, R_L the load resistance and W, h and ℓ the strip-line

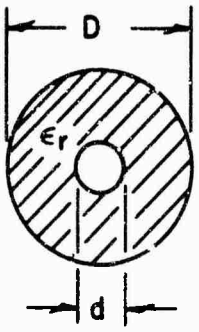

Co – Axial

$Z_o = 60 \frac{v}{c} \ln D/d$, where v = Velocity of an electro – magnetic wave in the dielectric media and c is its speed in vacuum.

$Z_o = 60 \frac{1}{\sqrt{\epsilon_r}} \ln D/d$

Strip Line

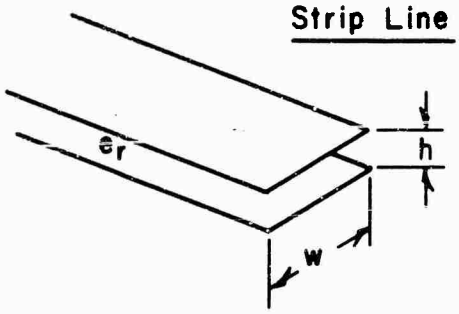

$Z_o = 377 \cdot \frac{h}{w} \left(\frac{v}{c}\right)$

$= 377 \frac{h}{w} \frac{1}{\sqrt{\epsilon_r}}$

Single Wire — Ground

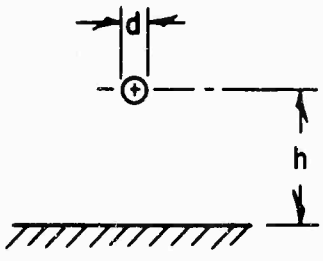

$Z_o = 138 \frac{v}{c} \log_{10} \frac{4h}{d}$

$= 138 \frac{1}{\sqrt{\epsilon_r}} \log_{10} \frac{4h}{d}$

Figure 1 Three Types of Transmission Lines and the Corresponding Line Impedance Formulae.

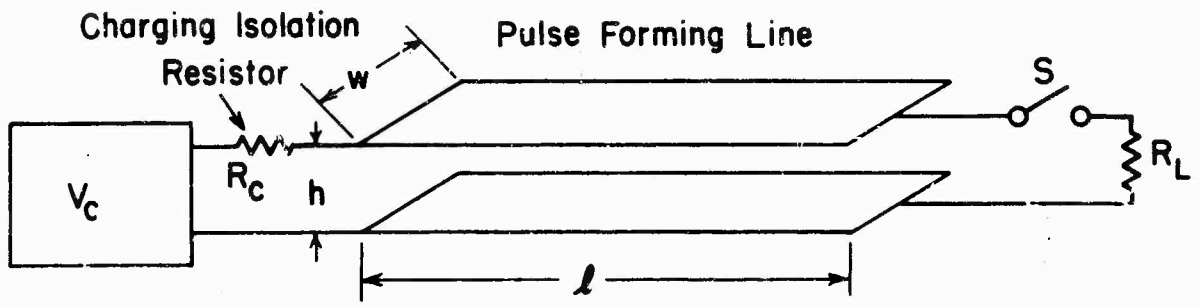

Figure 2 Typical Circuit Employing a Transmission Line as a Pulse Generator.

width, spacing, and length respectively. The characteristic impedance of this type of transmission line, neglecting edge effects, is

$$Z_o = \eta_o \frac{h}{w} \frac{1}{\sqrt{\epsilon_r}} \tag{1}$$

where η_o is the intrinsic impedance of free space

$$\eta_o = \sqrt{\mu_o/\epsilon_o} = 377 \text{ ohms} \tag{2}$$

ϵ_r the relative dielectric constant, and ϵ_o and μ_o the permitivity and permeability of free space. The switch S isolates the energy stored in the line pulser from the load R_L, which is assumed to be an impedance match to the pulser for the present discussion:

$$R_L = Z_o \tag{3}$$

Upon switch closure a voltage wave, which can be approximated by a step function if the switch is nearly ideal, develops across the load at a voltage level (for the matched impedance case):

$$V_o = V_c/2 \tag{4}$$

The pulse length of the voltage applied across the load is twice the electrical delay length ℓ/v of the transmission line of Figure 2, or

$$2\tau_o = \frac{2\ell}{v} = \frac{2\ell\sqrt{\epsilon_r}}{c} \tag{5}$$

where v is the velocity in the dielectric and c the velocity in free space. The transient phenomena of this discharge process will be discussed in some detail later in this section.

For the case of a matched-load impedance all the energy W stored in the line during charging will be delivered to the load in the time $2\tau_o$, and will equal the VIt product:

$$W = V_o It = \frac{V_c^2}{Z_o} 2\tau_o = \frac{V_c^2 \tau_o}{2Z_o} \tag{6}$$

Noting that the electric field or stress E for the strip line is

$$E = V_c/h \tag{7}$$

and by substitution of equations (1), (5) and (7) in equation (6) one obtains the stored energy W in the line as

$$W = \frac{(Eh)^2 \ell w \epsilon_r}{2h\eta_o c} = \epsilon_o \epsilon_r \frac{E^2}{2} \, hw\ell \tag{8}$$

since

$$c = 1/\sqrt{\mu_o \epsilon_o} \tag{9}$$

Noting that the volume of dielectric in the strip line is $hw\ell$ and the electric stress E is approximately uniform over this volume (if edge effects are neglected), one immediately obtains the energy density in the dielectric:

$$W/_{\Delta v} = \epsilon_o \epsilon_r \frac{E^2}{2} \tag{10}$$

This well-known formula (Ref. 2), obtained for the strip line in this example, generally applicable to dielectric energy storage and will be used in subsequent sections (e.g., Section II-7 and Figure 15) for general design and comparison purposes.

A brief discussion of elementary considerations regarding current and voltage conditions on a charged line, prior to and during termination in a load, may aid in predicting current and voltage wave shapes at any point along a line.

Initially, the energy in a charged unterminated line can be considered to be divided equally between two traveling waves of a voltage amplitude $V_c/2$ having the same polarity and proceeding in opposite directions, each being constantly reflected from the open ends of the line. The resultant voltage at all points along the line is equal to the charging voltage, while the currents are equal and opposite and their sum is everywhere zero. (Refs. 3, 4). When the termination at either end of the line is perturbed (such as connecting the line to a load) the reflection at that end of the line is also altered. Only the open, shorted, or matched impedance cases will be considered here.

The subsequent distribution of voltage and current along the line as a function of time and position can be forecast by treating the oppositely directed waves independently, considering the reflections that occur at each end of the line and then reconstructing the wave by summing up the component waves at any point in space or time. A voltage reflected at an open circuit experiences no change in polarity, while reflection at a short circuit results in a reversal of the reflected voltage. Applying these principles to the simple case of a charged line shorted at one end at time t_o while remaining open at the other end, Figure 3 shows the resultant voltage (heavy trace) as a function of position along the line; this voltage, which is the sum of the two waves (cross-hatched and plain) in the line, is given for several specific times expressed in terms of single transit time units, τ, following shorting at one end at time t_o. In Figure 3, the voltage is given at all positions along the line for five different times, namely some time prior to t_o and at integral multiples of $\tau/4$ up to $1\text{-}1/4\,\tau$ following switch closure. It can be shown that the sequence repeats once every 4τ, following shorting at one end at time t_o. Figure 4 depicts the same information in another

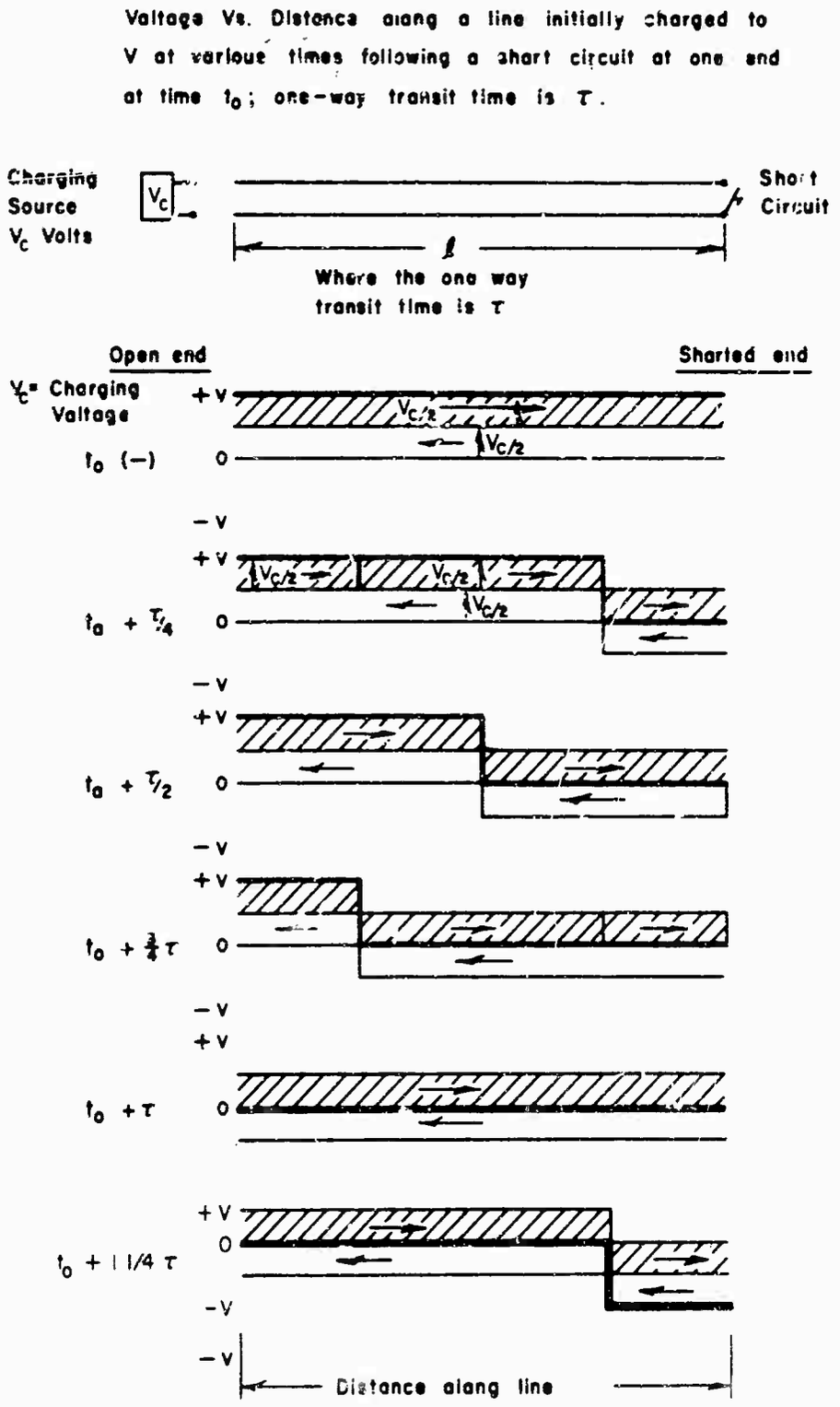

Figure 3 Voltage (heavy line) as a Function of Position Along a Transmission Line, at Various Times Following the Time t_o at Which One End of the Lire is Short-Circuited.

Voltage Vs. Time at various points along a line initially charged to voltage V_C, shorted at time t_0; line length = ℓ; one-way transit time = T.

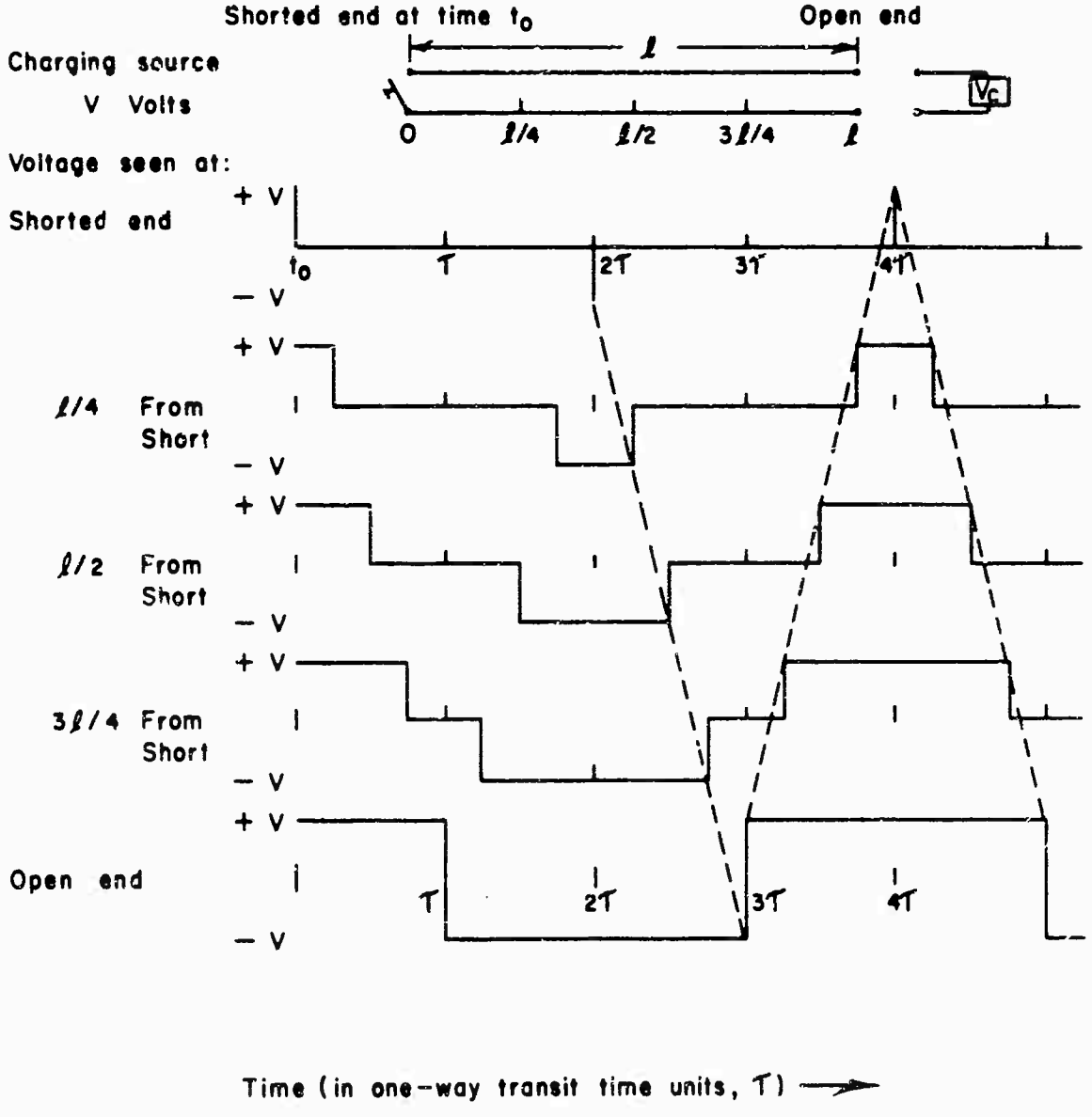

Figure 4 Voltage Along a Transmission Line as a Function of Time, Following the Time at Which One End of the Line is Short-Circuited.

manner and shows the voltage as a function of time at the shorted end and at each 1/4 length of the line thereafter to the open end.

The open end voltage is of major interest here since most field reversal pulsers short the line at an end opposite the load; the reversed voltage arrives at the open end τ seconds later, and then persists for 2τ seconds.

While the open circuit voltage pulse from a single line is equal to the charging voltage, the voltage developed across an impedance matching load is only one-half the charging voltage.

3. Marx-surge Circuits

For high-power-line type pulsers having impedance networks, the voltages on the networks tend to become high, and may reach values of 50 kv or more. Such high voltages, particularly for direct current charging, frequently lead to engineering difficulties, and some form of impulse-voltage multiplication is desirable. The Marx multiplier circuit (Ref. 5) may easily be adapted to this use.

A typical four-stage circuit of this type is shown in Figure 5, including effective internetwork capacitances and network capacitances-to-ground. The charging resistance R_c and isolating chokes L serve to conduct currents to the several pulse-forming networks during direct current charging, while preventing the condensers from being short-circuited through the gaps during the pulse. These chokes L must therefore have a sufficient inductance to prevent an undue portion of the pulse current from being lost through them. After being charged, the pulser is discharged by triggering the initial gap S_1 either by means of a third electrode or by some form of radiation such as ultraviolet or X-ray excitation. The subsequent gaps S_2, S_3 and S_4 are then discharged by a combination of overvoltage and ultraviolet irradiation, the latter requiring adequate optical coupling between S_1 and subsequent gaps.

Figure 6 is indicative of the pressure-voltage relationship which may be measured for the gap firing conditions with a Marx-surge pulser

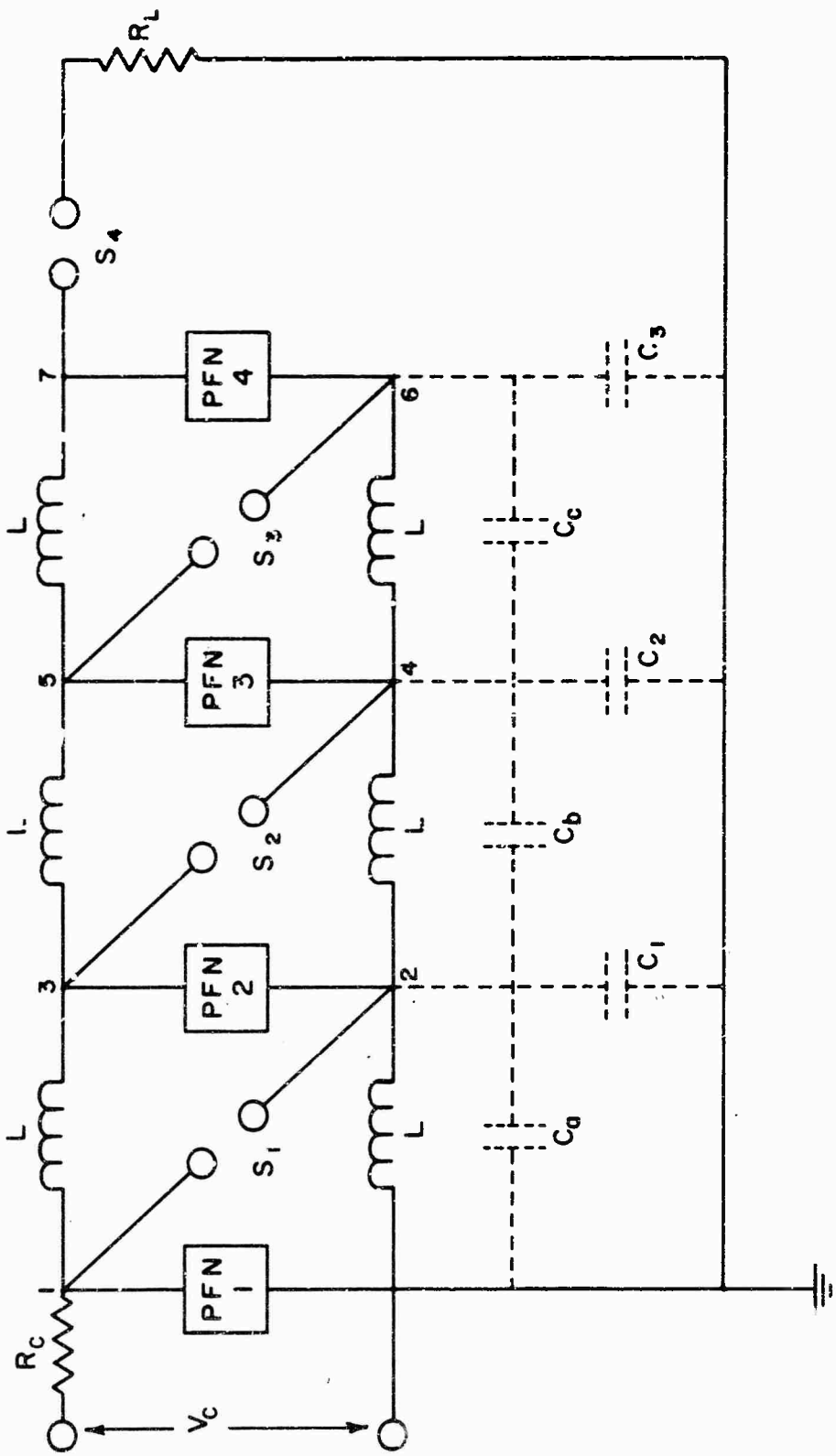

Figure 5 Schematic Circuit for the Marx-Surge Generator, Indicating Energy Storage Elements, Switches, Isolation Charging Impedance, Load and "Stray" Capacitances.

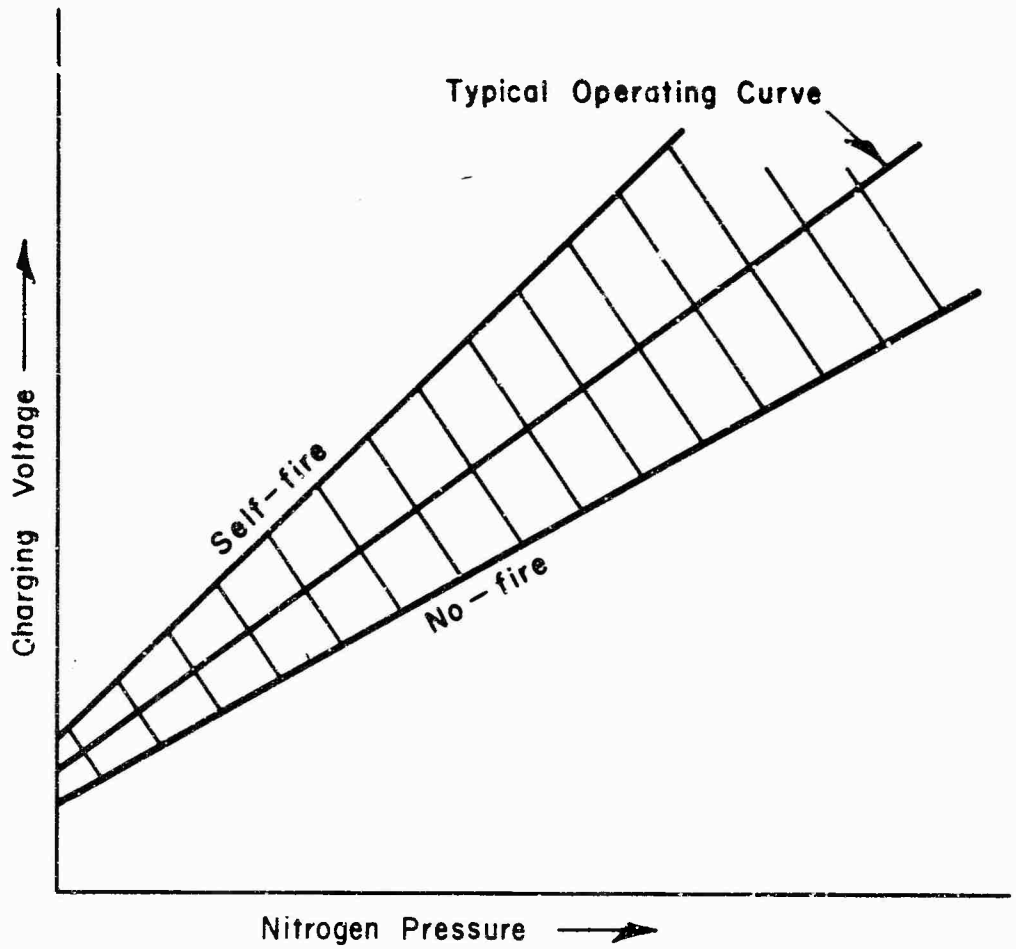

Figure 6 Pressure-Voltage Relationship as Affecting Switch Gap Firing for a Typical Marx-Surge Pulser.

where the spark gaps are enclosed in a controllable pressure chamber filled with some gas such as nitrogen. If the dc charging voltage is too high with respect to gap pressure, the pulser will discharge spontaneously, termed self-fire. If the voltage is below a certain critical level, triggering of the spark gap S_1 will result in discharge of only that gap, with the energy stored in the pulse-forming networks being discharged through S_1 rather than R_L. The pulser is normally operated at an intermediate level as indicated in Figure 6. These spark-gap-firing conditions may be understood qualitatively by a more detailed examination of the circuit of Figure 5, taking into consideration the internetwork capacitances (C_a, C_b and C_c) and the network-to-ground capacitances (C_1, C_2 and C_3). The method of explanation is an expanded version of that presented by Vorobyev et al., in their book: High-Voltage-Testing Equipment and Measurements, 1960 (Ref. 6). This book is recommended as a general text covering high-voltage equipment and techniquies, both dc and pulsed, and providing general background for more recent high-voltage developments.

At a time just before triggering of spark gap S_1, the pulse-forming networks (PFN 1, etc.) are completely charged by means of the power-supply voltage V_c through R_c and the several charging inductors L. The circuit junctions 1, 3, 5 and 7 (Fig. 5) are then at a potential V_c, with junctions 2, 4 and 6 at ground potential.

When the first spark-gap switch S_1 is triggered, the potential at junction 2 will increase rapidly to the same potential as junction 1. The rise time is dictated primarily by the inductance and resistance of S_1 and associated wiring which impedes the flow of current, and by the effective capacity-to-ground at point 2(C_1, C_a, etc), which must be charged. The inductances L and resistance R_c are selected large enough to permit very little current flow from junction 2 to ground during the switching rise time; hence the potential (after switching) at junction 2 will be just below V_c, provided the energy storage of PFN 1 is substantially greater than the energy required to charge the capacity-to-ground at this junction.

Since PFN 2 was fully charged, junction 3 will then be elevated in potential to just below $2V_c$ by discharge of S_1. The potential at junction 4

will then depend on the relative values of the various internetwork and network-to-ground capacitances. Referring to Figure 5, C_b is effectively shunted across S_2, and will tend to raise the potential of junction 4 with respect to ground. However, junction 4 is coupled directly to ground through C_2, and indirectly through C_b and C_1, C_c and C_3, etc. The potential at junction 4 will jump by the same amount V_c as the change in potential at junction 3 if C_b is much larger than the capacitance-to-ground, or to a value of about V. If C_2 is much larger than C_b, however, junction 4 will tend to remain at approximately ground potential. In the first case, the voltage difference across S_2 will remain at about V_c, and gap breakdown will not occur. For the latter case, the voltage difference is about $2V_c$ and S_2 will break down, provided the gap pressure and spacing are proper.

The pressure-voltage relationship of Figure 6 is thus explained: the no-fire potential point for a given pressure will then be substantially lower than the self-fire point, provided that the Marx-surge pulser has substantially higher capacity-to-ground than internetwork capacity. Conversely, relatively low capacity-to-ground, compared to the internetwork capacity, will result in the no-fire point being very close to the self-fire point.

Even with substantial overvoltage of gap S_2 breakdown will occur quicker with less time jitter (Ref. 7) when illumination of gap S_2 is achieved by ultraviolet coupling between gap S_1 and S_2. Coupling of all of the gaps in this manner results in "priming" or creation of charged particles in the gaps. These particles initiate electron avalanches in the presence of sufficient gap voltage. Exposure of a spark gap to sufficient ultraviolet radiation can lower the self-fire point below the unirradiated self-fire potential by as much as 10 percent, although with considerable delay and jitter at this extreme value. It is therefore possible to discharge gap S_2 somewhat below the self-fire curve of Figure 6 even with little or no capacity-to-ground, provided ultraviolet gap coupling is employed.

Spark gap switch S_3 (and additional gaps of pulsers having more sections than shown in Figure 5) is then discharged in a similar manner. The final or "output" gap (S_4 of Figure 5), which isolates the load R_L from

the charging potential, is overvolted and breaks down when the potential jumps at junction 7 since the other electrode is kept at about ground potential by coupling through R_L.

With a circuit such as that indicated in Figure 7, it may be possible to obtain successful operation of a Marx-surge generator well below the self-fire level, but without the necessity of network capacity-to-ground. It is thus perhaps practical to extend the techniques to strip line (as shown in Fig. 7) or coaxial distributed-energy-storage networks, which are characterized by relatively high internetwork capacitance and little inherent capacity-to-ground.

Pulsed or dc charging is accomplished through the two sets of inductors at the far end of the storage elements, with the inductors at the switch end being employed to maintain the trigger needles at mid-gap potential during charging. In the charged condition, much more energy is stored in the dielectric material (1) than in (2), in part by providing a larger spacing in (2) than in (1). Initiation of the discharge process occurs with firing of the bottom gap, either by overvolting (i.e., pulse charge), or by triggering with the needle electrode as indicated. This then raises the potential of the following gap with respect to its needle electrode, causing this gap to break down, etc., until with breakdown of the top gap the output voltage appears across the load.

The output impedance of a generator of this type is the sum of the line impedances of the individual storage dielectric stages (1); however, the rise time is in general less than that calculated by adding the inductances of the several gaps, since the voltage is not applied to the load until the final gap breaks down.

4. Blumlein Circuit

A Blumlein circuit is a simple but rather ingenious extension from a single pulse-forming line to a line which contains two stages but requires only one switch located at the line end opposite the load. Its output voltage into a matching load is equal to the charging voltage (twice that of the single-stage matched line), its pulse length is twice the one-way transit time τ of either one of the line sections (the same as that of a single line of

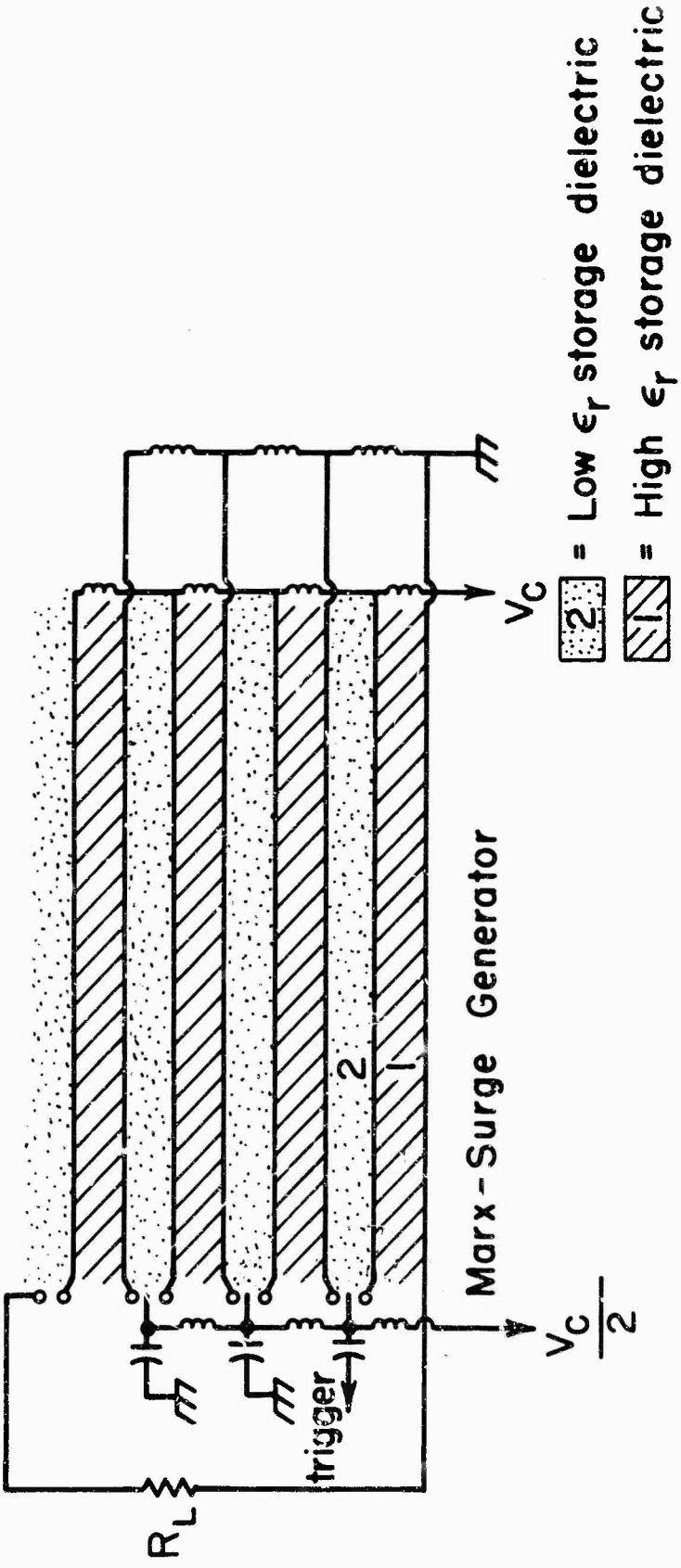

Figure 7 Possible Marx-Surge Generator with Three Electrode Switches. Strip Line Energy Storage Elements are Indicated, but the Method is General.

equal length), and its impedance is the sum of the impedance of the two lines. Figure 8 is a simple Blumlein circuit. Both line sections are charged prior to pulsing; however, no voltage appears across the load until after one line section is shorted by the switch S at time $t_o = 0$. The voltage reverses at the open end AA' one transit time τ later. At this time the voltage across AB (the sum of the reversed voltage and the voltage across the unswitched line) is equal to twice the charging voltage in the absence of a load, and equal to the charging voltage in the case of a matching load, since the lines are in essence connected in series. This voltage pulse persists for a period equal to 2τ.

It is re-emphasized that, while the output voltages of the two lines add directly, their impedances also add directly.

The two-stage Blumlein circuit can be considered as a building block from which extensions to higher voltage can be made by the addition of similar building blocks in a stacked circuit as illustrated in Figure 9a. Similar to the two-stage Blumlein circuit, the multiple-stage or stacked circuit in the charged condition (prior to switching) has alternating field lines that cancel each other, resulting in zero voltage across the load. Thus a load can be directly connected to the pulser without requiring switch isolation of the pulser from the load. Several advantages appear in favor of the stacked circuit over that of the Marx circuit (shown schematically in Fig. 9b). Since energy storage in all the dielectric volume becomes available to the load, one achieves greater efficiency of energy storage as well as a higher output voltage for a given stack height. The stacked circuit lends itself to simple assembly and construction techniques. Perhaps the greatest advantage is that, in comparison to the Marx-surge, the stacked Blumlein circuit requires only one-half as many switches per storage element. The avoidance of an output switch in the case of the Blumlein circuit, although an advantage, imposes a more stringent requirement on switch synchronization time if a good output pulse waveform is to be achieved; a major problem area in the stacked circuit is that of attaining the necessary synchronization of a multiplicity of switches. If it is found that pulse synchronization problems cause

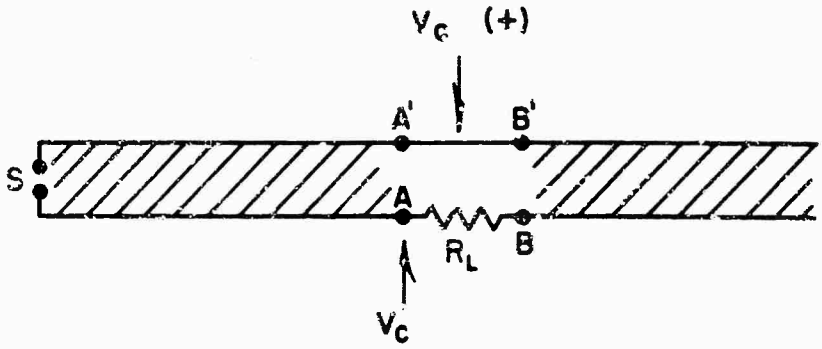

Strip Type Blumlein (Unfolded)

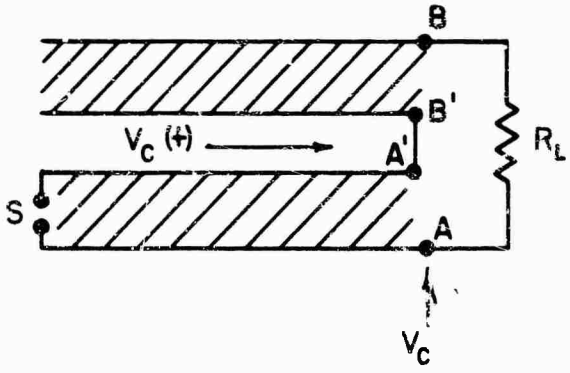

Strip Type Blumlein (Folded)

Two configurations of the Blumlein Circuit. The same circuit can employ co-axial lines rather than the strip lines shown.

Figure 8 Two Configurations of the Blumlein Circuit. The Same Circuit Can Employ Coaxial Lines Rather Than the Strip Lines Shown.

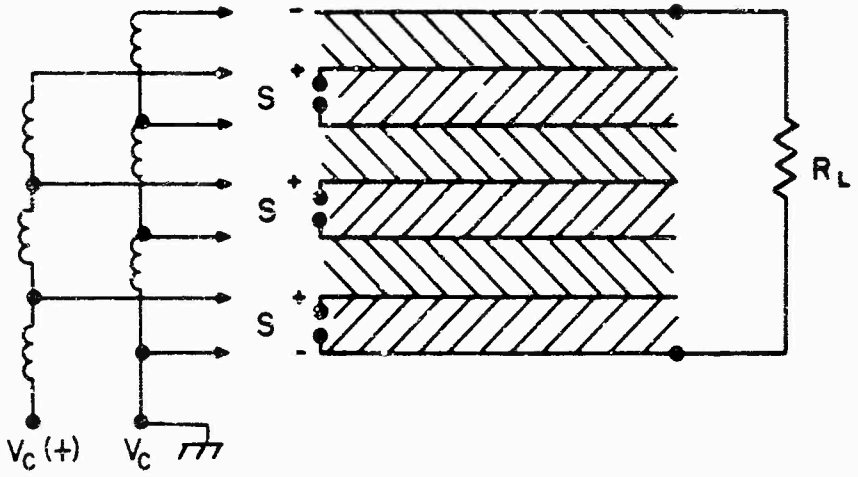

(a) Stacked Blumlein Circuit (Strip Lines)

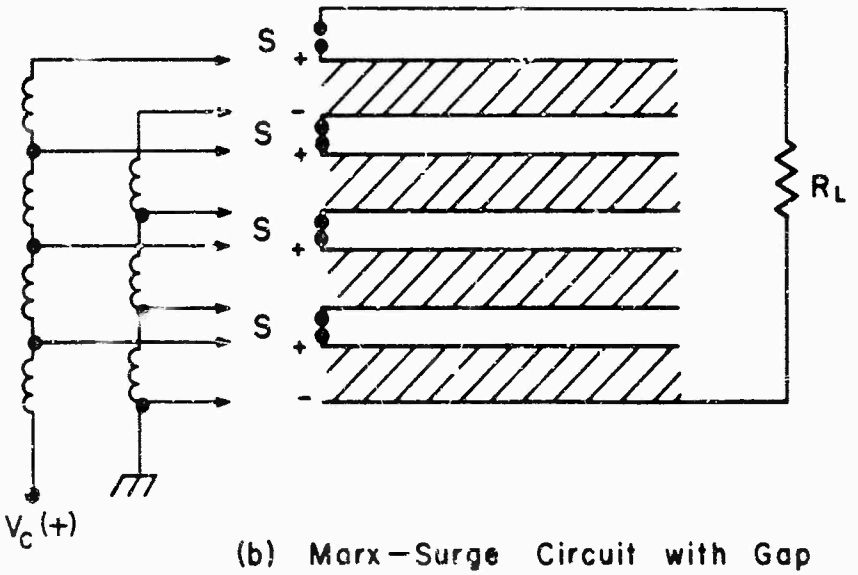

(b) Marx–Surge Circuit with Gap Switching (Strip Lines)

Figure 9 The Stacked Blumlein (a), and the Marx-Surge Generator with Strip Line Energy Storage (b).

degradation of rise time, an output switch can be inserted between the load and the pulser in the Blumlein circuit as it is in the Marx-surge circuit or the spiral circuit; however, addition of an output switch will not correct fall time degradation due to poor synchronization of the input switches.

The stacked Blumlein can be fabricated in either a strip-type configuration or in a coaxial configuration. The latter is a more desirable geometry from the standpoint of connecting to a transducer chamber and from consideration of edge effects at the termination of electrodes since edge effects in one dimension are eliminated in the coaxial configuration; however, they remain in the other dimension. The coaxial arrangement provides excellent shielding, is a very low loss configuration and provides a better match to the transducer chamber; however, it is difficult to switch. The well shielded geometry reduces the capacitance-to-ground normally experienced in the Marx-surge circuit. Therefore, the firing of one or two gaps does not result in overvolting of the other gaps in the line, and other means of switching must be provided. Several possible switch designs are considered later in this report; laser switching (Ref. 8) AFWL paper in solid or liquid dielectrics appears promising.

5. Spiral Coaxial Generator Circuit

The spiral coaxial generator, schematically represented in Figure 10, employs the field reversal principle in a two-stage Blumlein configuration composed of two strip lines. Voltage multiplication in the circuit results from the ingenious spiral physical arrangement of the lines. A unique feature of the circuit is that the output pulse energy is removed orthogonally to the direction of propagation of the reversal wave in the strip line.

Referring to Figure 10, the construction of the spiral coaxial generator utilizes a sandwich consisting of two conductors separated by a dielectric (1), with a second dielectric (2) attached to the outer face of the inner conductor. When arranged in a spiral, as indicated, the conductor and dielectrics form two separate transmission lines. Lines 1 and 2 become storage elements, i.e., both dielectrics become stressed when the conductors A and A' carry charge. (During the charge time, no potential difference exists between outer contact O and inner contact O' since alternate dielectric

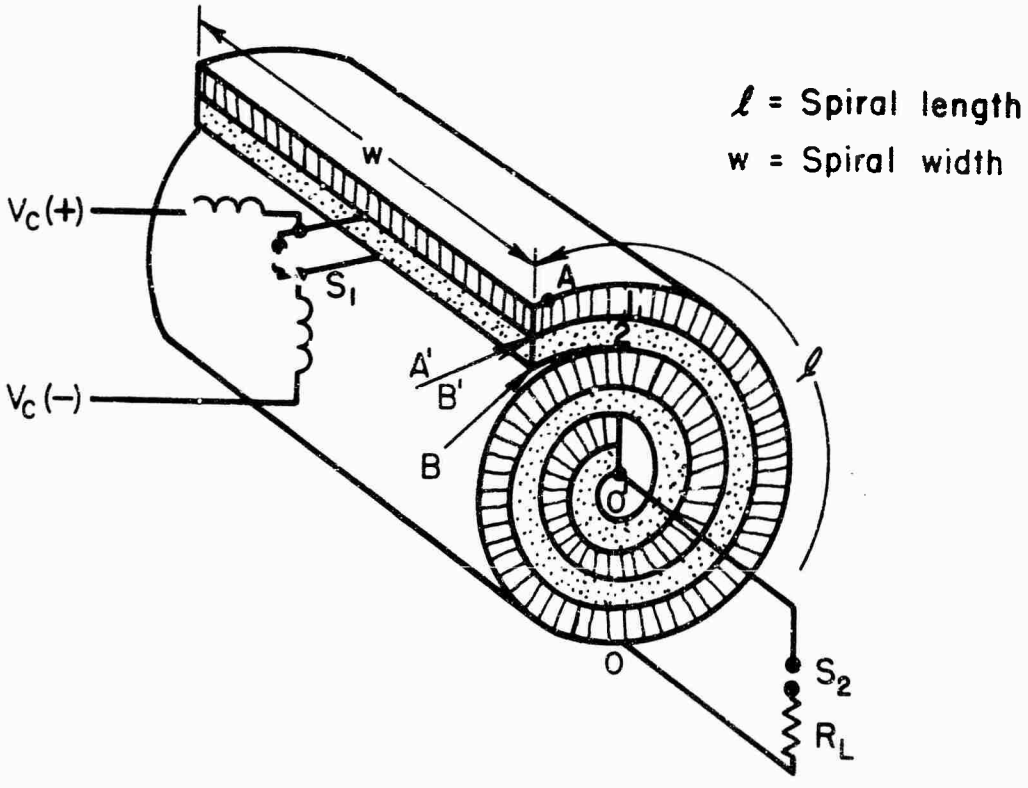

Figure 10 Spiral Coaxial Pulse Generator.

layers are charged oppositely).

One of the lines is equipped with a shorting switch S_1 which, when shorted, initiates on line 2 a voltage reversal (Fig. 3) which propagates down line 2 toward the center of the spiral. Each time the wave front passes through an imaginary radial line, e.g., OO' the voltage between points O and O' increases by an amount V_c. As the wave front reaches the open end of the line at O' it reflects back on itself according to Figure 3 and, each time the reflected wave front passes the line OO', the potential between O and O' further increases by V_c until the potential at all points of line 2 are reversed. Thus, for example, if there are 20 wraps of line 2 and 20 wraps of line 1, the maximum potential between O and O' becomes 40 V_c. The dielectric is still fully stressed (with fields in lines 1 and 2 now adding) and the potential difference between OO' is a maximum, as shown in Figure 11 which depicts the build-up voltage as a function of time.

Energy can now be extracted from the end of the wrapped line (axial direction) when the output gap S_2 is closed at time t_2 so as to make connection to the output load. The output pulse, for the above example and for a matched load, will yield a voltage of 20 V_c and will have a pulse length equal to twice the one-way transit time of an E-M wave in the axial direction of the pulser (w of the strip lines). The generator output impedance will be approximately that of a coaxial line of outer radius OO' and inner radius of the diameter at O'. The input impedance at S_1 will be that given by the strip line formula and will be low compared to R_L in the case cited.

Switch S_1 should have very low dissipation loss because of the very high current it must pass. The inductance of this switch should permit full current rise in a time substantially less than the voltage build-up time. Switch S_2 must be a high-voltage switch capable of very fast switching at the desired voltage point during the charging voltage build-up.

As represented in Figure 10, the output energy is available between points O and O'. This output energy can be carried to the load either by a wire or a strip type transmission line. A more desirable configuration from the standpoint of impedance matching would be that of a

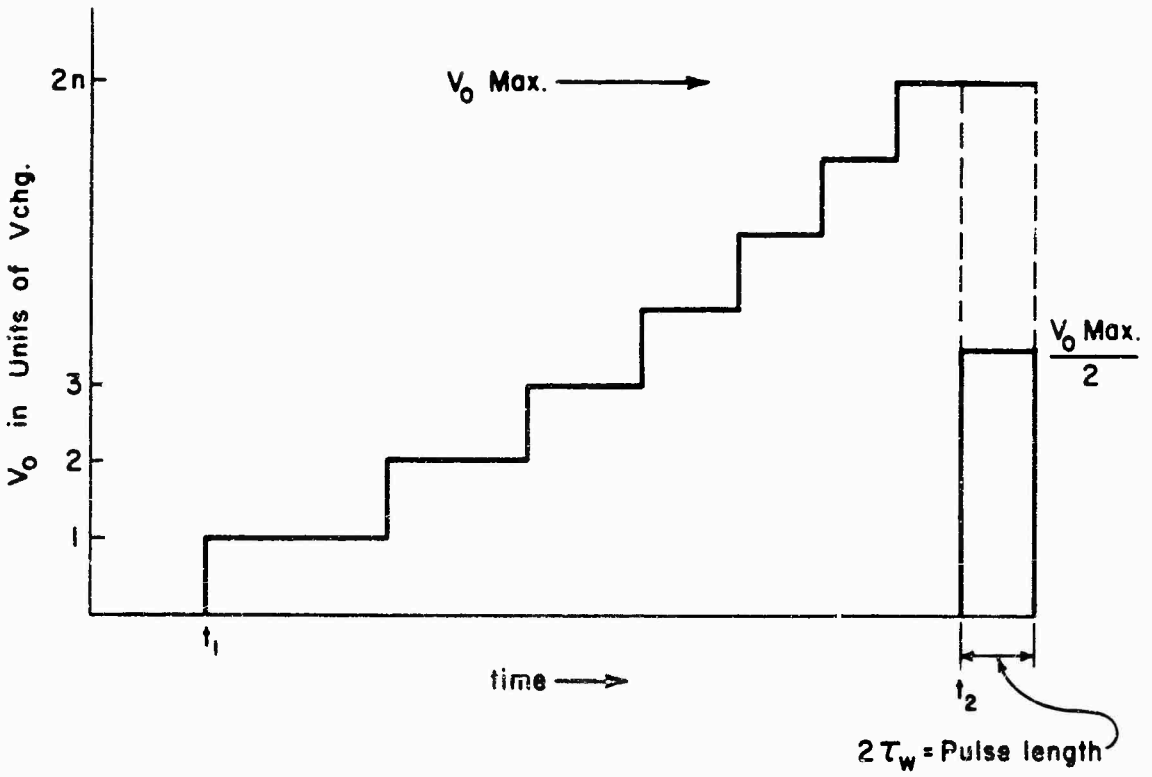

Figure 11 Voltage Rise, VA'B', as a Function of Time (ramp-up) to 2n Vchg where Vchg = Line Charging Voltage and n is the Number of Wraps of Either Line in the Spiral.

coaxial line; however, it is not yet apparent how to accomplish this because of the difference in potential that exists between points A and B during the pulse time.

The practical open-circuit voltage is less than the theoretical maximum $2nV_c$; Fitch and Howell (Ref. 9) discuss three loss factors:

a) The first depends on the inductance of S_1---the switch time constant should be about one-tenth that of the voltage build-up for a drop of 10 percent.

b) The second depends on resistive skin losses in the conductors and hence on resistivity and certain generator dimensions.

c) The third loss factor is related to the interconnecting of regions of different potential by the two continuous conductors, permitting some energy flow during the charging build-up which reduces the potential difference.

This loss increases as the ratio of the outside diameter of the generator to the inside diameter increases, i.e., as the generator output impedance increases. A 30-ohm generator would thus be expected to have a lower ratio of measured-to-theoretical output voltage than a 10-ohm model.

At relatively low-impedance levels, the spiral coaxial pulser appears desirable as a multiple-stage voltage-step-up pulser, since fewer switches are required than for the stacked Blumlein or Marx-surge circuits of Figure 9. Both the stacked Blumlein and the spiral generator have an advantage over the Marx-surge circuit because all of the dielectric material is, in principle, used for deliverable energy storage.

At impedance levels of the order of 20 ohms or greater, the third loss factor mentioned above becomes sufficiently great that the delivered energy is appreciably less than the stored energy, and consequently the stacked Blumlein may in principle be more desirable. A final choice would require further development of both types of pulsers.

6. Rise Time Considerations

Pulse rise time in several of the above pulser designs is affected by several parameters subject to varying degrees of control. Certain applications may stress rise time, while others may relegate it to a lesser role. The following rise time discussions are confined to the switch end of a Blumlein circuit; rise time considerations dealing with the output end of the pulser will be discussed later, in connection with Transducer Chamber design.

For switching a Blumlein pulser circuit, i.e., providing a short circuit at the line end remote from the load, a desirable switch would be one which had the following characteristics: constant impedance from the line to the switch, little or no inductance in the switch itself, a distributed switch which shorted simultaneously every point of the transmission line termination, minimum energy dissipation in the switch, and finally very long switch life or at least a switch design permitting easy maintenance.

6.a Switch Inductance

Switch inductance will be distributed between the inductance of the leads connecting the line to the switch and the switch gap itself.

The minimum gap distance in the switch is determined by the dielectric strength of the switch material. This distance can be very short, particularly for the case of solid or liquid dielectrics; however, following switch breakdown solid dielectrics have to be replaced.

The length of switch leads will be determined by design considerations involving space requirements around the switch, i.e., charging access to the pulser, switch insulation, gap spacing, provision for plug-in switches, arc-residue control, etc. The effect of switch inductance is to degrade rise time, which is determined by the L/R time constant (where L is the switch inductance and R is the resistance of the line and gap). Rise time between the 10 and 90 percent points is equal to 2.2 times the L/R time constant. Since the lines described herein are generally of very low impedance, switch inductance must be correspondingly low and becomes a very important parameter requiring minimization.

6. b Transit Time Effects

Solid, liquid or gaseous dielectrics may be utilized as switch dielectrics. Such dielectrics can generally be broken down at discrete

points but seldom continuously over a large area. The present availability of laser-type switching may provide a new and very desirable flexibility in switching techniques. For fast-rise-time pulse generation, it becomes important that the switch provide a short circuit continuously along the entire end of the line, if at all possible. Under these conditions a voltage reversal propagates uniformly with radial symmetry from the switch at the shorted end of the line. However, shorting at point A of Figure 12 results in a perturbation which will not be felt at point B until a period of time following switching equal to the single transit time between point A and B through the storage media. Thus, following switching, a reversal wave at A begins to propagate toward C but will not begin to propagate from B toward D until a later time. Thus an asymmetrical wave propagates down the line and arrives at the load end resulting in the load experiencing a rise time which is not a step function but is a ramp having a length related to the transit time from A to B. It becomes important then to switch at as many points around the periphery of the Blumlein as is possible. By using a technique such as beam splitting, laser triggering appears well suited to the simultaneous triggering of many parallel gaps. A further advantage is gained by the absence of electrical connections, with consequent simplification and probable improvement in gap stability (Ref. 8).

A seemingly apparent alternative is to switch at a point everywhere equidistant from the end of the Blumlein. This point would necessarily lie along the axis of the line. However, as can be seen in Figure 13 if the section connecting the transmission line to the switch has uniform dielectric constant the impedance is found to increase from the line to the switch; for example, the impedance at AA' is greater than the impedance at a cut through BB' which is greater than the impedance at a cut through CC'. Thus transit time variations can be avoided, but at the expense of introducing a nonuniform impedance between the end of line CC and the switches. One means of circumventing this difficulty would be to provide a graded dielectric material between the end of the line and the switch such that, to as high a degree as possible, a uniform impedance is found at any point through

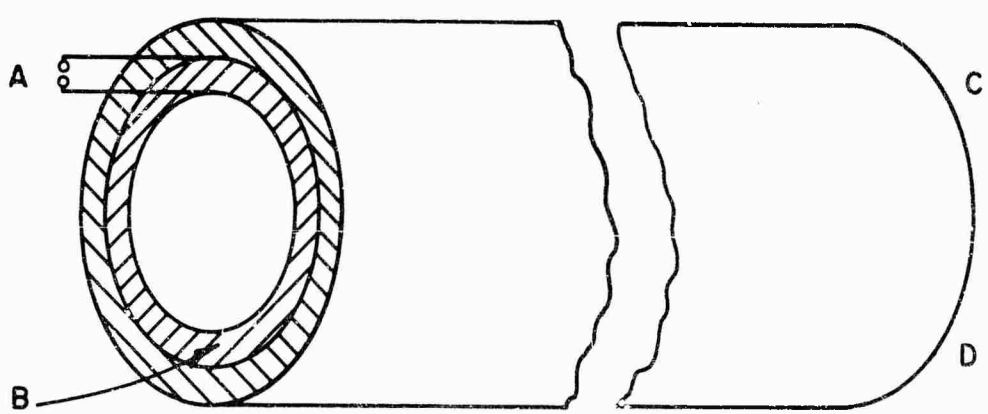

Figure 12 Blumlein Single Switch Which Generates an Assymetrical Wave in the Line.

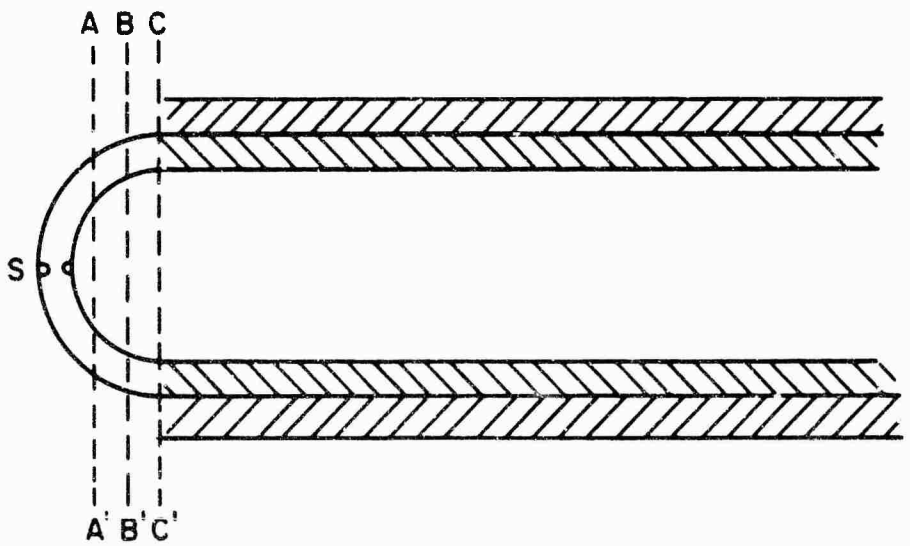

Figure 13 Blumlein Single Switch Which Introduces Non-Uniform Impedance in the Line.

the cross section. Such a dielectric material is not known to be readily available or easy to construct for applications where high dielectric hold-off is required.

7. General Design Considerations

The output pulsed voltage durations of interest for the proposed generators are of the order of tens of nanoseconds and are probably produced most efficiently by discharge of distributed-line pulsers, where the storage elements are coaxial or strip lines. When viewed with respect to the load, the pulsed generator output circuit behaves as an individual line having specific values of open circuit voltage V_{oc}, characteristic impedance Z_o and pulse duration $2\tau_o$. The output voltage V_{oc} when the generator is operated with a matched load (i.e., $R_L = Z_o$), which will be assumed in the following discussion.

The pulser output power delivered to the load, in joules per nanosecond, is

$$W/\Delta t = 1000\ V_o^2/Z_o \text{ joules/nanosecond} \qquad (11)$$

if V_o is in megavolts and Z_o in ohms. The factor of 1000 results from conversion from standard (mks) units to those specified. For convenience this relationship is shown in graphical form in Figure 14. For example, consider the desired exploding-wire specifications of 1000 joules to be delivered in 10 nanoseconds (i.e., 100 joules/nanosecond) into a matched load at an output voltage of 500 kv. Assuming no loss and zero rise and fall times, a 2.5 ohm generator impedance is indicated.

The problem of size is also of interest in generator design, since excessive volume not only may be bulky and costly, but also may give rise to excessive inductance and/or capacitance, depending on the particular design employed. A brief discussion of some factors affecting size is therefore appropriate.

A general formula for the energy storage density was given as equation (10) in Section II-2; this can be expressed in more convenient units as

$$W/\Delta V = 195\ \epsilon_r E^2 \text{ joules/foot}^3 \qquad (12)$$

where ϵ_r is the relative dielectric constant and E the electric field in Mv/inch.

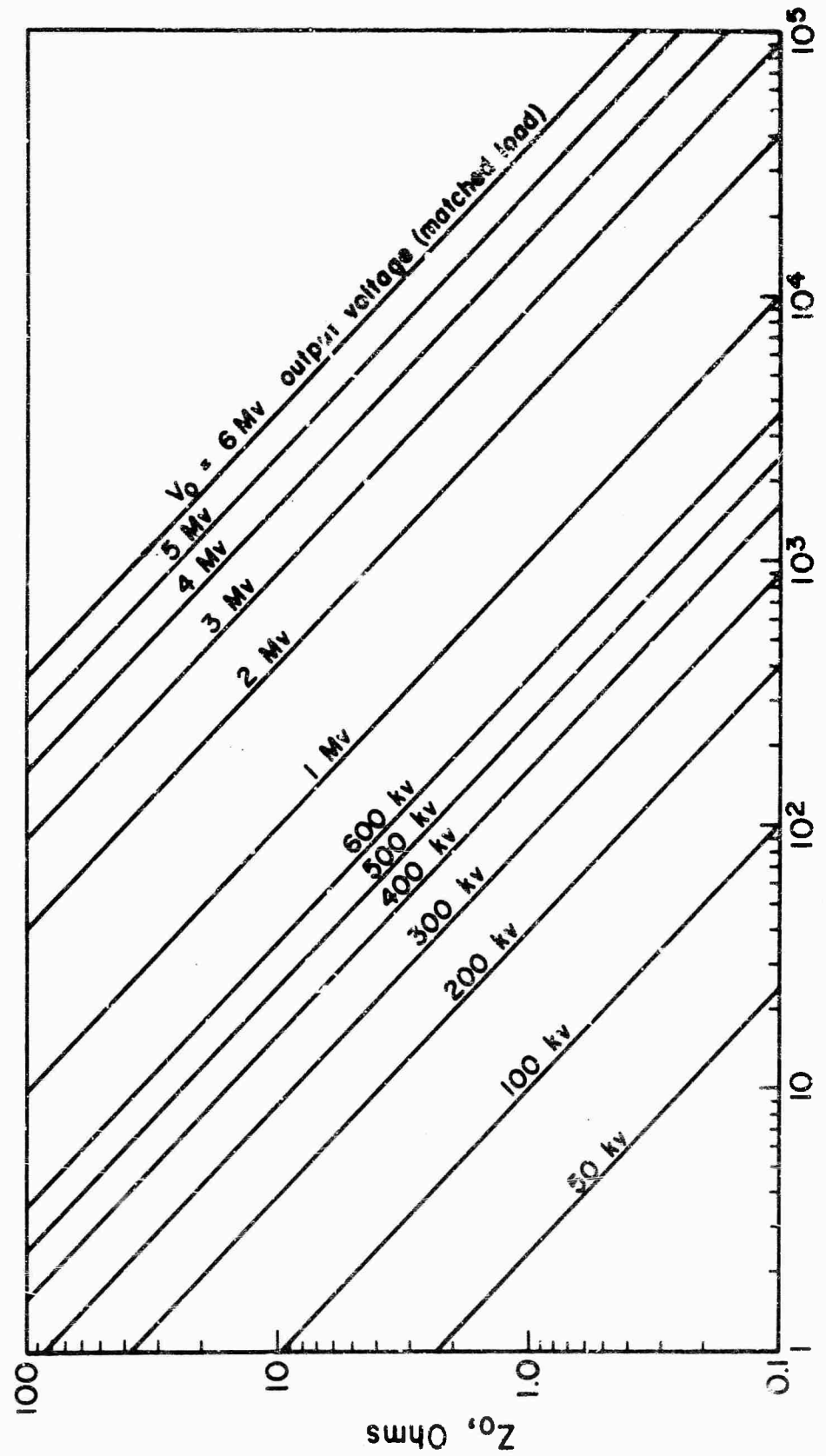

Figure 14 Relation Between Charging (or open circuit) Voltage, Characteristic Impedance and Energy Storage per Nanosecond Output into a Matched Load.

This relationship is presented graphically in Figure 15. A word of caution is in order concerning certain ceramic materials --- the dielectric constant may decrease substantially at higher voltage gradients, and hence a detailed study of dielectric constant versus electric field is required for an estimate of energy storage density.

Also of interest is the pulse length $2\tau_o$ obtained from a distributed line with relative dielectric constant ϵ_r. Expressing equation (5) above in more convenient units one obtains the pulse length per unit line length as:

$$2\tau_o/\ell = 2.03\ \epsilon_r \text{ nanoseconds/foot} \qquad (13)$$

A 1-foot line would thus give a pulse length of 2.03 nanoseconds for vacuum dielectric, about 3.0 nanoseconds for polyethylene or certain transformer oils (ϵ_r=2.2), about 18 nanoseconds for water (ϵ_r=78) and about 100 nanoseconds for ceramic dielectric (if ϵ_r=2430). It is immediately apparent that the length of energy storage lines is quite short for high-dielectric-constant materials, particularly for the short pulse durations of interest. This short length requires increased width and/or height to attain a given stored energy, compared to energy storage at the same energy density with a lower dielectric constant. Also end effects problems are exaggerated, particularly since the maximum electric fields are considerably lower than those permissible with the other dielectrics. Referring to equation (1) and Figure 1 above, the problem of impedance matching is also more difficult. The successful use of relatively-high-dielectric-constant material in a low impedance system (i.e., 4.7 ohm at 320 kv) has, however, been noted. (Ref. 1).

Two of the more popular dielectrics, polyethylene and water are considered as examples for the higher voltages and short pulse lengths of interest in this study. Based on design support data mentioned later in the report, maximum electric field values (pulse charged) of 1.0 Mv/inch for polyethylene and 0.5 Mv/inch for water are assumed for the following design discussion.

At first examination, use of a strip line pulser geometry appears quite attractive, since all the space is used for dielectric storage, in contrast

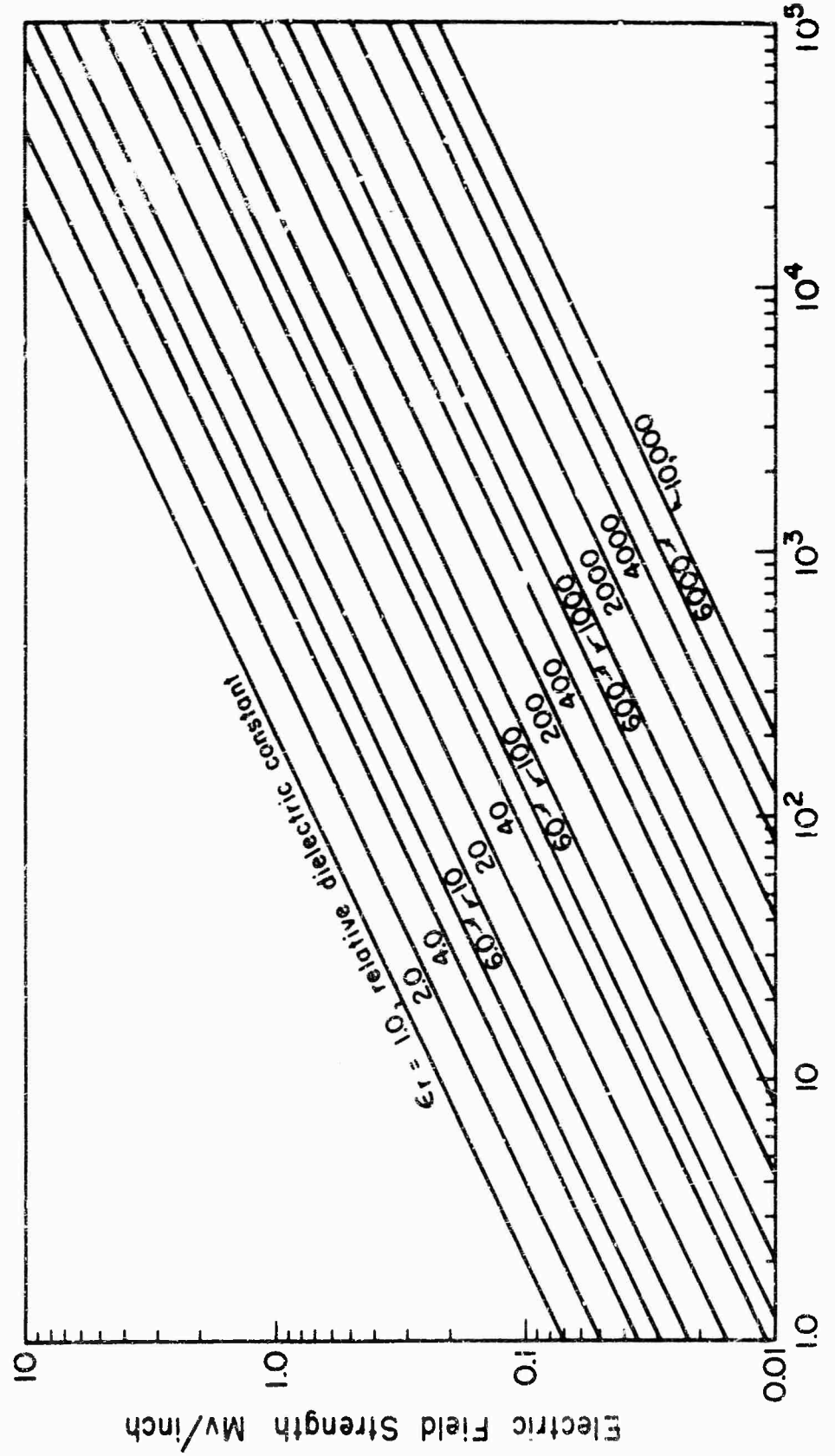

Figure 15 Relation Between Dielectric Constant, Electric Stress and Energy Density for Dielectric Storage Material.

with the volume wasted within the inner conductor of a coaxial pulser. The latter coaxial design, however, has several advantages over the strip line design:

a) The high voltages (and electromagnetic radiation) can be contained with a minimum of design problems,

b) connection to a coaxial (and perhaps hollow-beam) tube or other load appears to be practical with minimum inductance and difficulty, and

c) field enhancement edge problems are encountered at only two ends, compared with both the sides and ends of the strip line.

The coaxial design is therefore the only type considered for the relatively low impedance systems of interest in this study.

Overall dimensions are important, since excessive size may prove undesirable with respect to construction, service and required facilities. Figures 16 and 17 are provided to indicate the minimum sizes that can be expected for the dielectrics and maximum field strengths specified, covering voltages and impedances of interest in this study. Actual diameters will be larger - after allowances for edge field enhancements (for the simple Blumlein design) for intermediate conductors (for multiple-stage Blumlein designs or for conductors and insulation (for Marx-surge designs).

Comparison of Figures 16 and 17 would indicate that water dielectric generators are more compact below an impedance level of 10 ohms, for the same output voltage and impedance. The increase in diameter at higher impedance values arises from sizeable field enhancement at the relatively small inner conductor required to give a high impedance.

The use of water dielectric appears impractical for an 80 ohm generator impedance, as specified for the X-ray generator design, because of the extremely small inner-to-outer diameter ratio (about 10^{-5}) required to give this impedance in a coaxial geometry. Referring to Figure 17, a minimum outer diameter of 2.5 feet at 2 Mv or 5 feet at 4 Mv would be required with polyethylene at an 80 ohm impedance level. A length of 6.6 feet

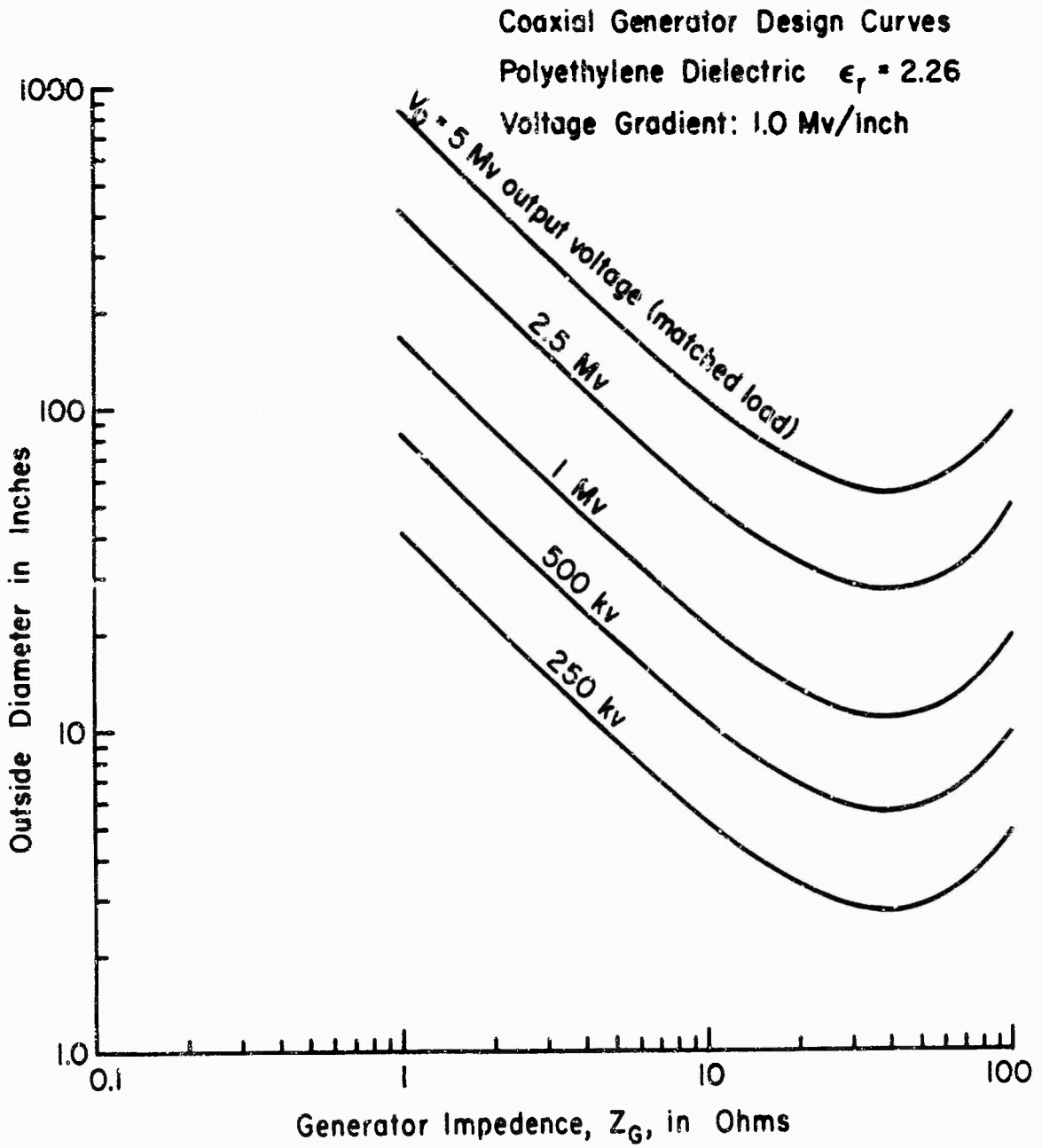

Figure 16 Coaxial Generator Design Curves for Polyethylene Dielectric and a Maximum Electric Stress of 1.0 Mv/inch. The Outer Diameter is Shown to Depend on Characteristic Impedance and Open Circuit Voltage.

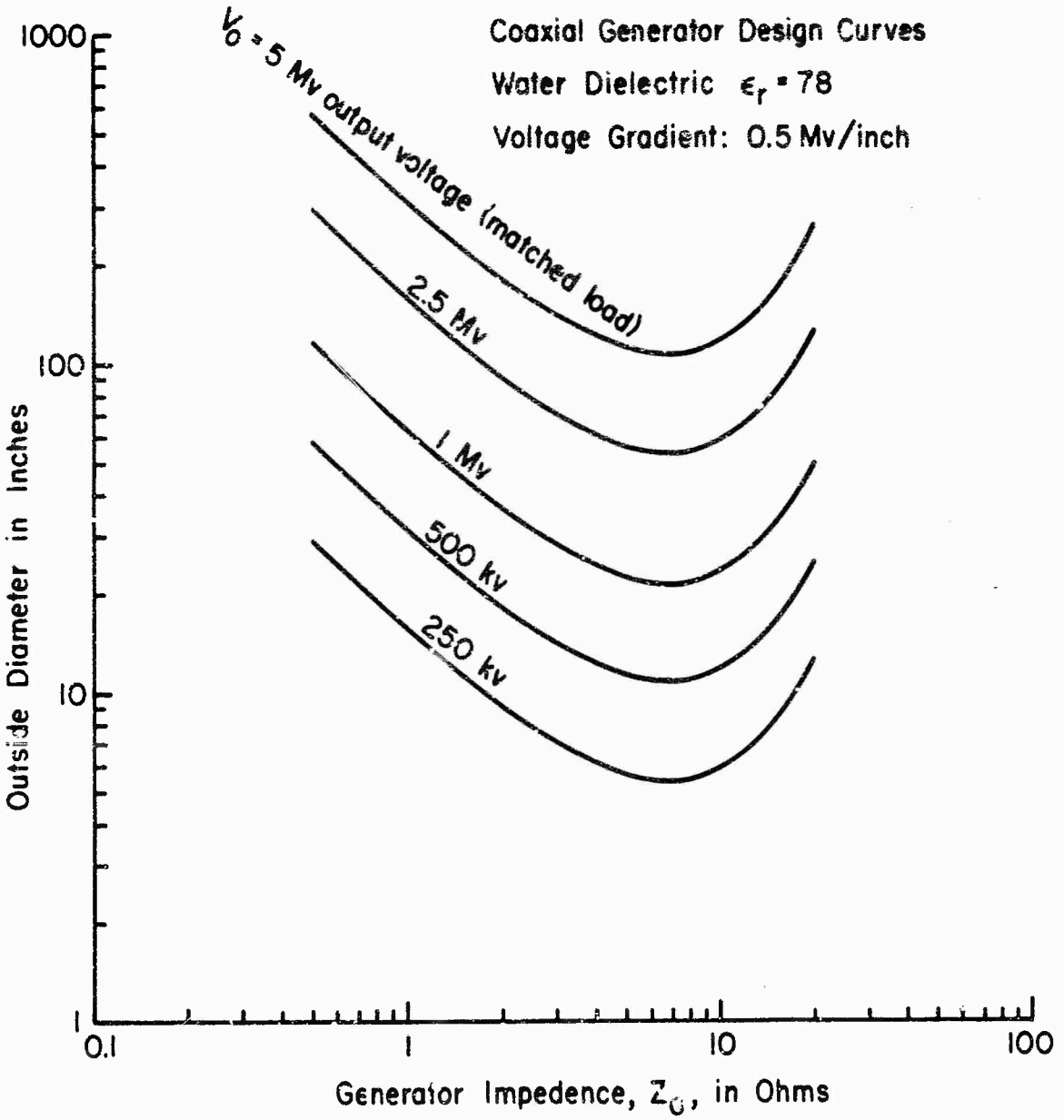

Figure 17 Coaxial Generator Design Curves for Water Dielectric and a Maximum Electric Stress of 0.5 Mv/inch. The Outer Diameter is Shown to Depend on Characteristic Impedance and Open Circuit Voltage.

for 20 nanoseconds or 16 4 feet for 50 nanoseconds would be required, using equation (13) and a dielectric constant of 2.26.

An impedance level of 1 or 2 ohms, with corresponding matched-load voltages of 300 or 500 kv, is specified for the exploding wire pulser design, with a pulse length of 10 nanoseconds. A minimum outer diameter of 1.5 feet and length of 0.56 feet would be required with water dielectric, or about a 4 foot outer diameter and 3.3 foot length with polyethylene, based on Figures 16 and 17 and equation (13). The choice of dielectric in this case would depend on consideration of all problems, since both types are possible geometrically.

8. Pulse Charging Considerations

As indicated in the design support data section of this report, advantages may frequently be obtained by pulse charging the energy storage dielectric in the case of certain designs such as Blumlein Pulsers. With such pulse charging it is frequently possible to operate at substantial voltage gradients with liquid dielectrics at high gradients. Surface "creep" breakdown is also frequently minimized for such pulse charging.

Initial calculations and certain experimental studies referred to later were performed to determine the energy and voltage transfer efficiencies when a capacitor C_1, charged to V_c, is discharged through an inductor into a second capacitor C_2. The voltage across C_2 is a damped sinusoidal function of time, which during the first half cycle goes through its maximum value $V_{o\,max}$ corresponding to a maximum energy transfer $W_{o\,max} = 1/2\, C_2 V^2_{o\,max}$. The first order expressions derived for the circuit of Figure 18 are given below:

$$\rho_{v\,max} = \frac{V_{o\,max}}{V_c} = \frac{C_1}{C_1 + C_2}\left[1 + \exp\left(\frac{-\pi}{2}\frac{R}{\sqrt{L/C}}\right)\right] \qquad (14)$$

$$\eta_{max} = \frac{W_{o\,max}}{W_c} = \frac{C_1 C_2}{(C_1 + C_2)^2}\left[1 + \exp\left(\frac{-\pi}{2}\frac{R}{\sqrt{L/C}}\right)\right]^2 \qquad (15)$$

where ρ_v is the voltage transfer ratio, η the energy transfer ratio, and C is the equivalent series capacitance (i.e., $1/C = 1/C_1 + 1/C_2$).

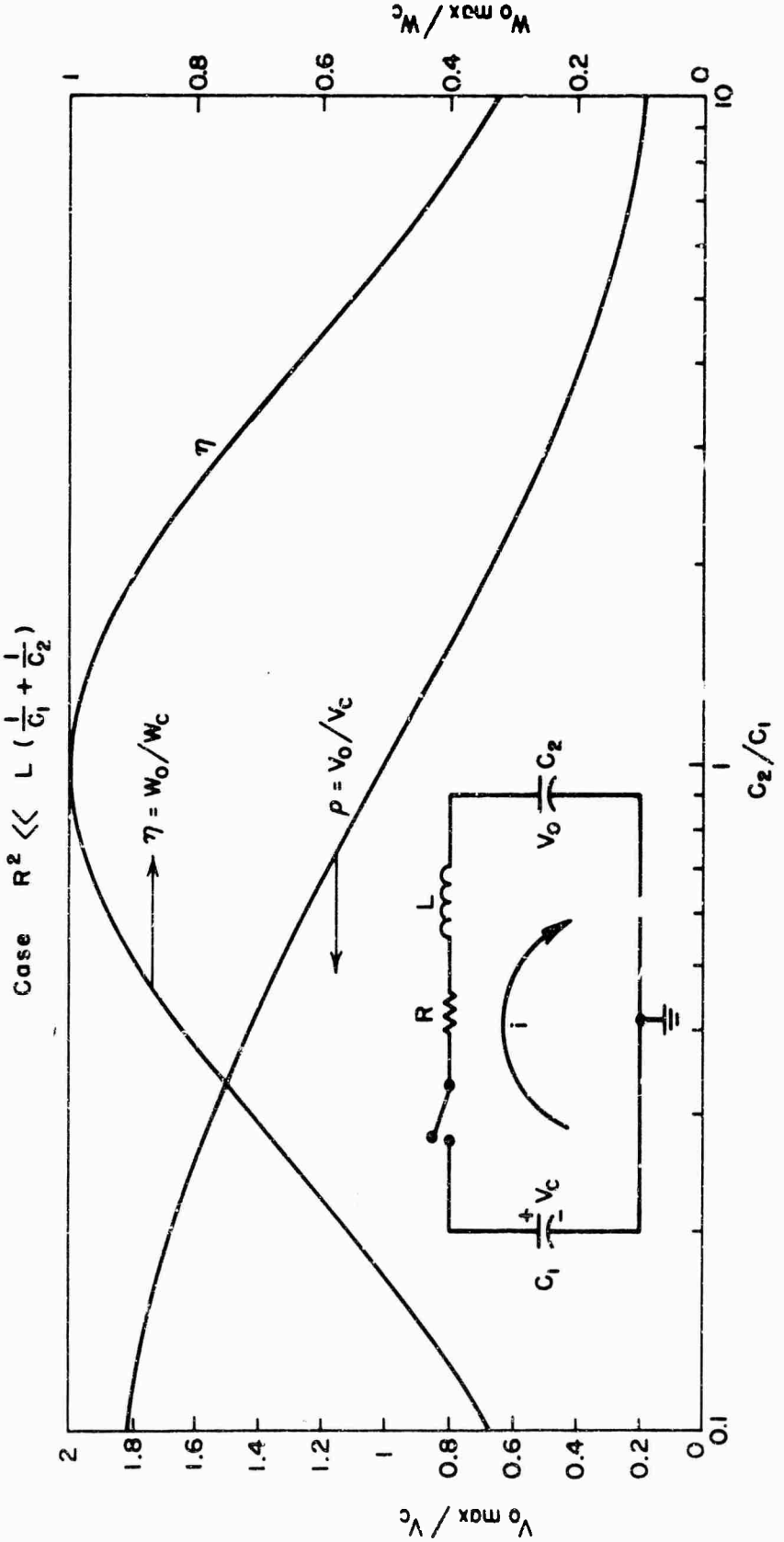

Figure 18 Calculated Efficiency and Voltage Transfer Between a Charged Capacitor Inductively Charging a Second Capacitor. The Equivalent Circuit Used in the Calculations is also Shown.

Figure 18 is a plot of these ratios as a function of the ratio of output to input capacity, assuming the equivalent series resistance for the system is relatively small, as defined at the top of Figure 18, i.e., assuming the exponential factors above to be essentially unity.

Of special interest is the fact that the energy transfer efficiency can be made to be 100 percent for matched values of capacity in the primary and secondary storage, irrespective of the inductance value. Therefore, when charging a Blumlein generator from a Marx-surge capacitor primary pulser, the effective series output capacity of the Marx-surge pulser should equal the input capacity of the Blumlein circuit as seen during charging, if one seeks the most efficient possible use of the energy stored in the Marx-surge stage. As will be noted later, the distributed inductance in the charging circuit does not adversely affect the energy transfer efficiency. On the other hand, the foregoing equations and Figure 18 indicate the existence of a trade-off, and show that it is possible to achieve a significant voltage step-up $\rho_{v\,max}$ at the cost of some loss in energy transfer efficiency (e.g., $\rho_{v\,max} = 1.4$ at $\eta_{max} = 84\%$).

9. Impedance Transformers

Tapered transmission lines have been used in certain circumstances to provide impedance transformation where it is necessary to match a load resistance of one value to a generator or transmission line having a different characteristic impedance. For constant power, a given voltage transformation by some factor x requires an impedance transformation x^2. For example, if operation of a load resistance of 20 ohms at 6 megavolts is required from a 3-megavolt (matched-load) generator, this generator would have to have an internal impedance of 5 ohms for optimum power transfer. Referring back to Figure 16 and interpolating, the required 6-megavolt open-circuit 5-ohm generator would have an outer diameter of about 8.3 feet, somewhat larger than the corresponding 12-megavolt open-circuit 20-ohm generator diameter of about 7 feet. This increase in physical size, however, might be offset by advantages of operating at a lower storage voltage and having more uniform gradients.

A practical limitation of uniformly tapered transmission lines is the electrical length required for minimum pulse distortion and energy reflection. As a rule of thumb, the line should be approximately 3 wave lengths long at the frequency corresponding to the fundamental of the Fourier pulse analysis. For a 30-nanosecond pulse, this would correspond to an electrical length of about 180 nanoseconds; a physical length of 120 feet would then be required with polyethylene, or about 20 feet with water. It might be possible to reduce these figures substantially by employing a spiraled inner conductor, but this would in turn introduce problems of voltage gradients and termination connections.

Shatz and Williams (Refs. 10 and 11) have indicated the practicality of maintaining low pulse distortion with exponentially-tapered lines for certain conditions (e.g., pulse lengths of 5 to 20 nanoseconds and voltage step-up ratios of 2 to 4). The shape required in the tapered conductor is given by the expression for the ratio of radii (in terms of sending end ratio of radii R_2/R_1) as

$$r_2/r_1=(R_2/R_1)\exp(\gamma x)$$

where r_2 and r_1 are the inner and outer radii at the output end, R_2 and R_1 the inner and outer radii at the input, γ the flare coefficient and x the line length. Design curves given by these authors permit ready computations of the conductor taper, pulse distortion, efficiency and voltage step-up ratio. For example, consider such a transformer for a 10 nanosecond pulse, with water dielectric, 5 ohm input (generator) impedance and 20 ohm output impedance. The input and output radii ratios are 2.11 and 20 respectively and a line length of 22 inches would give a maximum pulse distortion of 5 percent and a voltage step-up ratio of 1.8, or 90 percent of theoretical. A sketch of such a transformer is shown in Figure 19.

10. Transducers

The function of a transducer chamber is to couple energy from the pulse-forming line (e.g., the Blumlein circuit discussed above) to the transducer (e.g., an exploding wire or a flash X-ray tube). It must in many cases accommodate internal as well as external diagnostics, such as optical

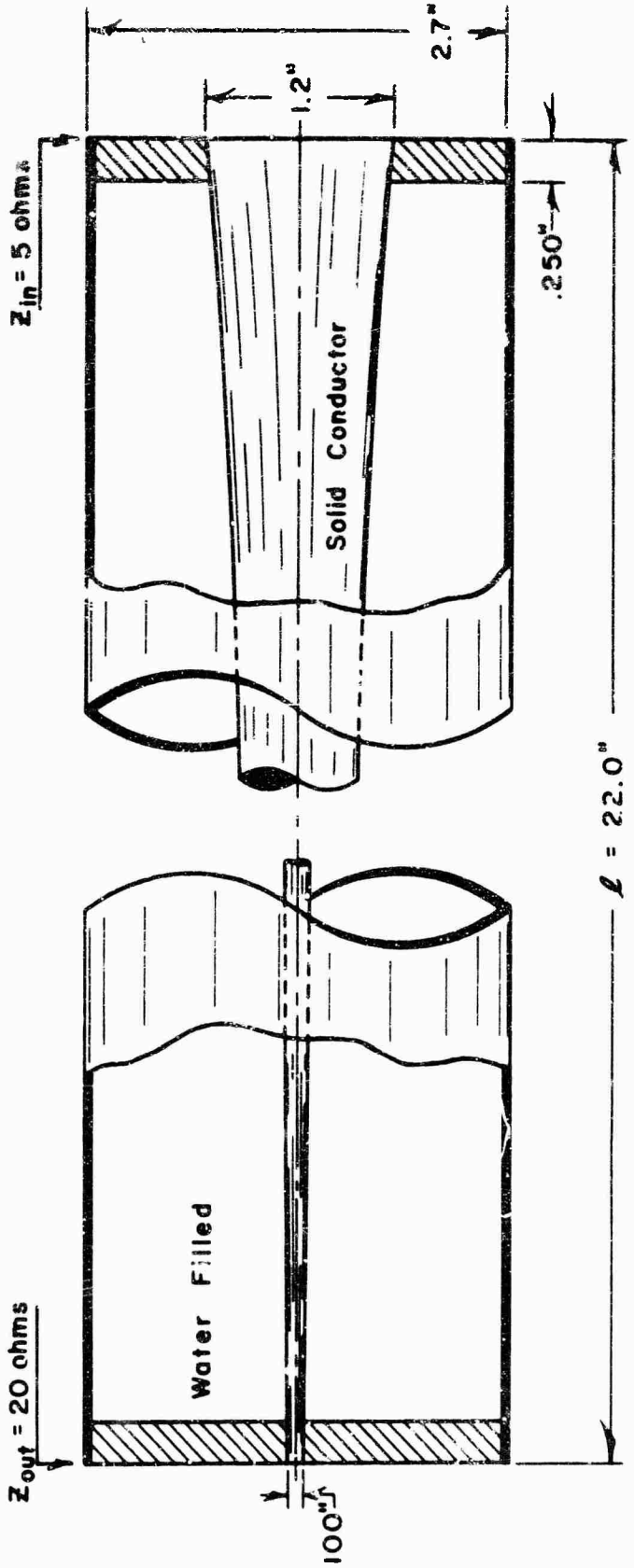

Figure 19 Sectioned View of 5 to 20 ohm Exponential-Line Pulse Transformer.

viewing of the event from outside the chamber (e.g., exploding wire phenomena, EWP) or electrical measurements performed inside or close to the chamber. The chamber should also be capable of withstanding significant overvoltage in the event of an impedance mismatch between the load and generator. Furthermore, the energy must be delivered to the transducer in the desired pulse shape, which normally requires that the chamber and transducer present to the pulser a matched impedance load with minimum inductance.

The impedance matching problem may be a serious one since transmission lines of some type will be employed, and the only adjustable parameters controlling impedance are line dimensions (spacing) and the dielectric constant of the insulating media. If the transducer is inevitably much smaller than the dimensions of the coaxial generator, as in the case of an exploding wire load, obtaining a good impedance match may be difficult or even impossible. This can be better understood with the aid of Figure 20, showing a cross section of a disc-transmission line which can be considered to be a simplified approximation to a hemispherical chamber having small spacing at the apex. The impedance of this disc-type line, considering the pie-shaped section of Figure 20 and applying the impedance formulae for strip lines (Figure 1) indicates that the spacing must decrease steadily as the transducer size (diameter in this case) decreases. Thus, good impedance match to a small transducer such as a wire may imply a chamber spacing too small for satisfactory voltage hold-off and therefore prove unfeasible.

Two obvious alternatives exist. One is to maintain sufficient spacing to provide adequate voltage hold-off resulting in an impedance mismatch wnich will appear as added circuit inductance. The other alternative is to grade the dielectric constant of the line as it approaches the transducer in order to maintain constant impedance while varying line spacing. This implies a flexibility not fully available at present in selection or construction of dielectric materials and certainly impossible with gases. Although at the cost of some mismatch, transition from low to high dielectric constant material may be made in one abrupt step (e.g., from a storage line

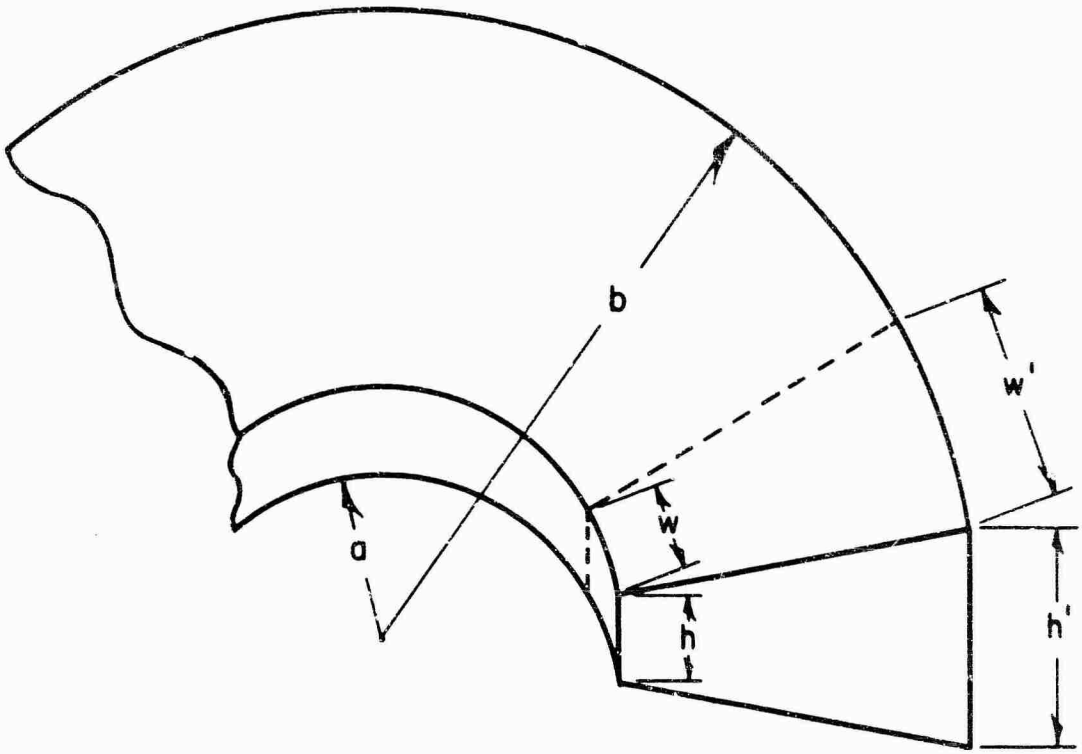

$$h/w = h'/w'$$

Figure 20 Schematic Representation of Disc Type Transmission Line. For Constant Impedance the Ratio S/W Must Remain Constant for any Radius a, thus Adapting to a Small Transducer (small a) May Imply a Chamber Spacing too Small for Satisfactory Voltage Hold-Off.

solid dielectric of low dielectric constant to a liquid of high dielectric material in the vicinity of the load permits the use of greater spacing usually resulting in greater voltage hold-off). Specific application will dictate where liquid and/or solid dielectric materials can be employed in the vicinity of the transducer.

As indicated in the foregoing discussion, the primary function of the transducer chamber is to convey as efficiently as possible energy from the pulse generator to the device being excited. A case of immediate interest to this study is the design of an exploding wire chamber. A secondary but important function in the design is incorporation of features for diagnostics, including voltage, current and di/dt monitoring as well as use of aperturing and suitable dielectric media (e.g., vacuum gas) for optical viewing.

Relative to time scales considered here, the use of modest apertures does not appear to greatly affect the energy delivered or its rate of transfer, nor does the inclusion of various electric diagnostic sensors. Thus the problem centers on maintaining a constant impedance in the transmission system. However, since this cannot be readily accomplished in most chambers, the problem becomes one of minimizing the effective series inductance by maintaining as small a spacing between electrodes as possible, while avoiding breakdown which would shunt energy from the exploding wire.

Consideration of various possible geometries leads to selection of spherical geometry, as illustrated in Figure 21 which gives a schematic view of a pulse-charged Blumlein generator, wire chamber and load. This spherical geometry gives a minimum inductance coupling between the generator and exploding wire, consistent with uniform voltage gradient throughout the chamber region and adaptation to viewing parts for optical diagnostics.

As an example, some inductance calculations have been performed for an outer chamber radius of 12 inches. The formulae employed, given in the Appendix give a value higher than the actual inductance since the capacitance between the inner and outer chamber domes (Figure 21) acts to cancel a portion of the inductance.

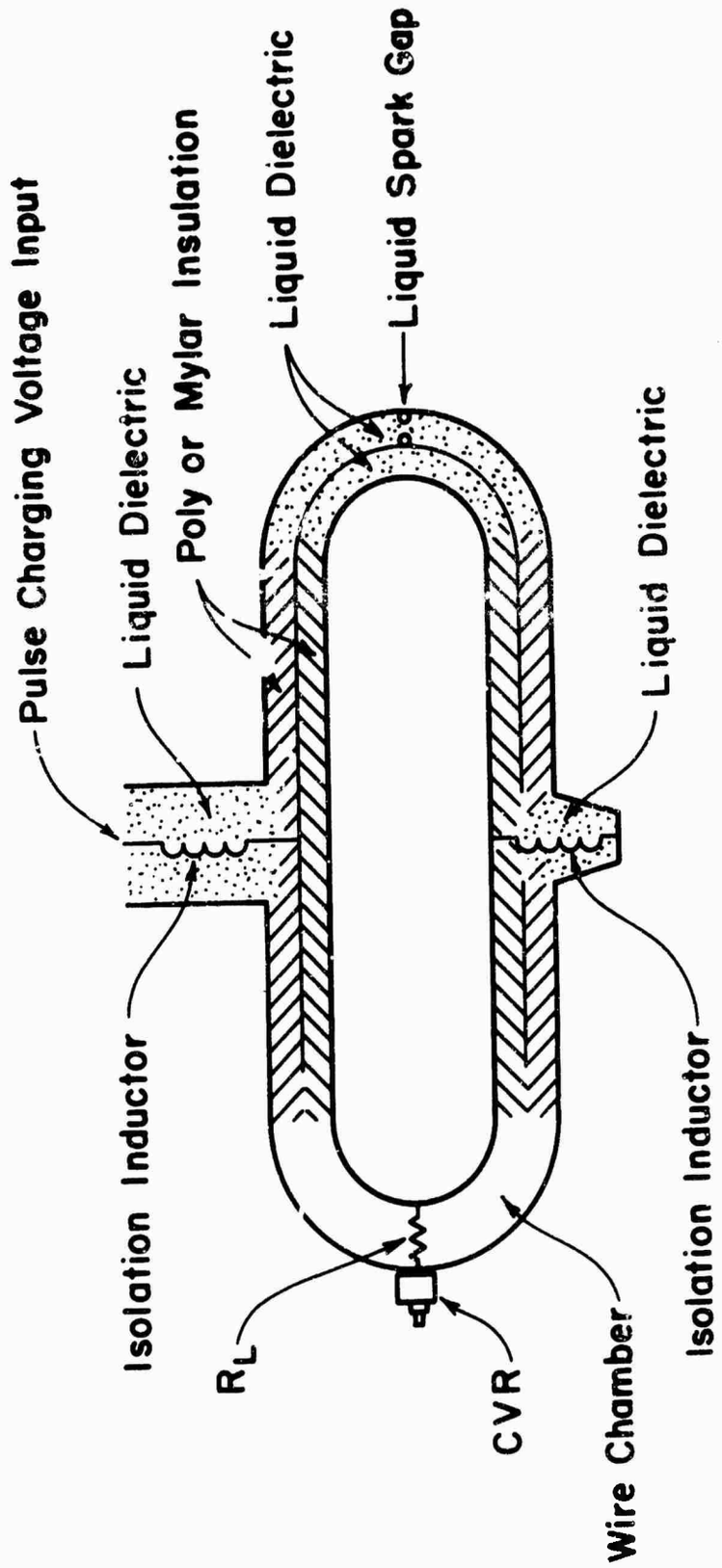

Figure 21 Schematic Diagram of Exploding Wire System, Indicating Hemispherical Geometry of Transducer Chamber.

Chamber spacings of 0.15 and 0.6 inch were selected for computation with wire diameters ranging from 2 mils (0.002 inch) and up, and inductance arising from magnetic build-up within the wire was ignored, skin depth considerations would appear to justify this assumption:

$$\delta = \frac{1}{2\pi} \sqrt{\frac{\lambda \rho}{30 \mu}}$$

where ρ is the resistivity of the conductor in ohm-centimeters, μ is the permeability of the conductor, λ is the free-space wave length, a δ the skin depth in centimeters. (Ref. 12). The inductance obtained in this manner was reduced to allow for the distributed chamber capacitance and the results are listed in Table I, with the rate of current rise, di/dt, being computed as the quotient of open circuit voltage (600 kv assumed to be across the wire inductance initially) and wire inductance.

TABLE I

Exploding Wire Chamber Parameters
Chamber Radius = 12 inches

Chamber Spacing inches	Wire Diameter, mils	Estimated Inductance, nanohenries	di/dt, initial amp/sec
0.6	2	29.7	2×10^{13}
0.6	20	22.7	2.6×10^{13}
0.6	200	15.7	3.8×10^{13}
0.6	787	11.5	5.2×10^{13}
0.15	2	6.62	9.1×10^{13}
0.15	20	4.87	1.23×10^{14}
0.15	200	3.12	1.92×10^{14}
0.15	787	2.08	2.9×10^{14}

The importance of minimizing chamber spacing is at once evident from examination of Table I, since the inductance increases even faster than linearly with chamber spacing. For a given spacing, specific energy deposition in a wire would be expected to increase with decreasing wire diameter d, since the mass decreases and the resistance increases as $1/d^2$, while the inductance increases only as a log 1/d.

Preliminary data, given in Section III of this report, indicate that dielectric strengths of 2 to 4 megavolts/inch may be practical with solid

or liquid dielectric media. This, together with relative dielectric constants which would further minimize inductance, would permit inductance values perhaps even lower than those in Table I corresponding to the 0.15 inch spacing. Pressurized gases appear capable of withstanding gradients somewhat in excess of one megavolt per inch, with inductance values corresponding to the larger spacing in Table I. It thus appears that such insulation techniques would be suitable for obtaining quite high energy deposition rates, where compatible with required diagnostics.

Vacuum insulation is, however, often preferred or even necessary for certain types of diagnostics such as spectroscopic examination of the exploding wire. Examination of Figure 22 shows data variations of over an order of magnitude in spacing at a given voltage, with a lower limit of perhaps one centimeter being obtainable with relatively large area electrodes at 600 kv. Preliminary data obtained with the EWP system built (Ref. 1) for the AFWL indicate initial breakdown at gradients as much as an order of magnitude lower, occurring in this instance with electrode surfaces and vacuum conditions not yet optimized.

There is also the problem with vacuum insulation with respect to the gas sheath which surrounds a wire soon after energy is introduced, thereby shunting the current flow from the wire itself (Ref. 13). Both the electrode surface and vacuum conditions require considerably more investigation with the pulse-width and rise-time of exploding wire systems presently available and proposed in this report.

One important mechanism leading to vacuum breakdown is thought to be field emission of electrons from microprojections on the negative electrode, followed by bombardment of the anode and release of gas, the process then being regenerative until the energy is dumped. The dependence of breakdown upon electrode area is presumably a result of higher energy storage (capacity between electrodes) being available for dumping in the arc in a short time, of greater difficulty of avoiding some sharp projections on a large area electrode, and of greater effect of gas release at the anode on the gas pressure in the gap. These mechanisms and some possible

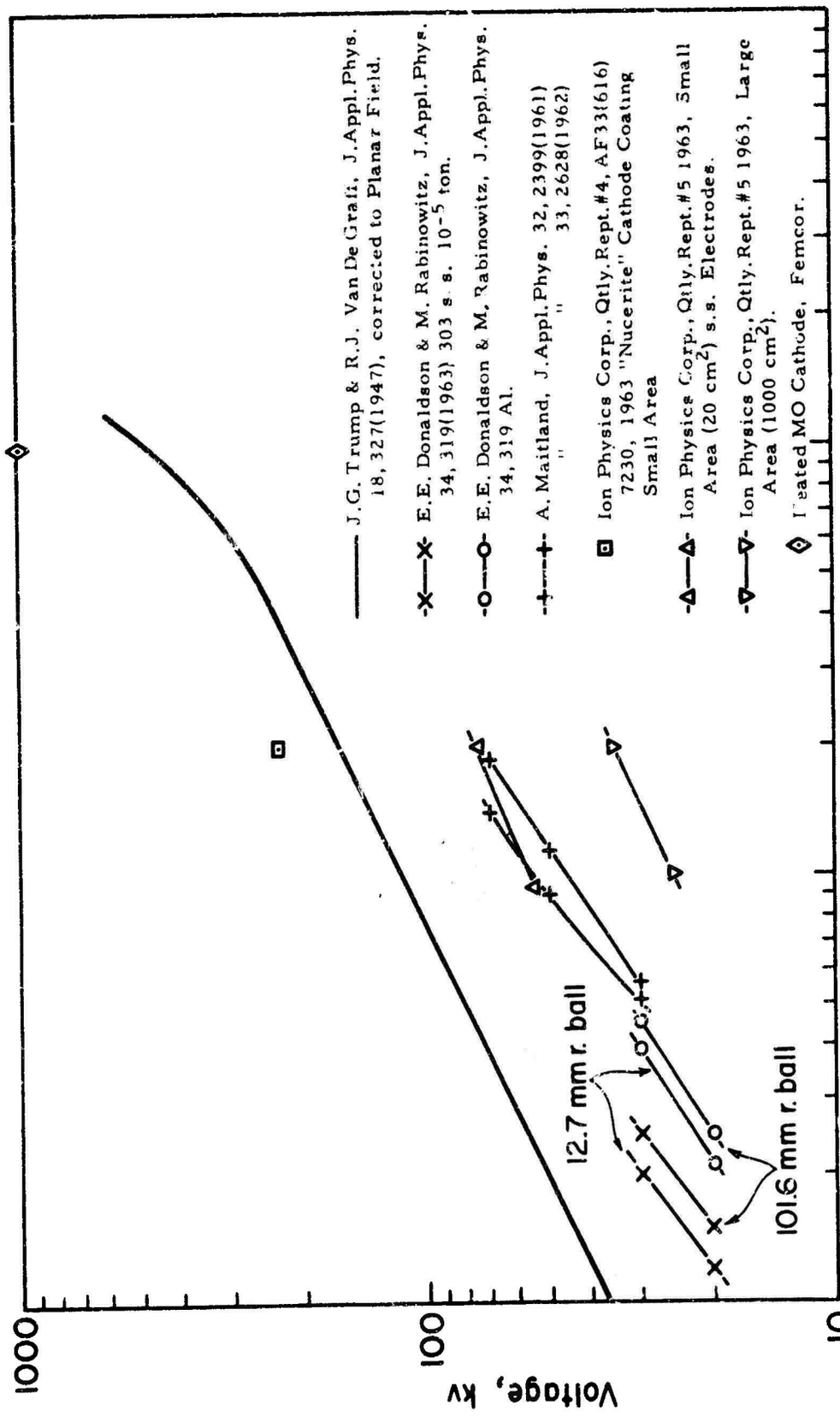

Figure 22 Vacuum Breakdown Voltage as a Function of Pulser Electrode Spacing.

techniques for improvement in breakdown strength are discussed in Section V below.

If a short rise time is to be preserved in a flash X-ray system, it is madatory that the inductance of the transducer chamber and vacuum tube be held to a minimum. One effective way of accomplishing this is to design the transducer chamber and tube in a coaxial geometry, the tube serving as the inner conductor and the transducer chamber as the return outside conductor. For example, assuming vacuum dielectric, the ratio of inner to outer diameters for a 20-ohm system would be 1.4. This approach would apply rigorously only if a hollow electron beam is employed (so that no magnetic field is generated inside the electron beam by the tube current), and if the outer chamber is tapered down in the vicinity of the target to compensate the drop in the voltage between the inner and outer "conductors".

A schematic cross section of a flash X-ray system with such a transducer chamber and tube geometry is shown in Figure 23, indicating the method of connecting a hollow-beam tube to the Blumlein high-voltage generator. In this design it is important that the spacing between the tube and transducer chamber (or magnetic focus coil) be adequate to avoid electric breakdown of the insulating medium surrounding the tube; such a breakdown would probably not only affect tube output, but also damage the tube envelope. The use of hollow-beam tube geometry not only decreases the effective load inductance but will also be shown to be desirable with respect to target loading and radiation uniformity.

11. X-Ray Generation

11. a Tube Design

The design of a tube was not a specified objective of this contract. An applicable detailed discussion of X-ray tubes is given in Reference 14. The following limited discussion is however presented to clarify the relationships between the generator and a tube which is employed as a load.

The maximum target temperature reached during an X-ray pulse is of prime importance where multiple-pulse target life is

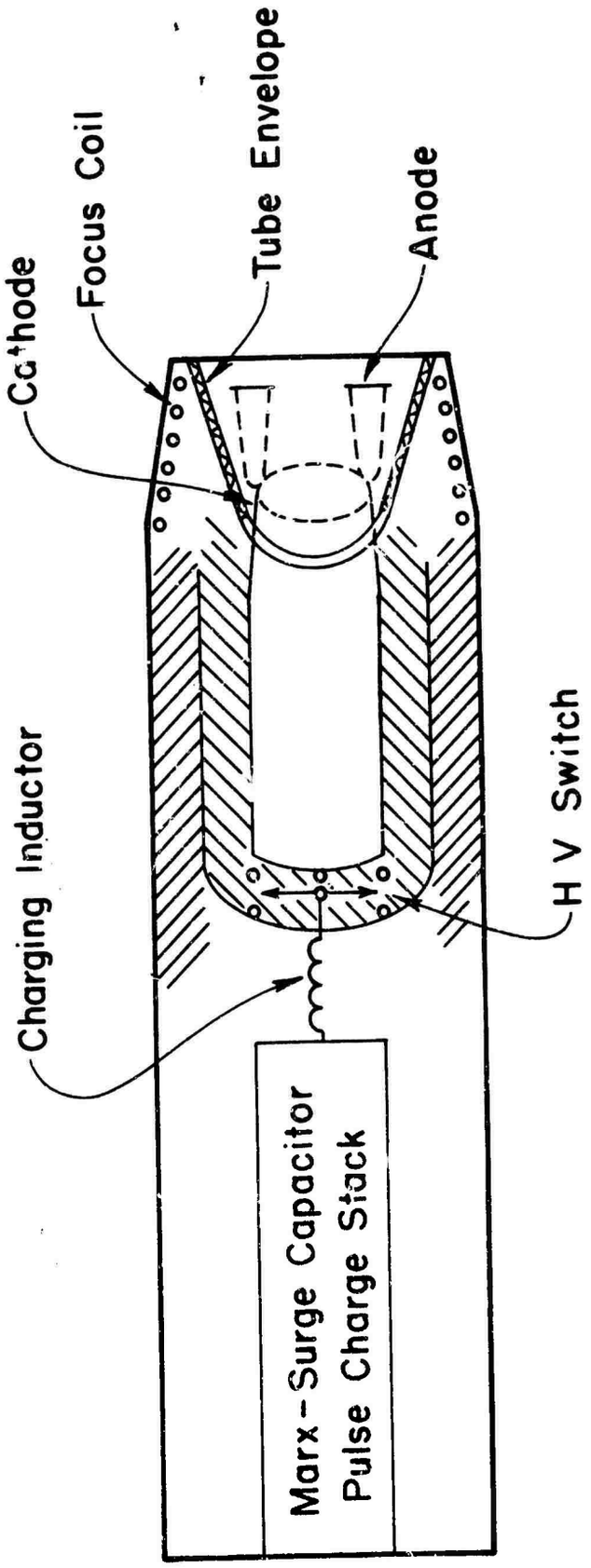

Figure 23 Schematic Cross Section of a Flash X-ray System Showing a Method of Connecting a Hollow Beam Tube to a Blumlein Generator.

desired. Consider for an example a 6-Mv, 20-ohm, 30-ns system; the electron beam energy to be dissipated in the target is 5.4×10^4 joules/pulse. Assuming for the moment a solid beam of 8 inches diameter, the target area is seen to be about 324 cm^2. For the relatively large electron penetration, very high peak powers and very short pulse length of present interest, the target heating is adiabatic and governed by the volume of tungsten or other target material in which the electron beam energy is expended (i.e., thermal conduction and radiation remove during the pulse only a negligible fraction of the electron beam energy). The electron range is therefore an important tube design parameter. Examining Figure 24 it is seen that the maximum electron range at 6 Mv is about 1 mm. Based on the range data of Figure 24 and on the profile of beam energy loss versus depth in the target, one can derive (e.g., the nomograph of Figure 25) as a function of voltage, the maximum beam energy density $W_{max/A}$(joules/cm^2) which can be deposited in an arbitrarily short pulse in a tungsten target initially at room temperature and not allowed to exceed a given temperature (e.g., $T_{max} = 2300^{\circ}C$) low enough to keep target evaporation at a minimum. Thus, assuming $V_o = 6$ Mv and a solid electron beam 8 inches in diameter and with uniform current density, an energy per pulse of over 1.1×10^5 joules could be absorbed instantaneously by the target without resulting in significant target erosion. Since this is twice the energy per pulse of this assumed system, such a tube would probably be relatively free from excessive target erosion provided fairly uniform current density can be obtained at the target. The same target loading can be also obtained with hollow-beam tube geometry, for the same voltage conditions, if the inner and outer beam diameters at the target are 6 and 10 inches respectively.

Thus, one is led to the important conclusion that at the relatively large beam diameters which are suggested by impedance matching and voltage hold-off considerations, the specific energy loading can be made sufficiently low that multiple-pulse operation would not be precluded by target erosion. Hence, serious consideration should be given to multiple-shot operation in view of its inherent advantages in terms of operating rate

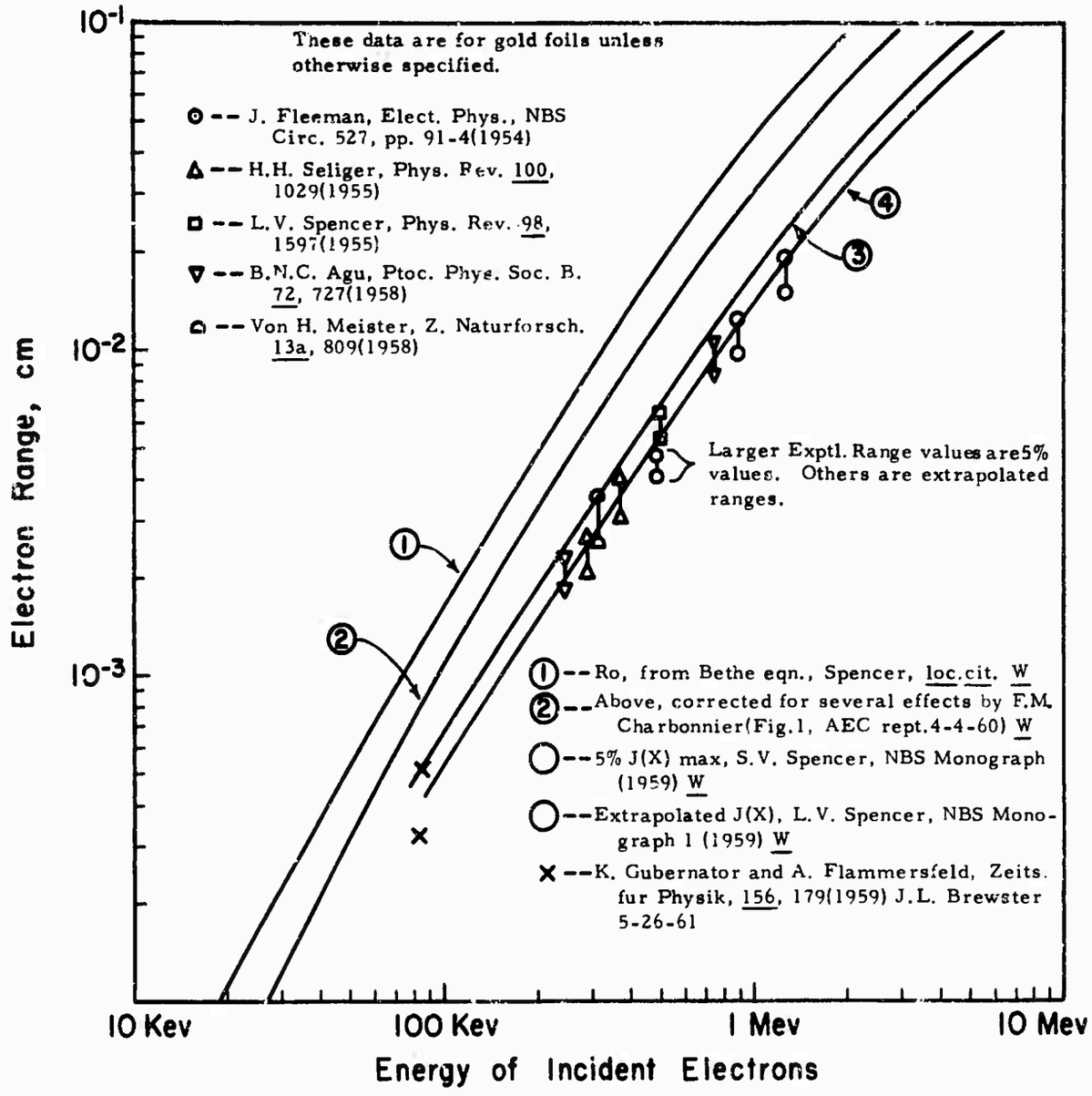

Figure 24 Electron Range in X-Ray Tube Target as a Function of Beam Voltage.

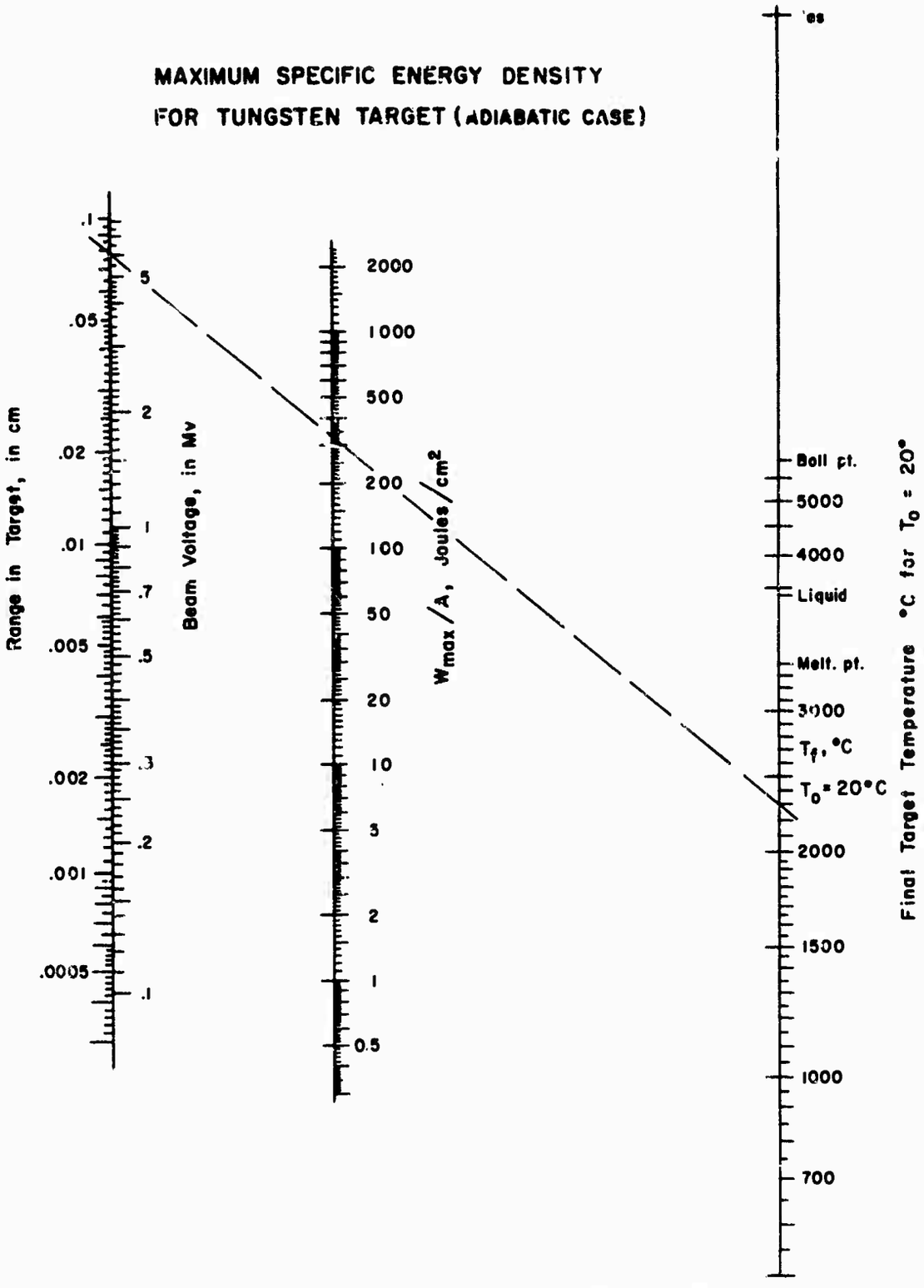

Figure 25 Nomagraph Relating Beam Voltage, Current Density and Peak Target Temperature for a Tungsten Target.

and cost per shot.

Remaining tube design factors include the tube envelope, cathode configuration and cathode-to-target spacing. Reasonably good first approximations may be obtained by extrapolation from present tube designs, and subsequently refined through analysis of direct experimental system tests. Tube insulating envelope problems requiring special study include sealing and expansion matching (in view of the large tube diameter) and the desirability of contouring and potential grading.

It is proposed that a strong magnetic field be employed for tube focusing, similar to the approach used successfully in a 2-Mv system recently delivered to the AEC. The magnetic field not only confines the primary electrons, but also reduces tube deterioration due to back-scattered electrons and ions which are produced at a high rate during the pulse.

11.b X-Ray Output Characteristics and Source Geometry

A limited amount of data has been published with respect to the X-ray performance characteristics of megavolt machines such as Van deGraaff and Linear accelerators. Figure 26 shows the X-ray dose yield for tungsten or gold targets as a function of voltage in the forward direction, or that of maximum intensity. The X-ray yield is normally specified in terms of roentgens per minute per milliampere at a distance of one meter from the target; however, for convenience in high power pulsed applications such as the present this has been renormalized to give roentgens per joule at a distance of one meter from the target. This figure may be applied to a point source cathode by multiplying by the tube pulse energy in joules to obtain the dose per pulse at one meter, then dividing by the pulse width to obtain the dose rate at this distance. The difference between the upper and lower sets of curves in Figure 26 appears to be primarily a result of dose reduction in the latter case due to use over a range of voltages of targets having a fixed thickness thus resulting, at lower voltages, in unnecessarily high target absorption of the emitted X rays. Data taken at Field Emission Corporation under Sandia Corporation (Ref. 15) support in

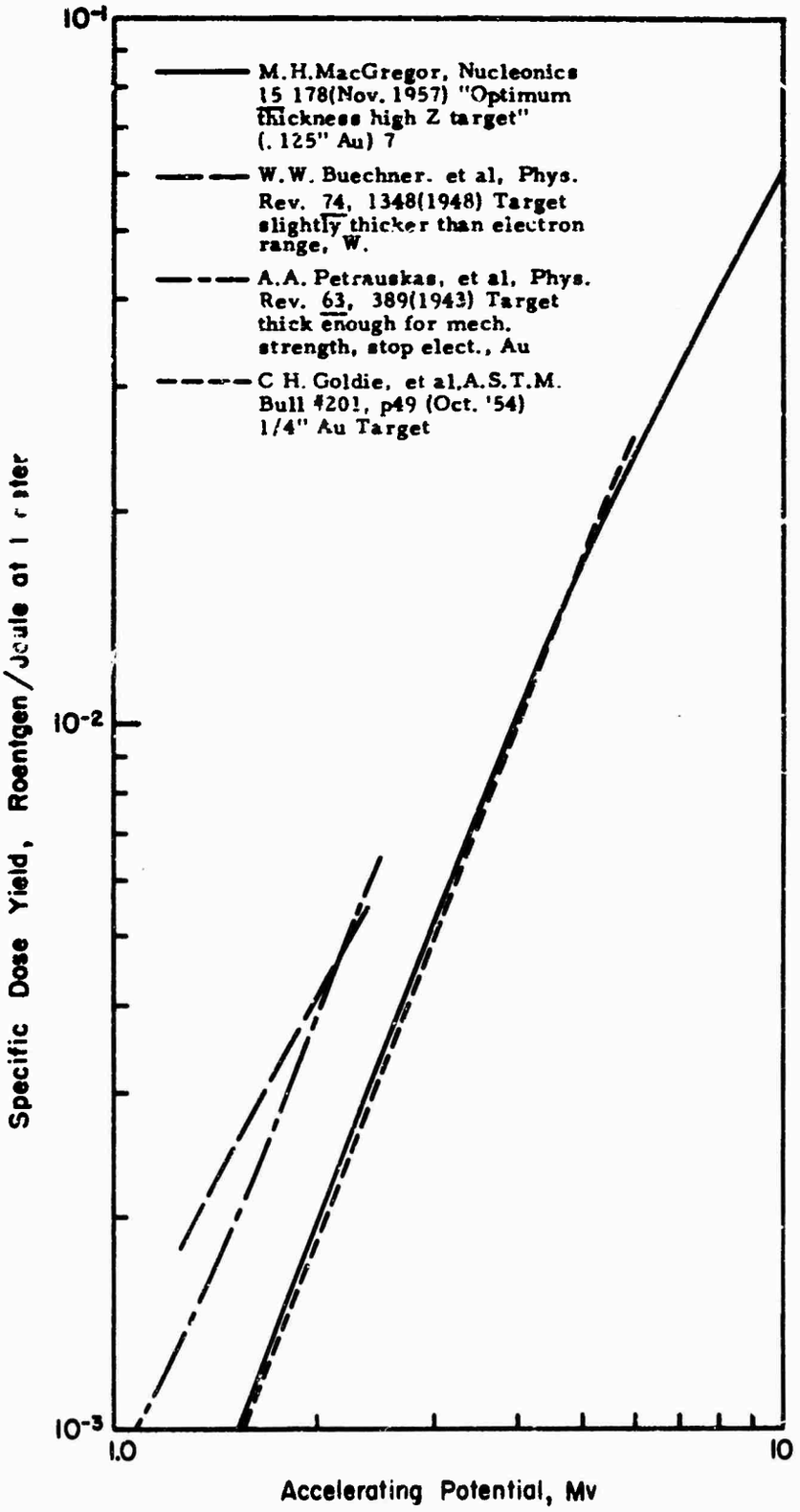

Figure 26 Specific X-Ray Yield for a Tungsten Target as a Function of Voltage.

general fall between the two sets of curves, approaching the upper limit with optimum-thickness targets and gas-free tube operation.

The X-ray spatial distribution at very high voltages is shown by the upper and lower curves of Figure 27 corresponding to thick and thin X-ray targets respectively. It is seen that in general the 22 million volt data, taken with a platinum target, follow this distribution. Data in the vicinity of 2 million volts, obtained with Van deGraaff accelerators, have been plotted employing the same normalized product of voltage and angle which is believed to be universal at higher voltages. The spatial distribution is affected by the nature and thickness of the target and by the amount of subsequent filtration of the emitted X rays. The dotted line drawn in Figure 27 has been employed for the following calculations, assuming that it is also valid at 6 million volts and with the type of magnetic focusing employed.

An estimate of the X-ray dose rate distribution for the 6 million volt 20-ohm system discussed above has been calculated, using a (pessimistic) specific dose yield value of 2.4×10^{-2} roentgen per joule at one meter, from Figure 26, and the dashed line for X-ray spatial distribution in Figure 27, as well as the familiar inverse square distance law of geometrical attenuation of the X-ray beam intensity. Two cases were assumed: a) an ideal point source target, and b) an ideal cylindrical line source target having a diameter of 8 inches. Calculations were performed to give the distribution in "subject planes" normal to the tube axis and at specified distances from the target, with the results being shown for the two cases in Figure 28.

It is seen that for a given distance between target and object plane the highest peak dose rates are obtained with a point source, being about 10^{12} roentgens per second in the forward direction and 8 inches away from the target, but the radiation is sharply peaked and is uniform to within 20 percent over a diameter of only 1.6 inches. A comparison of the two X-ray source geometries (point and ring) under equal dose rate conditions is obtained by observing the point source cathode at 16-inch spacing

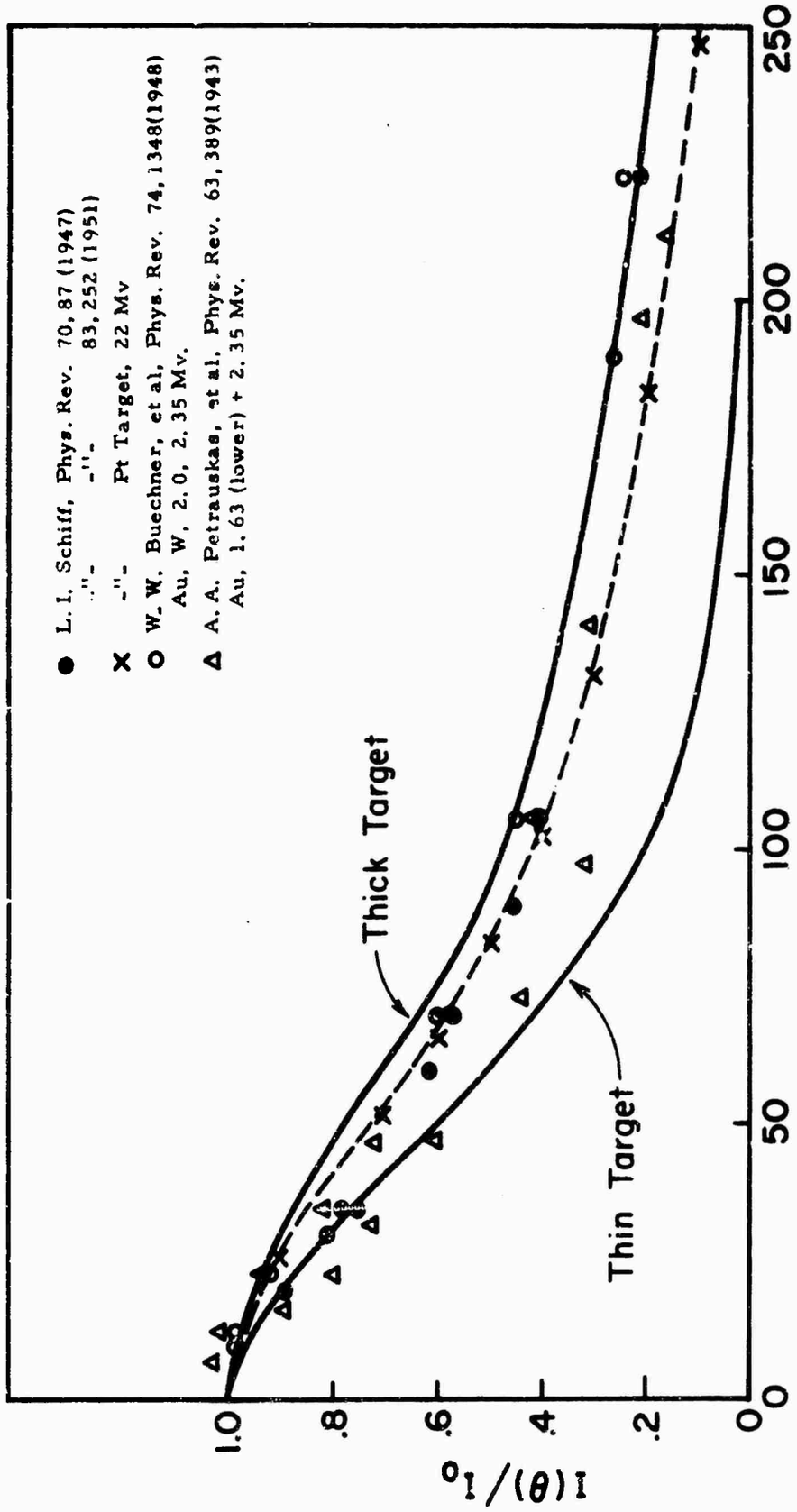

Figure 27 X-Ray Spatial Intensity Distribution in the Megavolt Region.

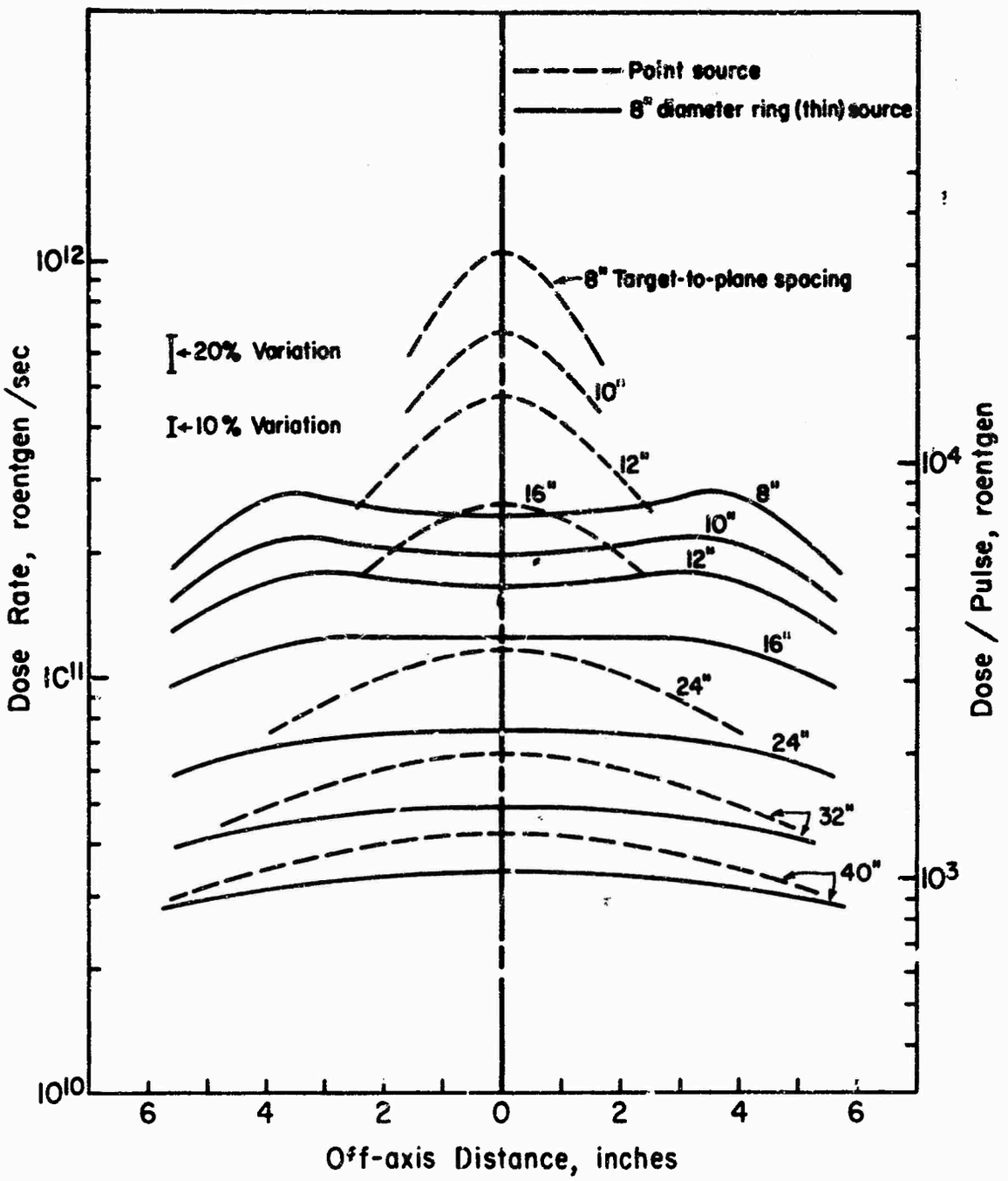

Figure 28 Estimated X-Ray Dose Rate Distribution in Plane Normal to Tube Axis.

compared with the ring source cathode at 8-inch spacing; the point source cathode is uniform to within 20 percent for a diameter of about 3.2 inches while the ring source target gives the same dose rate and uniformity over a diameter of about 10 inches. The dose rate in both cases is about 2.5×10^{11} roentgens per second and the dose per pulse, 7500 roentgens. The physical reason for the apparent increase in coverage is the utilization of most of the X-ray yield from the "tail" from one side of the ring target, while this is not possible with a point source target. At distances of the order of ten times the ring radius (i.e., 40 inches) it is seen that the improvement in uniformity is still substantial although not as striking as at the higher dose rate levels.

The ring source curves in Figure 28 can be used to estimate the dose rate where larger areas are to be illuminated with a source having a larger ring diameter. For example, doubling the diameter of coverage would give four times the area and consequently one-fourth the dose rate, but with the same distribution profile. It would appear practical to construct several tubes with different beam diameters, but capable of being installed in the same pulser, thus giving a fair degree of versatility for different studies.

The main conclusion which can be drawn from the comparison of "point" and "ring" X-ray source presented in Figure 28 is that, at high voltage where the X-ray beam produced by each target point is sharply collimated in the forward direction, the ring source is far superior to the point source (in terms of rate per watt of electrical power) when a high and uniform dose rate is required over a specified area. Assuming for instance a requirement that the dose be uniform within $\pm$ 10 percent over a circular area 9 inches in diameter, Figure 25 shows that the distance d between X-ray source and object plane can be reduced to 8 inches, resulting in a dose rate of 2.5×10^{11} roentgens per second for the case of an 8-inch diameter ring source; the same requirement for a point source forces a distance d greater than 40 inches and reduces the dose rate approximately an order of magnitude (for a given electron energy). Departures in practice

from the idealized model of Figure 28 (e.g., the need for enough X-ray source to handle beam power dissipation or the existence of a spread in the directions of the electrons striking the target) would reduce somewhat the difference between "solid" and "ring-shaped" X-ray sources but would not alter the general conclusion that hollow electron beams and ring-shaped X-ray sources have very significant overall advantages for the applications of present interest.

11.c Optimum Load Impedance

Assuming a pulse generator of given characteristics (open circuit voltage V_{oc}, characteristic impedance Z_o and pulse length $2\tau_o$), one can to some extent control the actual output into a load by varying the load impedance R_L. In view of the steep increase of X-ray yield with voltage, it would at first glance seem advantageous to increase the load impedance above Z_o. The purpose of this subsection is to give the necessary background relations and to evaluate the desirability of mismatching the load.

General Expressions:

Let V_m, I_m and P_m be the output voltage, current and power for a matched load, i.e., $a = R_L/Z_o = 1$. In the case of a mismatch, the output consists of a series of steps of duration $2\tau_0$, and the subscript j is used to denote output during the j^{th} step corresponding to $(j-1)2\tau_o < t < j\,2\tau_o$. Attention is focused here on the case of high impedance mismatch ($a > 1$) which is the only one of interest from the standpoint of maximized radiation output. It is further assumed that the X-ray dose rate $\dot{x}$ is proportional to tube current and to the n^{th} power of the tube voltage, i.e., $\dot{x} \propto IV^n$ (the specific value of n depending on the type of radiation produced, the direction relative to the electron beam and the electron energy; e.g., n=3 for X rays in the forward direction). The following expressions are readily derived for the ideal case of a loss-less generator and tube-independent load impedance (P_{rf} is the power reflected to the pulser during the first step):

$$\frac{V_1}{V_m} = \frac{2a}{a+1} \tag{16}$$

$$\frac{I_1}{I_m} = \frac{2}{a+1} \tag{17}$$

$$\frac{P_1}{P_m} = \frac{4a}{(a+1)^2} \tag{18}$$

$$\frac{P_{rf}}{P_m} = \left(\frac{a-1}{a+1}\right)^2 \tag{19}$$

$$\frac{V_j}{V_1} = \frac{I_j}{I_1} = \sqrt{\frac{P_j}{P_1}} = \left(\frac{a-1}{a+1}\right)^j \tag{20}$$

$$\frac{\dot{x}_1}{\dot{x}_m} = \frac{2^{n+1}\, a^n}{(a+1)^{n+1}} \tag{21}$$

$$\frac{\dot{x}_j}{\dot{x}_1} = \left(\frac{a-1}{a+1}\right)^{j(n+1)} \tag{22}$$

Some of these expressions are shown graphically in Figure 29. For a given n, $\dot{x}_1$ goes through a maximum $\dot{x}_{1\,max}$ when a = n. The value of this maximum, relative to the dose rate for a matched load, is given by:

$$\frac{\dot{x}_1}{\dot{x}_m}_{max} = \frac{2^{n+1}\, n^n}{(n+1)^{n+1}} \tag{23}$$

Application to forward X ray with n = 3:

In the case of X rays taken in the forward direction (i.e., in the direction of incidence of the electrons in a parallel, high voltage beam),

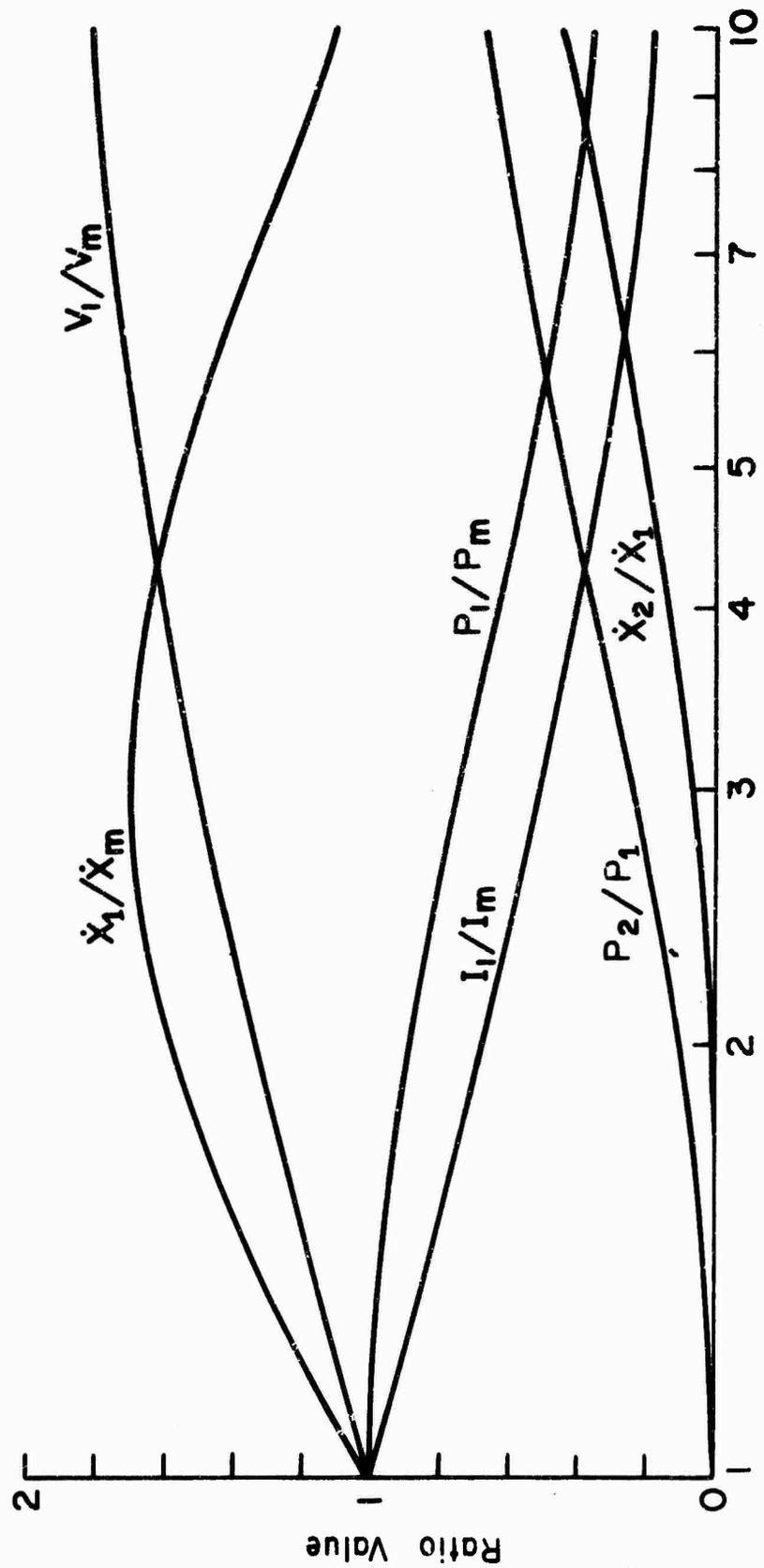

Figure 29 Dependence on Mismatch Factor "a" of the Relative Output Voltage, Current, Power and Dose Rate.

the dose rate $\dot{x}$ is approximately proportional to the cube of the voltage, according to the following expression:

$$\dot{x} \cong 650 \frac{I V^3}{d^2} \qquad (24)$$

where $\dot{x}$ is in r/sec, I in amperes, V in million volts, and d is the distance in meters between the X-ray source and the point where $\dot{x}$ is measured (with optimum target thickness and high vacuum, values as high as 1000 have been obtained for the numerical coefficient; hence, the expression just given for $\dot{x}$, while functionally correct, is rather conservative in terms of the maximum X-ray dose rate which can be achieved at given I, V, and d values).

The relative dose rates $\dot{x}_1/\dot{x}_m$ and $\dot{x}_2/\dot{x}_1$ are plotted in Figure 29 for the case of n = 3. Thus, from the standpoint of maximizing the X-ray dose rate in the forward direction, one should use a load impedance three times the matched load, thereby achieving a 70 percent increase in $\dot{x}$ over the matched case. Under these conditions the electrical characteristics for the first step are: $V_1 = 1.5V_m$ $I_1 = 0.51_m$ and $P_1 = 0.75\ P_m$; hence, the voltage is increased by 50 percent over the matched load voltage and 75 percent of the generator energy is transferred to the load during the first step. The $\dot{x}(t)$ profile then consists (ideally) of a series of steps of duration $2\tau_o$, the intensity during each step being only 6 percent of that in the previous step (and even less if there is significant filtration of the output). It is open to question whether a 70 percent increase in dose rate is sufficient compensation for the difficulties resulting from having to increase the tube voltage by 50 percent since, assuming a matched load and fixed generator impedance, the same 70 percent increase in dose rate could be achieved by means of a voltage increase of only 14 percent and without undesirable power reflection and stair-stepping of the output.

Effective Voltage Dependence of the X-Ray Dose Rate:

A strong additional argument against high impedance mismatch results from examination of the effective voltage dependence of the X-ray dose rate, when the radiation output requirements are

stated in terms of maximizing dose rate over a specified area (of diameter D) and within a specified maximum relative variation of dose $\sum$ over that area where $\sum$ is equal to

$$\sum = 2 \frac{\dot{x}_{max} - \dot{x}_m}{\dot{x}_{max} + \dot{x}_m} \qquad (25)$$

As the tube voltage is increased, the forward dose rate does increase proportionally to V^3 but the beam becomes more and more sharply collimated in the forward direction so that the maximum angular size $2\theta_{max} = D/d$ of the irradiated area, viewed from the X-ray source, must be reduced to maintain dose uniformity. Hence, for given D and $\sum$, the target to object distance d must be increased as V is increased, resulting in an increase of $\dot{x}$ with V which is much slower than V^3. The actual dependence of $\dot{x}$ on V, at fixed D and $\sum$, is very complex in the practical case of a distributed X-ray source and of a nonparallel electron beam with nonuniform current density. However, the effect of beam collimation can be illustrated by considering the simple idealized case of a point source of X rays and a parallel beam. At voltages above 2 Mv, theory and experiment indicate that the normalized spatial distribution $I(\theta)/I_o$ is a function of $V\theta$ only. Thus for a given permissible dose variation $\sum$, the product $V\theta$ must be held constant (at least at the voltages of present interest where beam collimation strongly predominates over the distance factor, equal to $\cos^2 \theta$ for a plane target, in creating dose variation across the area of interest). It follows readily that θ_{max} is inversely proportional to V and, at given D and $\sum$, the dose rate $\dot{x}$ which is proportional to V^3/d^2 increases only linearly with voltage. The approximate formula given below is convenient for the purpose of estimating the power required to generate a given dose rate $\dot{x}$ over given area of diameter D and with a given maximum relative variation $\sum$ of the dose rate over the area. The formula is obtained by noting that, for $I(0) \geq 0.7\ I_o$, the data $I(\theta)$ of Figure 27 are reasonably well represented by

$$I(\theta) \cong I_o (1 - 0.4\ V^2 \theta^2) \qquad (26)$$

where V is in Mv and θ in radians. Assuming $\dot{x}(\theta)/\dot{x}_o \cong I(\theta)/I_o$, which is true

above 4 Mv for a plane area, and making appropriate substitutions, finally yields:

$$\dot{x} \cong 6.5 10^{-4} \, d \, \frac{P \sum}{D^2} \qquad (27)$$

where $\dot{x}$ is the dose rate in r/sec, P = IV is the beam power in watts, D is the irradiated area diameter in meters, $\sum$ is the permissible relative dose variation across the irradiated area, and d is a numerical factor equal to 6 for the case considered (parallel electron beam, point X-ray source). In a more complex practical case, the relation just given would in first approximation still hold but with a different numerical value of d. It is also found that both the use of a distributed X-ray source (particularly the ring source discussed earlier) and a nonparallel electron beam (within limits) increase the value of d and are therefore desirable.

An important aspect of the foregoing formula is that it shows the dose rate (at given D and $\sum$) to be directly proportional to the electron beam power P. Hence, use of a mismatched load, which can only decrease the power delivered to the load during the first step of duration τ_o, is definitely undesirable.

12. Neutron Generation*

In the range of voltages of primary interest (i.e., below 10 Mv where the uranium γ, n reaction becomes more prolific), it appears that neutrons can be generated most efficiently by the photo disintegration reaction in beryllium, ie. e.:

$$h\nu + {}_4Be^9 \longrightarrow {}_4Be^8 + {}_0n^1 - Q \qquad (28)$$

*An applicable and somewhat more detailed discussion of pulse neutron generation is also given in AFWL TR 65-63 (Ref. 14).

While we have not yet made direct studies of neutron generation by this technique, the reaction is well known and the following data summarize published results, derived primarily from the Handbuch der Physik XXXIII-2, pp 141-145, and from the survey article "Using Accelerator Neutrons", Nucleonics Vol 18, pp 64-68, December 1960, by Burrill (HVE Co.) and McGregor (Ref. 16).

1) The threshold of the reaction (Q value) has been accurately measured and is:

$$Q = 1.664 \pm 0.003 \text{ Mev} \qquad (29)$$

2) The angular distribution of the emitted photoneutrons is not too far from isotropic, and is approximately given by:

$$\frac{\sigma(0)}{\sigma_o} = 1 + 0.6 \sin^2 \theta \qquad (30)$$

3) The photoneutrons emitted are fast neutrons exhibiting a broad continuous energy spectrum, peaked in the 1 to 2 Mev region. The spectrum is not a sensitive function of electron energy, except for a slight increase in the high energy tail of the spectrum (> 4 Mev) in the case of very high electron energies.

4) Whereas the yield of the reaction is a complex function of the γ ray energy, with several additional reactions coming into play at high energies ($h\nu > 17$ Mev), the total neutron output for the continuous γ ray spectrum produced by Bremsstrahlung smooths these effects and shows a regular and very rapid increase of neutron yield with generator output voltage. Figure 30 shows typical overall neutron yields, expressed in neutrons/sec per ampere of electron beam current, according to Burrill and McGregor (Ref. 16).

5) In view of Figure 30, the voltage dependence of the neutron yield in the 4 - 10 Mv range is fairly closely approximated by a V^3 law. Hence, as in the case of the forward X-ray dose rate, neutron output is maximized if the load impedance is three times the pulser characteristic impedance. While the collimation argument does not apply since neutron

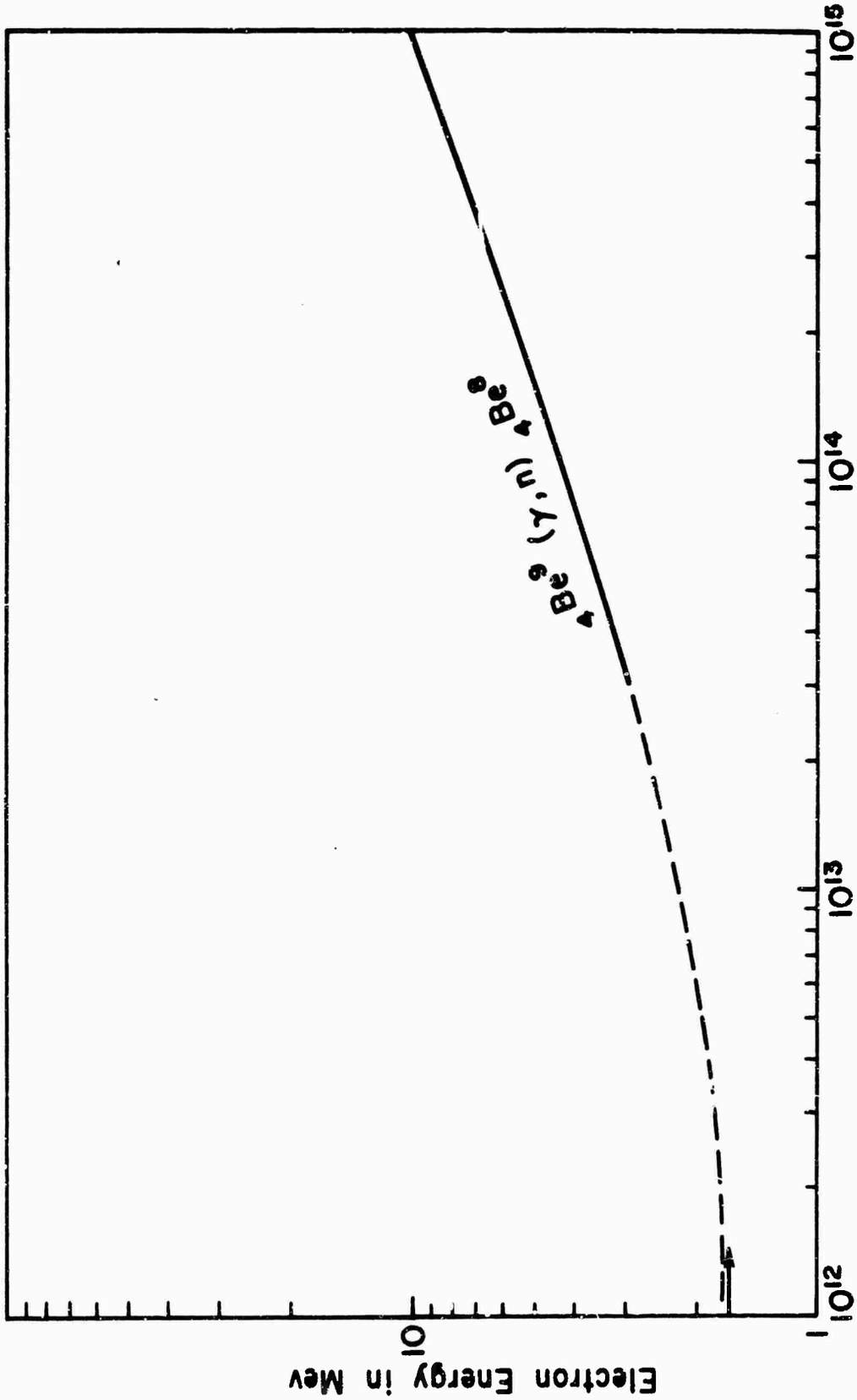

Figure 30 Dependence on Total Neutron Yield on Electron Energy. Curve Based on Linac Data.

spatial distribution is apparently fairly isotropic and insensitive to voltage, the other arguments against mismatching remain applicable.

At 6 Mv the peak neutron flux near the target is related to the electron beam current density by

$$N_{\text{neutrons/cm}^2\,\text{sec}} = 2.4 \times 10^{14} \; J_{\text{amp/cm}^2} \qquad (31)$$

Hence, with an electron beam current of 300,000 amperes and a beam cross section of the order of 350 cm^2, peak fast neutron fluxes well in excess of 10^{17} neutrons/cm^2 sec appear feasible. Even one meter away from the target, the average neutron flux during the pulse is approximately 2×10^{15} neutrons/cm^2 sec, and the total neutron output within a 20 nsec pulse exceeds 10^{12}.

SECTION III

EXPERIMENTAL STUDIES

1. Pulse-Charged Blumlein Generator

The general design and operating features of a Blumlein pulse generator were discussed previously, especially in Section II-4. Figure 23 shows schematically one possible configuration for an X-ray generator employing such a pulser.

As presently envisaged, the primary pulser would employ a Marx-surge pulser with an open circuit output voltage approximately equal to the system output voltage. This primary pulser would be coupled to a two-stage coaxial Blumlein storage unit through a suitable isolation charging inductor. A shorting switch across one of the Blumlein sections would be discharged immediately after the energy transfer from the charging pulser had reached its maximum value. Then the Blumlein circuit would deliver a short-duration high-voltage pulse to the load, such as a flash X-ray tube. Considerable attention has been devoted to the design parameters involved in the construction of such a pulser. This was followed by certain experimental studies as reported below.

Initial calculations performed to determine the energy and voltage transfer efficiencies with pulse charging and inductor coupling were indicated in Figure 18 above. Low-voltage model experiments were then conducted to compare with the theory of Section II-8, giving the experimental results shown in Figure 31. (The test circuit and component values are shown in the schematic Figure 31). The agreement with the theoretical curves of Figure 18 is quite good when the ratio of output to input capacity is not greatly different from unity; discrepancies are noted at extreme values, but are probably caused by instrumentation loading.

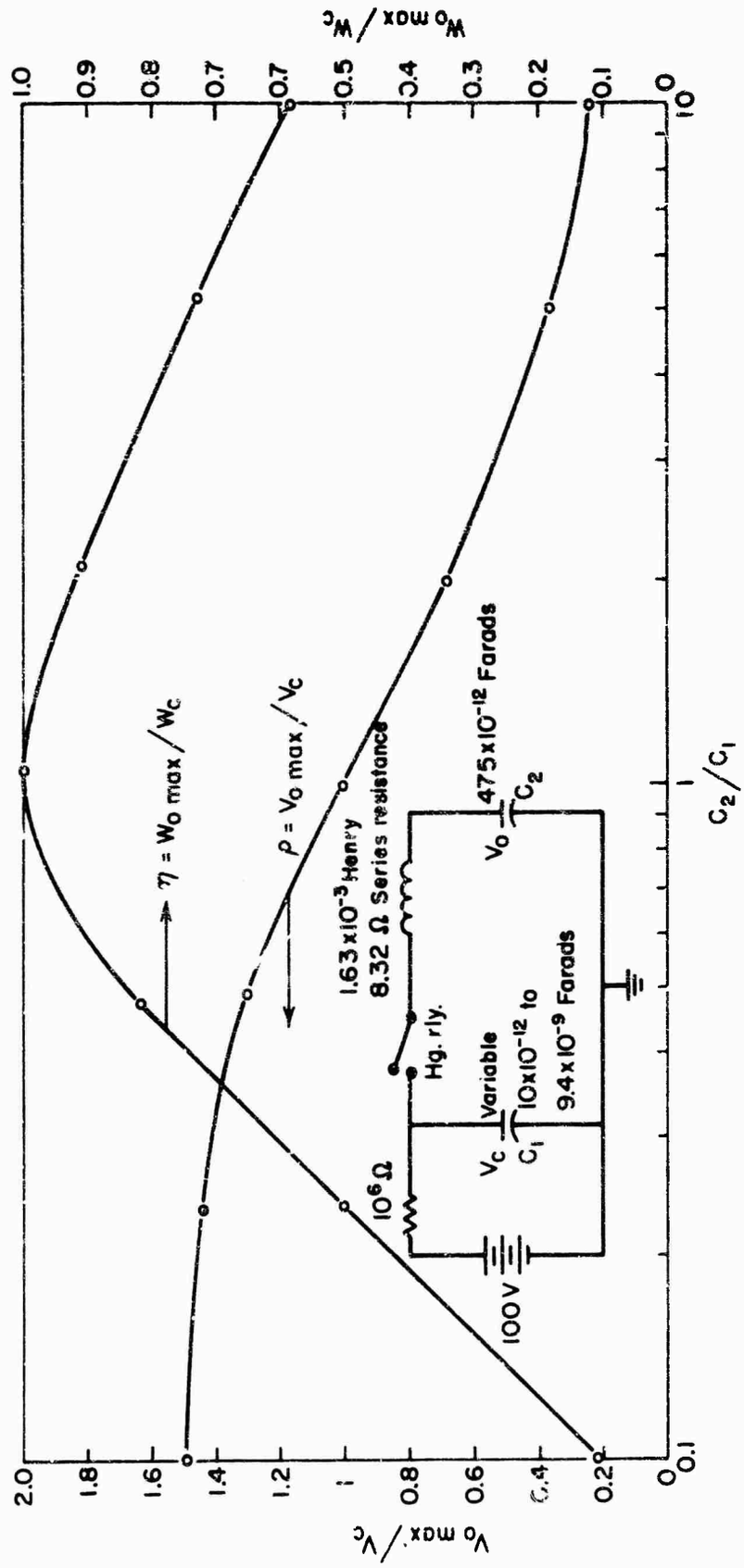

Figure 31 Experimentally Obtained Energy and Voltage Transfer Between a Charged Capacitor Inductively Charging a Second Capacitor. The Circuit Used Experimentally Including Component Values is also Shown.

Study of an equivalent circuit for the proposed Marx-surge primary pulser indicates that the very high feasible efficiency (fo C_2/C_1 close to 1) should not be affected by distributed inductance in the primary pulser arising from self-inductance of the capacitors, gap inductance, etc. To verify this assumption, a low-voltage model was constructed, according to the circuit of Figure 32A, and tested with the result that full efficiency of transfer to capacitor C_2 was indeed obtained despite sizeable distributed inductance.

These promising results suggested devising a model study system using an available 2-Mv. Marx-surge pulser as the primary charging pulser, together with an isolation inductor and Blumlein storage unit. (Fig. 32B).

The 2-Mv pulser had a relatively low effective output capacitance of about 80 picofarads. Hence, it was important to minimize the total capacity of the Blumlein to be charged; this total capacity being the sum of the capacities of the two Blumlein sections (which are charged in parallel although discharged in series).

A value of 50 ohms was selected as the highest practical output impedance, with two 25-ohm concentric coaxial line sections constructed in a concentric configuration as shown in Figure 33. The physical length of the Blumlein was selected to give an output pulse length of 5 nanoseconds, this value representing the minimum pulse length for which (because of end effects) the output voltage wave form could be expected to approach a rectangular shape. With this design, the Blumlein sections are 1.63 in length, with a total charging capacity of about 192 picofarads and a stored energy of about 96 joules at 1-Mv charging voltage.

Consideration of various dielectric materials (Section III-3) resulted in selection of transformer oil because of its relatively high breakdown strength, good healing ability, ease of handling, and low cost. Polyethylene was employed for the mechanical spacers because of its superior electric strength and the similarity of its dielectric constant to that of the transformer oil.

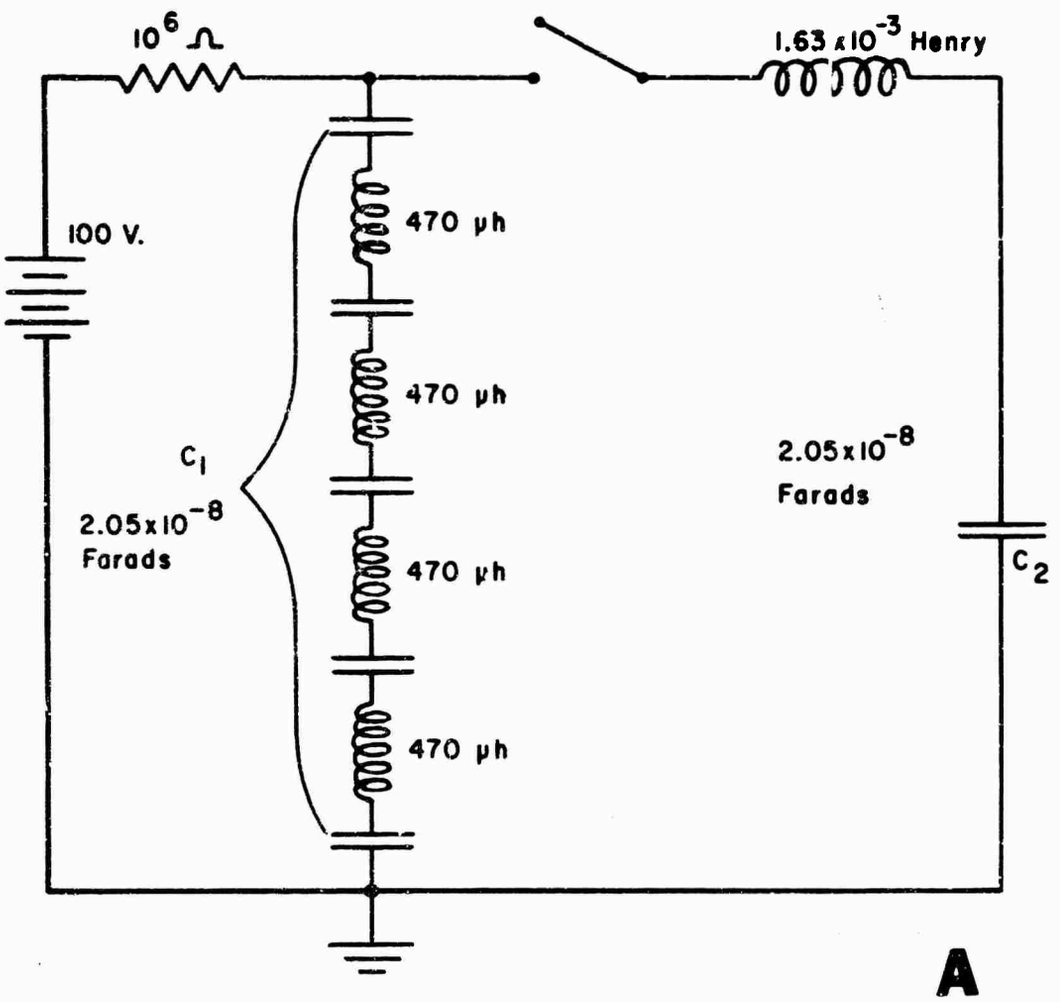

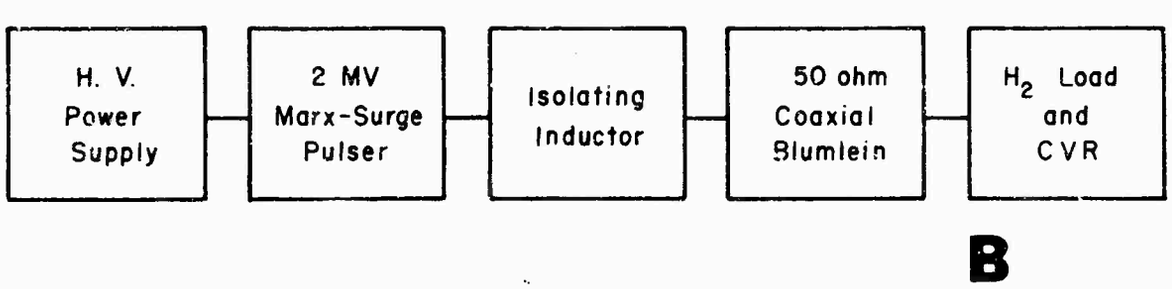

Figure 32 Circuit Used to Evaluate Experimentally the Effect of Distributed Parameters in the Primary Storage Unit.

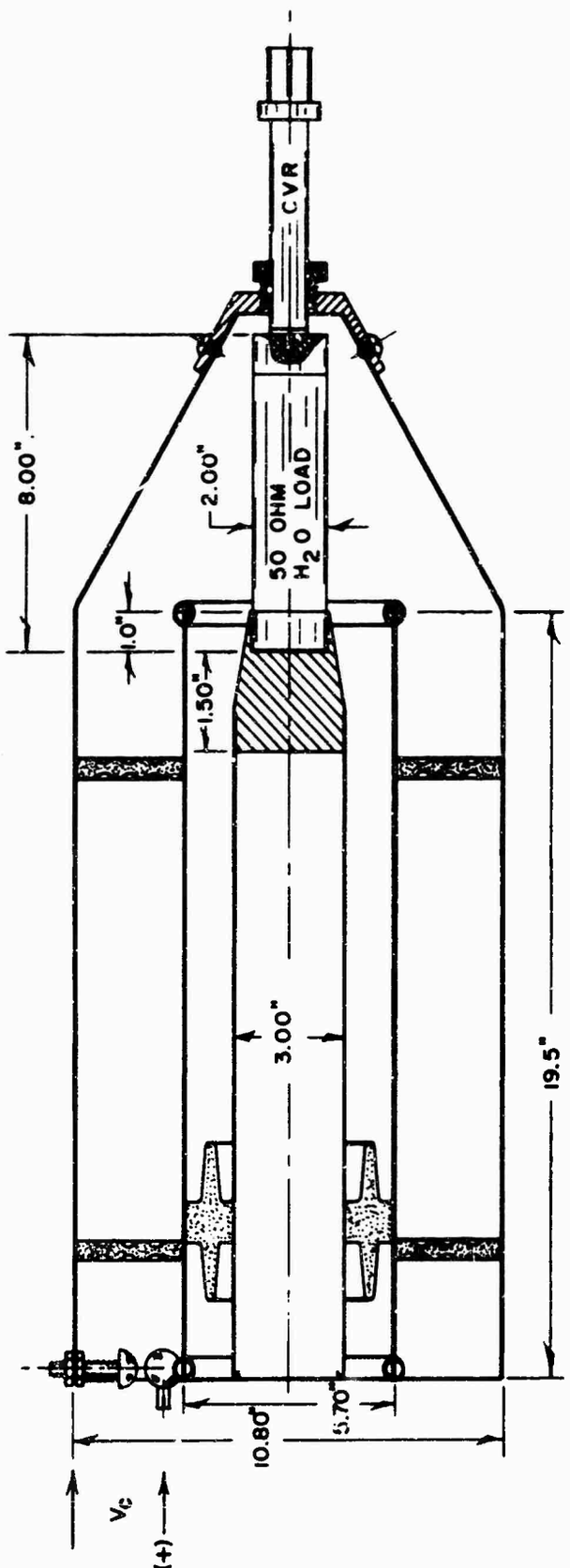

Figure 33 Sectioned View of 50 ohm 1 Mv Blumlein Including Water Load and Current Viewing Resistor.

A 50-ohm aqueous-solution load resistor ("water load resistor"), in series with current viewing resistor, formed the output load for the Blumlein. Switching was accomplished by over-volting a ball gap located across the outer coaxial line at the charging input end of the Blumlein. Figure 34 is a photograph of the assembled Blumlein, and Figure 35 shows the disassembled unit.

The 2-Mv Marx-surge pulser used as the Blumlein primary pulser employed 120 stages with each stage utilizing an artificial line made up of 5 ceramic capacitors having an individual capacity of about 2000 picofarads. The estimated pulser output capacity for this series-parallel configuration is $\frac{2000 \times 5}{120} = 83$ picofarads.

Adjustment of the charging voltage over the range from 10 to 30 kv would give an open circuit voltage varying from 1.2 to 3.6 Mv, reduced somewhat by stray capacity storages. From the known capacity ratio of 2.3, a voltage transfer ratio of about 0.6 and an energy transfer of about 88 percent were estimated from Figure 31. Any resistive loading of the pulser would of course reduce these values.

The use of artificial lines for energy storage in the Marx-surge primary pulser results in a voltage output having an approximately rectangular pulse shape of about 0.15 microsecond duration.

The value for the Blumlein charging inductor is ordinarly chosen to give a charging time sufficiently longer than the Blumlein output pulse time to avoid energy loss to the charging circuit after secondary switching. A discharge period of the order of 50 nsec, computed as the resonant period for the charging inductance and discharge capacitance (output capacitance of the primary pulser in series with the capacitance of one of the Blumlein lines --- the Blumlein gap shorts the other line), would thus ordinarily be employed. The primary pulser employed for this system, however, employed artificial line storage, with a pulse length of 120 nsec. A charging inductance of 500 microhenries was therefore selected to give a discharge period of about 1 microsecond long compared with the artificial line

Figure 34 Assembled Blumlein Showing the Input Gap to Corona Shield.

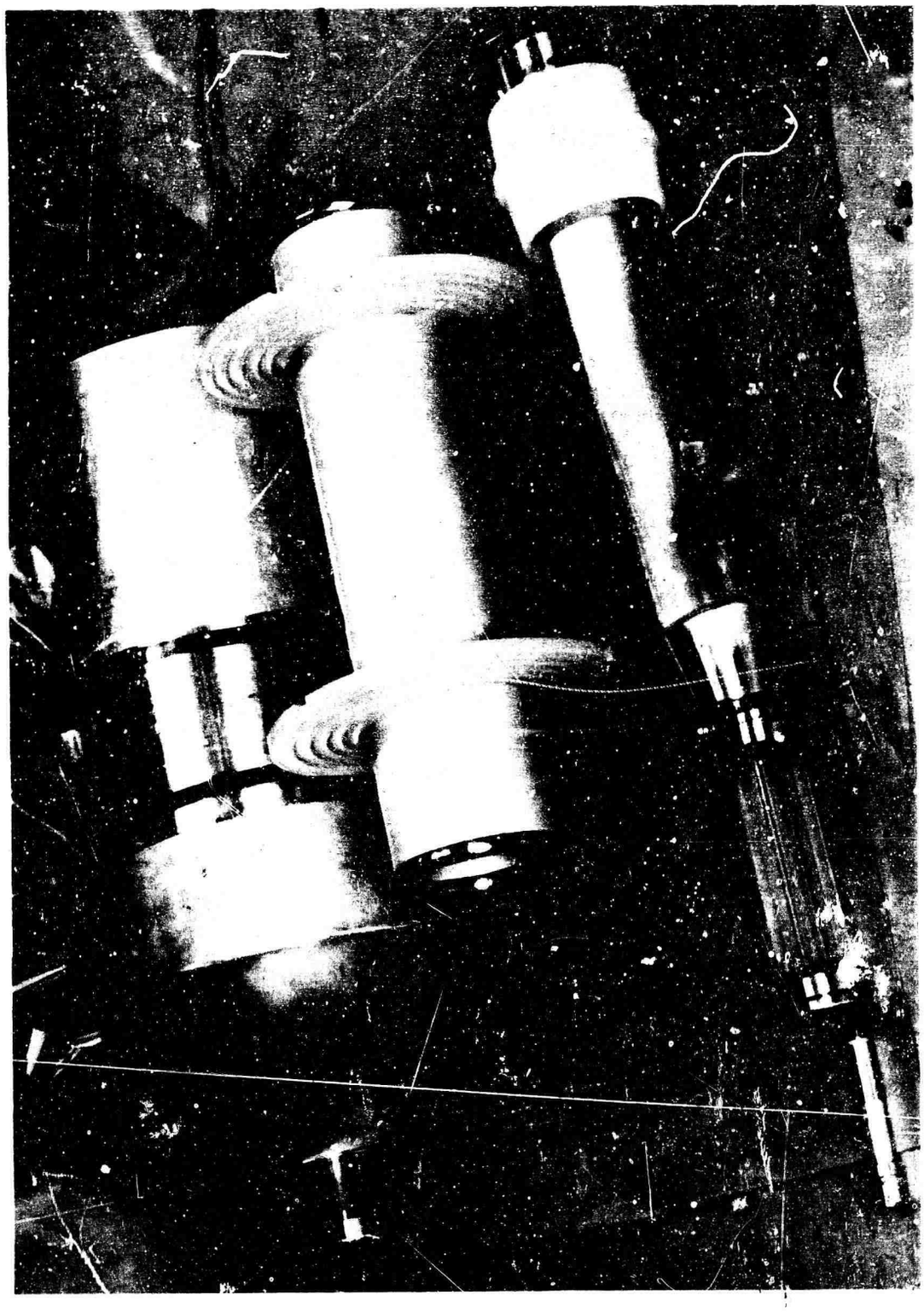

Figure 35 Blumlein Disassembled Showing all Components.

discharge period.

An inductance value of 500 microhenries was employed, using the following approximate design formula for a single layer solenoid:

$$L = N^2 \frac{r^2}{9r + 10\ell} \quad (32)$$

where N is the number of turns, ℓ the coil length and r the coil radius in inches. For the selected coil diameter of 12 inches and length of 24 inches, 64 turns are required.

Assuming the maximum applied voltage across the inductor to be twice the output of the primary pulser, the voltage between turns will be 31.2 kv (at 1-Mv charging voltage and assuming a linear gradient where N = 64).

Observing these design considerations, one-quarter inch diameter copper tubing was wound on a grooved lucite form with 2.65 turns per inch. The completed unit is shown in Figure 36.

Initial tests with the completed system resulted in certain modifications:

a) the current viewing resistor and water load mount were modified to reduce shunt capacity, with a substantial improvement in output rise time;

b) the polyethylene line spacers were redesigned with a longer voltage creep path to prevent voltage breakdown;

c) stricter grounding techniques, using low-inductance copper sheet between the primary pulser and the Blumlein, were employed to reduce "ringing" of the displayed oscilloscope traces; and

d) a 0.0127-ohm current viewing resistor which appeared to give poor signal-to-noise ratio was replaced with a 0.05-ohm current viewing resistor.

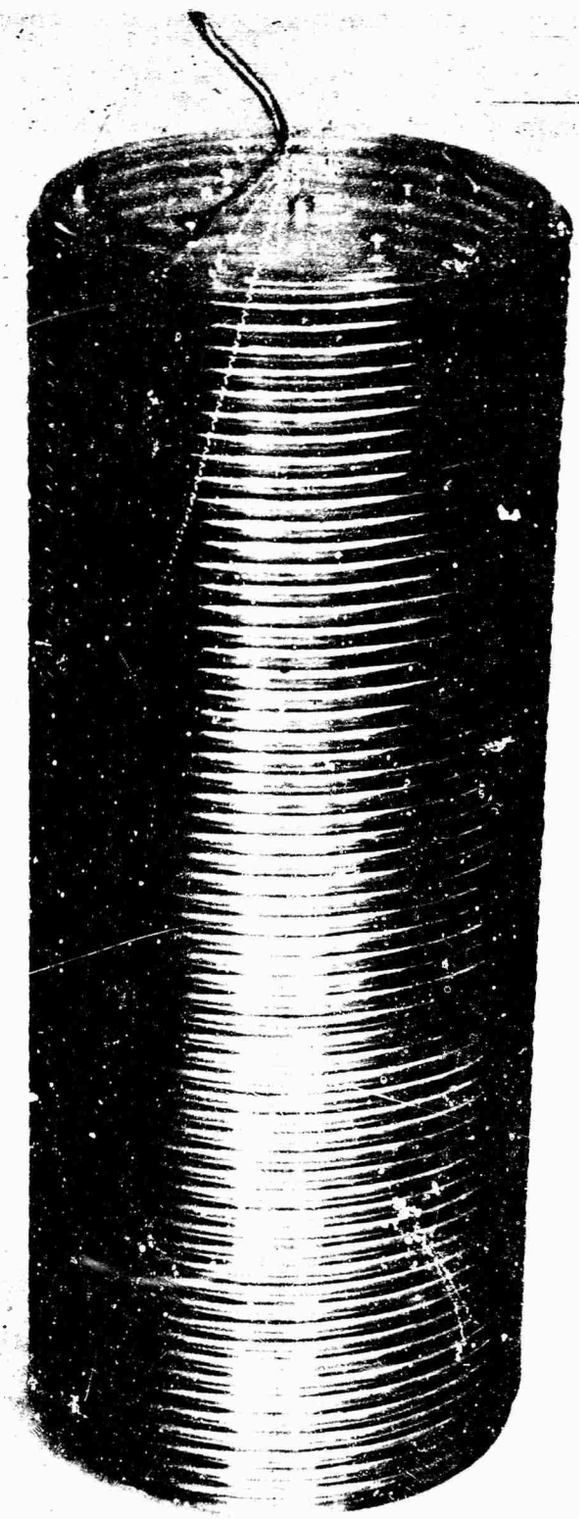

Figure 36 Blumlein Charging Inductor. The Inductor is 24 Inches Long, 12 Inches in Diameter and has 64 Turns.

These changes resulted in an output pulse which showed good agreement with calculations based on system design and measured pulse charging voltages. Figure 37 shows the Blumlein output pulse at voltage levels of 300 kv and 750 kv respectively. This output voltage was about 15 percent less than would be expected on the basis of measured voltage from the primary pulser and the capacity ratio, this discrepancy being attributed to early firing of the Blumlein switch ball gap (which was oil immersed and switched by over-volting). Data taken with breakdown of a solid (polyethylene) dielectric gap showed no significant change in output pulse shape.

Figure 38 shows the Blumlein output pulse wave forms when a dc source was employed to charge the line: a) with a 2.5-mil polyethylene switch gap and b) with a 5-mil polyethylene switch gap. The measured output pulse voltage shown in Figure 38 is in excellent agreement with the measured charging voltage of 22 kv. The improvement in pulse shape with respect to the high-voltage data of Figure 37 is attributed to two effects: a) a lower spark gap impedance because of smaller gap spacing and b) absence of electrical noise from the pulse charging circuitry.

Measurements were also made to study the effect of varying the charging inductor. For these tests a portion of the inductor was shorted out with a low-inductance copper strap, showing no resulting deterioration in pulse shape or amplitude.

The encouraging results of these model studies led to the design of a higher power system for use in tube design studies on another AFWL contract (Ref. 14). This later pulse design was used successfully in the test of several hollow beam, magnetically focused flash X-ray tubes.

The obvious advantages of this technical approach include high efficiency, simplicity and anticipated freedom from maintenance problems because of the self-healing switches used throughout the system.

2. Exponential Line Impedance Transformation

The possible advantages of using a tapered transmission line to achieve voltage step-up in the connection between a coaxial generator and load were noted in Section II-9, Figure 19 showing a sketch of such a device.

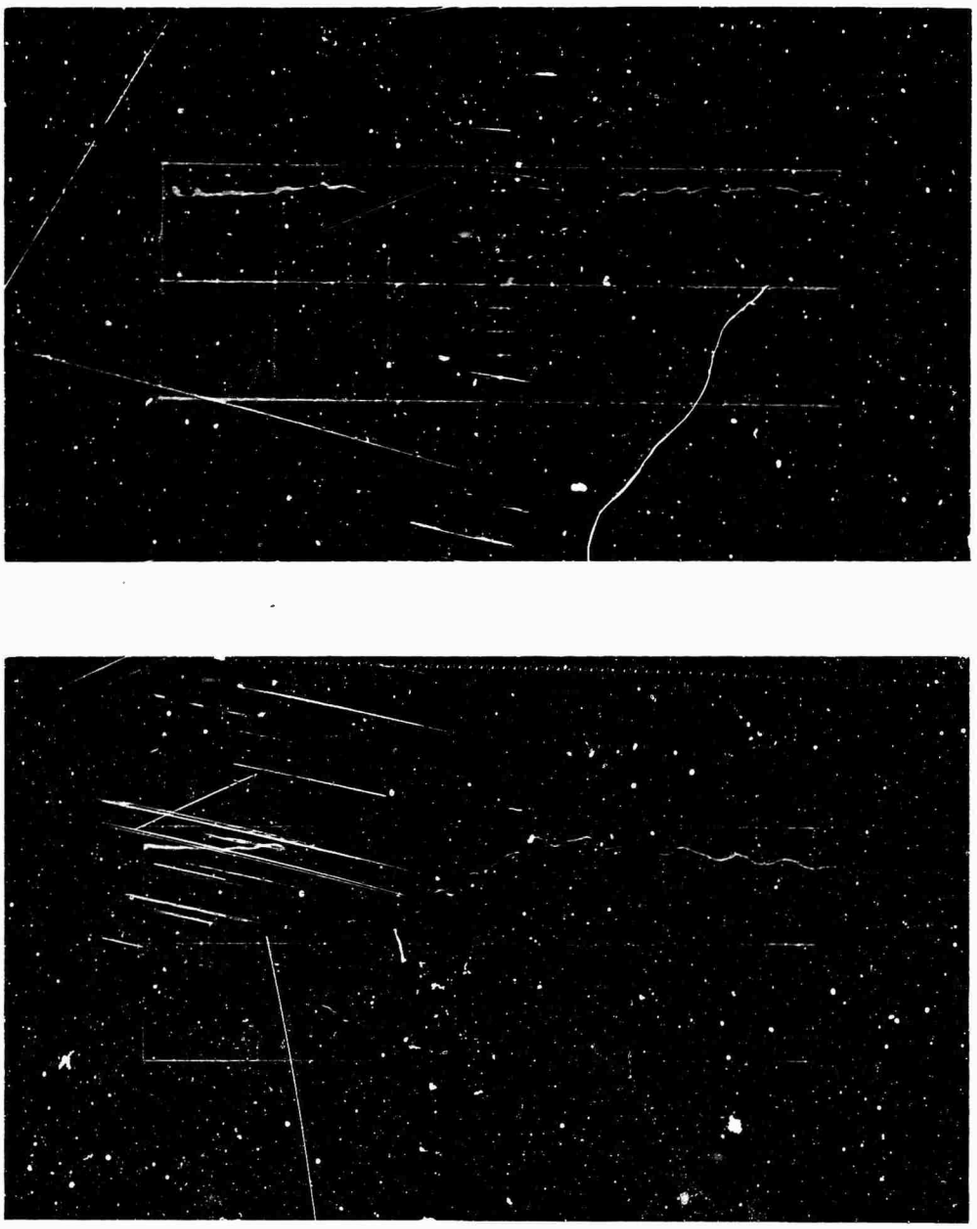

Figure 37 Blumlein Measured Output Pulse Using Primary Pulse Charging: Top 200 kv/cm; Bottom 500 kv/cm. Sweep Speed is 10 nsec/cm.

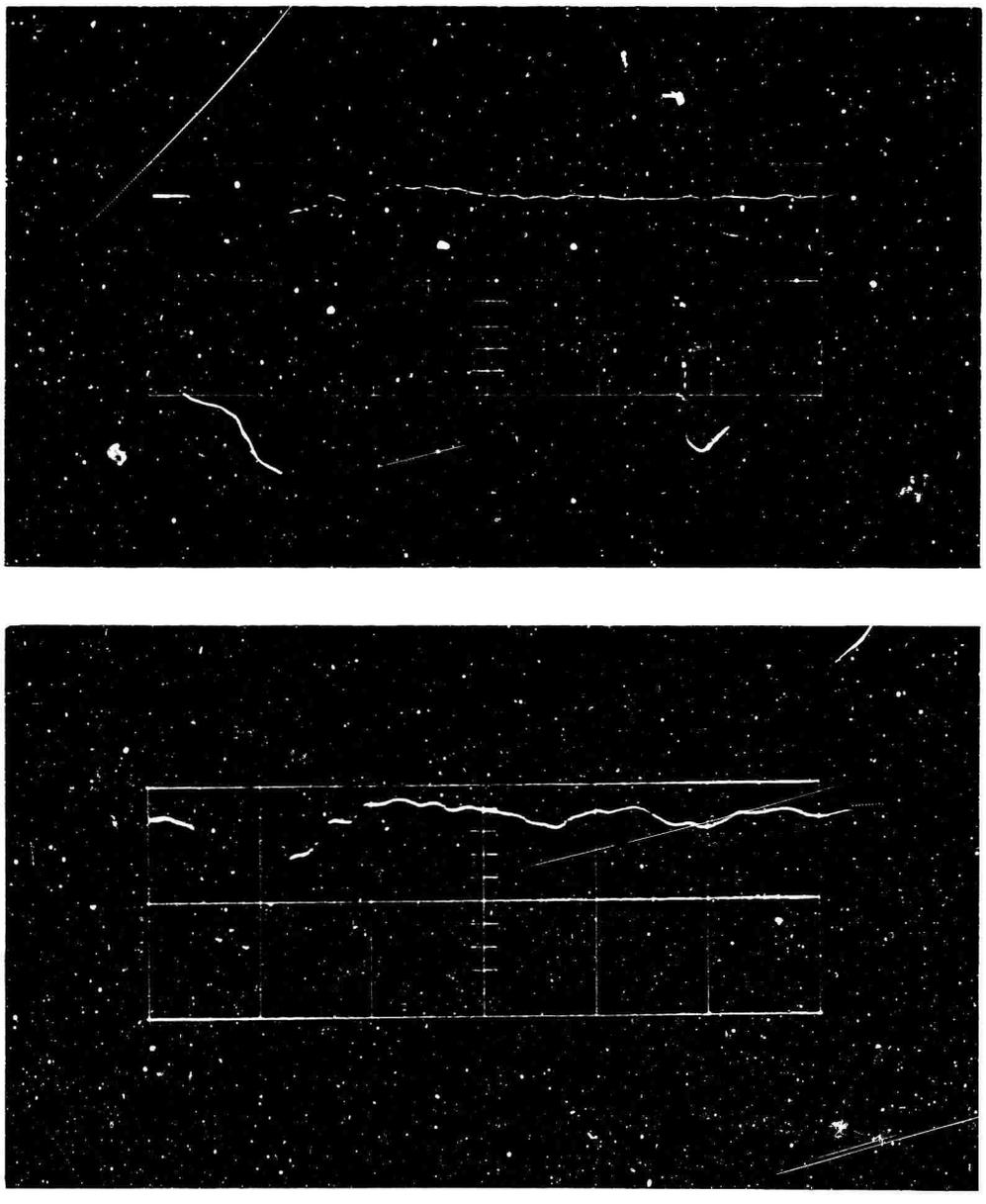

Figure 38 Blumlein Measured Output Pulse Using DC Charging. Output Amplitudes are 22 kv and Oscilloscope Sweep Speed is 10 nsec/cm. Top: 2-1/2 mils Polyethylene in Gap. Bottom: 5 mils Polyethylene in Gap.

An exponential line pulse transformer with a 5:20-ohm impedance step-up ratio was designed and fabricated to evaluate possible pulse wave shape transformation. This transformer employed water dielectric and had a physical length of 22 inches, corresponding to an electrical delay length of about 16.5 nanoseconds.

Rise time, voltage step-up and attenuation were measured with the following test arrangement. a Tektronix Model 110 pulse generator was coupled to the 5-ohm input, using a 50:5-ohm minimum loss impedance adaptor with low reflection G.R. type fittings. The 20-ohm transformer output was then connected to a Tektronix Model 519 oscilloscope with a 20:50-ohm low reflection adaptor and a Tektronix T50/N125 adaptor to match the 125-ohm oscilloscope input impedance.

With an input pulse rise time of less than 0.25 nanosecond and a pulse width of 10 nanoseconds, the output pulse rise time was 3.0 nanoseconds and no droop was observed. With a 20-nanosecond pulse, the rise time at the output was still about 3 nanoseconds and a droop of about 10 percent was observed. At 40 nanoseconds, the rise time was still the same with the droop increased to about 20 percent. Subsequent measurement of the input pad indicated that this degraded the rise time to 0.6 nanosecond while the output pad produced an increase of 2.0 nanoseconds; therefore, rise time degradation due to the line was probably less than 1.0 nanosecond.

The measured voltage step-up ratio was only 1.3:1, instead of the value of 2:1 expected on the basis of the impedance transformation ratio of 4:1. The discrepancy, which is much greater than could be accounted for by dielectric losses in water at the pertinent frequencies, is tentatively attributed to poor impedance matching and reflections at the two ends of the tapered line.

3. Dielectric Strength Studies

A knowledge of dielectric strength for solids, liquids and gases is important in the design of high-voltage pulse generators. The following tests were therefore performed with both dc and pulsed high voltages, some of the data reported here being obtained under the AFWL tube design program

(Ref. 14).

3.a Pulsed Voltage Tests

Tables II, III, and IV contain a tabulation of breakdown data on a variety of liquids and solids tested to date. In general, the entries represent single tests conducted to give engineering data on the dielectric properties of these materials under conditions similar to those which would be encountered in use. Therefore, the data do not reflect the intrinsic dielectric strength of these materials.

The pulsed voltage tests were performed with Marx-surge generators at pulse lengths ranging from 50 ns to 150 ns and at voltages from 150 kv to 2 Mv. One-inch diameter, stainless steel balls were used as electrodes in all cases.

The maximum field strength was found by applying the following approximate expression for the maximum field between spherical electrodes (Ref. 17), which holds at spacings not too small compared to the radius of the spheres:

$$E_{max} \cong \frac{0.9U}{d} \quad \frac{r + d/2}{r} \qquad (33)$$

where U is the gap voltage at breakdown, d is the electrode spacing and r is the radius of the electrodes.

3.b Dc Voltage Tests

Table IV is a tabulation of surface breakdown data on a variety of materials in several media; some of these data were obtained from pressurized gap tests described below.

These tests were performed with a 0-250 kv dc power supply, and the electrodes were 1-inch stainless steel or brass balls except as noted. The breakdown voltage was taken as the voltage at which arcing was continuous. In several cases intermittent arcing occurred at low voltages, probably a result of surface contamination. On the basis of these presently available data, polyethylene appears to be the solid dielectric most suitable for high-voltage storage purposes, particularly under dc

TABLE II

BREAKDOWN DATA TABULATION

IMPULSE BREAKDOWN						DC BREAKDOWN			D
MATERIAL	Spacing in Inches	Voltage in KV/inch	Maximum Field Strength (1) in KV/inch	Pulser	Pulse Length in ns	Spacing in Inches	Voltage in KV	Maximum Field Strength in KV/in.	Val
Polyethylene	0.50 (4)	1650	4,500	2 Mv	120	.060 (2)	250	4200	2.2
	0.50	1550	4,200	2 Mv	120	.020 (2)	115	5800	
						.050 (2)	100-160 (7) (8)	2000 - 3200	
						.075 (2) (3)	225 (9)	3000	
						.025 (2)	50 (8)	2000	
Mylar						.010 (2)	110	11000	3.
						.020 (2) (3)	210	11000	
						.030 (2)	250 (5)	8300	
						.060	250 (6)	4200	
Polypropolene						.031 (2)	150	4800	2.
Polycarbonate	.004	63	14,000	236	150				2.
Cellulose Acetate						.020 (2)	150	6300	3.2
Cellulose Acetate Butyrate						.020 (2)	140	7000	3.2
Nylon						.020 (2)	130	6500	3.4
Epoxy	.5	517 (10)	>1,000						4
Teflon	007	84	11,000	236	150	.031	105	3400	2.1
	.015	52.5	3,200	236	150				
	.030	80.5	2,500	236	150				
Acrylic	0.50 (4)	1100	3,000	2 Mv	120				2.2

FOOTNOTES:
1. See text for defining equation
2. Between 5" dia. flat Al. plate with edges radius to 1/8" in oil
3. Composed of .010" layers
4. Between 1" dia. balls in oil
5. After slow charge and 40 sec. at 250 KV
6. After slow charge and 1 hr at 250 KV
7. Charging rate: 10 KV steps each 10 minutes
8. Four tests
9. Charging rate: 25 KV steps each 30 minutes
10. Charging rate; 10 KV steps each 15 minutes
11. Did not break down
12. Machine Design Plastics Book 3H Sept. 20, 1962

TABLE II

BREAKDOWN DATA TABULATION

DIELE...		DC BREAKDOWN			DIELECTRIC CONSTANT ⑫		LOSS FACTOR ⑫		DIELECTRIC STRENGTH (Published)	
Value	Pulse Length in ns	Spacing in Inches	Voltage in KV	Maximum Field Strength in KV/in.	Value	Frequency in cps	Value	Frequency in cps	V/mil	Method
2.25-2.										
	120	.060 ②	250	4200	2.25-2.35	10^6	.0003	10^3	450-700	short time, 1/8"
	120	.020 ②	115	5800						
		.050 ②	100-160 ⑦ ⑧	2000 - 3200						
		.075 ②③	225 ⑤	3000						
3.0		.025 ②	50 ⑥	2000						
		.010 ②	110	11000	3.0	10^6	.016	10^6	7000	ASTM-D149, 1 mil.
		.020 ②③	210	11000					2000	ASTM-D149, 14 mil.
		.030 ②	250 ⑤	8300						
2.2		.060	250 ⑥	4200						
2.96		.031 ②	150	4800	2.2	10^6	.002	10^6	660	short time, 1/8" D-149
3.2 -7	150				2.96	10^6	.03	10^6	400	short time, 1/8" D-149
3.2 -6		.020 ②	150	6300	3.2 -7.0	10^6	.03-.33	10^6	250 - 365	short time, 1/8" D-149
3.4 -3.6		.020 ②	140	7000	3.2 -6.2	10^6	.03-.25	10^6	250 - 400	short time, 1/8"
4 - 5		.020 ②	130	6500	3.4 -3.6	10^6	.07-.14	10^6	385 - 470	short time,
2.1					4 - 5	10^6	.07-.10	10^6	330 - 550	short time, 1/8"
	150	.031	105	3400	2.1	10^6	.0006	10^6	1000 - 2100	short time, .010"
	150								400 - 500	short time, .080
2.2 -2.	150									
	120				2.2 -2.5	10^6	.07-.08	10^6	500 - 600	ASTM-D149, 1/8"
	1/8" in of	12. Machine Design Plastics Book 3H Sept. 20, 1962								

TABLE III

BREAKDOWN DATA TABULATION

IMPULSE BREAKDOWN (Exp.)						DC BREAKDOWN (Exp.)			DIELECTRIC	
MATERIAL	Spacing in Inches (1)	Voltage in KV	Maximum Field Strength in KV/inch	Pulser	Pulse Length in ns	Spacing in Inches	Voltage in KV	Maximum Field Strength in KV/in.	Value	Freq in
Freon TF	.063	275	4,200	Dagmar	150				2.44	6(
Carbon Tet.	.063	300	4,500	Dagmar	50	.97	25 - 30	150 - 160	2.44	1(
	.059	231	3,700	Dagmar	150					
	.075	300	3,800	Dagmar	50					
	.400	750-990	2400 - 3200	2 Mv	120					
Transformer Oil	.282	840	3,400	2 Mv	120	.250	140 - 150 (2)	630 - 680	2.2	1(
Castor Oil			4,000	2 Mv	120	.250	145 - 205	650 - 920	4.67	1(
Tap Water	.500	840	2,300	2 Mv	120				80	6
Tap Water with a small amt Photoflow	.500	900	2,400	2 Mv	120					
Polyglycol	.125	28(	2,300	Dagmar	50					
	.150	300	2,100	Dagmar	50					
FC-75 (3)	.40	1160	3,700	2 Mv	120	.063	57	970	1.87	10^6
	.063	200-300	3400 - 5600	Dagmar	150	.197	105	640 (4)(5)		
Dowclene EC	.40	1160	5,100	2 Mv	120	.025	6	220 (6)(7)	7.2	1(
	.14	230	1600	Dagmar	50	.050	20	380		
Chlorthene NU	.125	220	1800	Dagmar	50	.100	41	440		
Dioxane						.197	72	400		
						.591	100	240		

FOOTNOTES:
1. All tests were made with 1" dia. Stainless Steel balls.
2. Oil outgassed in vacuum chamber
3. FC-75 carbonized, oxidized the Stainless Steel balls.
4. Fluid was used, lower value may be due to this.
5. "Because of the very low dielectric constant of FC-75 in comparison to any contaminating particles, such particles tend to be drawn into the electrode gap causing an appreciable decrease in measured electric strength". This is pre- when forced circulation is present.
6. Quite a bit of scatter in this data. Average
7. Large DC currents were drawn during DC tests.

TABLE III

BREAKDOWN DATA TABULATION

DC BREAKDOWN (Exp.)			DIELECTRIC CONSTANT				DIELECTRIC STRENGTH (published)	
Spacing in Inches	Voltage in KV	Maximum Field Strength in KV/in.	Value	Frequency in cps			V/mil	Method
			2.44	60			320	ASTM-D149
.197	25 - 30	150 - 160	2.44	10^8			330	ASTM-D149
.250	140 - 150 ②	630 - 680	2.2	10^2			> 300	ASTM-D877
.250	145 - 205	650 - 920	4.67	10^6			350	ASTM-D877
			80	60				
.063	57	970	1.87	10^6			350 min.	ASTM-D877
.197	105	640 ④⑤						
.025	6	220 ⑤⑦	7.2	10^3			> 280	ASTM-D877
.050	20	380						
.100	41	440						
.197	72	400						
.591	100	240						
5. (cont'd) particles tend to be drawn into the electrode gap causing an appreciable decrease in measured electric strength". This is prevented when forced circulation is present.								
6. Quite a bit of scatter in this data. Average is given.								
7. Large DC currents were drawn during DC tests.								

2

TABLE IV

DC SURFACE (Creep) BREAKDOWN

DC SURFACE (Creep) BREAKDOWN

Surface Breakdown in Air		Surface Breakdown in Pressurized N_2						Surface Br
Material	Breakdown Voltage in KvDC	Material	Breakdown Voltage in KV DC ④					Materia
			25 psi	50 psi	100 psi	150 psi	200 psi	
4207 Epoxy ①	30	Nylon (convoluted) ⑤ ⑥	80	100	130	160 ⑦	180 ⑧	Polyethyle
4207 Epoxy w/Dow Corning High Vac Grease ①	24	Nylon (convoluted) ⑩ ⑥	120	150	175 ⑪		225 ⑫	Polyethyle
4207 Epoxy w/Dow Corning No. 3 ①	33	Nylon ⑬ ⑥	95	120	145 ⑪		200 ⑫	Polyethyle
4207 Epoxy (convoluted 5/32" deep) ①	29 ③	Polyethylene ⑬		160	210	240	250	Polyethyle
		Polyethylene w/DC #3 ⑬		240				
		Teflon ⑭	75	105	165	200	230 ⑮	

1.

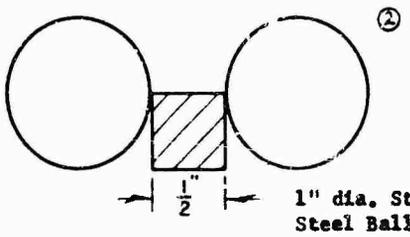

2. Balls alone breakdown at 37 KV DC.
3. Arcing jumped over top of convolutions.
4. Voltage at which continuous breakdown occurs.

5.

6. No marks on nylon after test.
7. Some arcing during charging.
8. Considerable arcing during charging.

10.

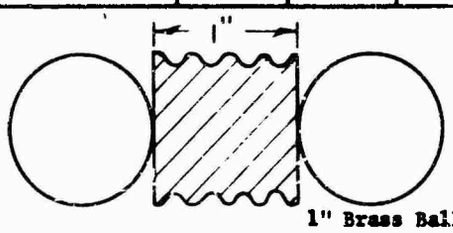

11. 90 psi
12. 180 psi

13.

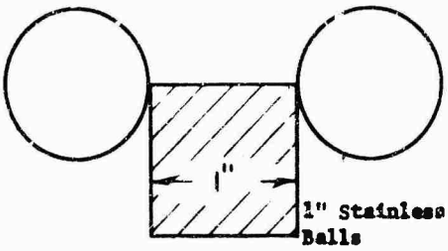

14.

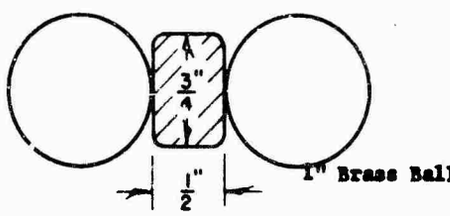

15. Very little arcing after sample was tested several times.

16.

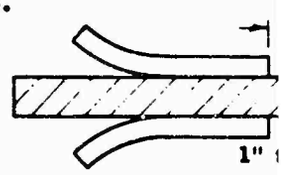

17. Sharp square corners
18. Round corners on copp
19. Burned deep grove in
20. In FC 75 (inserted f
21. In caster oil (insert
22. Breakdown occured aft 250 KV DC.
23. Veedol manufactured i

TABLE IV

DC SURFACE (Creep) BREAKDOWN

DC SURFACE (Creep) BREAKDOWN

Breakdown in Pressurized N_2					Surface Breakdown in Transformer Oil [23]		Surface Breakdown in FC-75 [24]	
Breakdown Voltage in KV DC [4]					Material	Breakdown [4] Voltage KV DC	Material	Breakdown [4] Voltage KV DC
25 psi	50 psi	100 psi	150 psi	200 psi				
80	100	130	160 [C]	180 [8]	Polyethylene [16] [17]	160	4207 Epoxy [26] [27]	150
120	150	175 [10]		225 [12]	Polyethylene [18] [19]	170 [15]	Teflon [28]	200
95	120	145 [11]		200 [12]	Polyethylene [18] [19]	240 [22]	Polyethlene	220
	160	210	240	250	Polyethylene [15] [19]	>250 [21] [22]		
	240							
75	105	165	200	230 [15]				

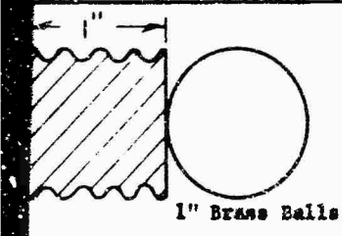

1" Brass Balls

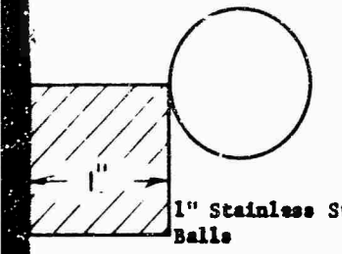

1" Stainless Steel Balls

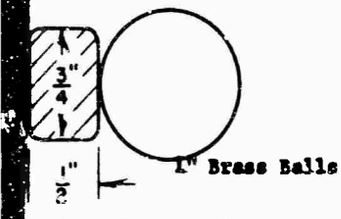

1" Brass Balls

arcing after sample was
al time.

16.

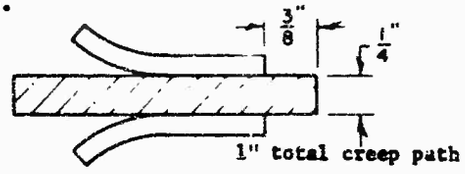

17. Sharp square corners on copper.
18. Round corners on copper.
19. Burned deep grove in polyethylene.
20. In FC 75 (inserted for reference).
21. In caster oil (inserted for reference).
22. Breakdown occured after 30 seconds at 250 KV DC.
23. Veedol manufactured by Tidewater.

24. Fluorochemical manufactured by 3M.

25.

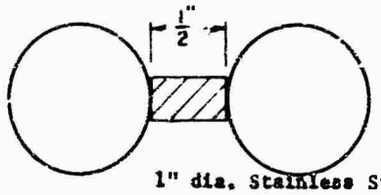

1" dia. Stainless Steel Balls

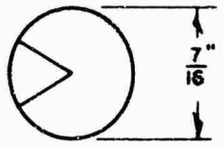

End view of test sample

26. Pitting and carbon path showed in grove after test.
27. Balls were dark with carbon.
28. Carbon holes penetrate volume. Markings on surface light.

2

conditions and with sizable edge field enhancement. While various reference books indicate the low-temperature optimum dielectric strength of pure polyethylene at about 18 million volts/inch, decreasing to 13 million volts/inch at 50°C and to less than 5 million volts/inch at 100°C, our data seem to indicate that the practical dielectric strength is probably much lower.

The present limited test data seem to indicate a maximum conservative breakdown strength of about 1 million volt/inch, or slightly greater under pulsed charging conditions. Some laminated mylar samples showed excellent breakdown strength but others were quite unsatisfactory. Mylar appears particularly susceptible to voltage creep and to corona damage.

Among the liquid dielectrics, transformer oil appears to have the most useful overall characteristics, particularly where both dc and pulsed voltage insulation is required and where switch breakdown requires self-healing. Fluorocarbon compounds have higher dielectric strength but are extremely costly and react with electrode materials on breakdown. Castor oil appears particularly attractive because of its high field strength and relatively high dielectric constant. However, use of castor oil for switch dielectric appears to pose serious problems because copious quantities of gas are released with each discharge and the highly viscous nature of the castor oil complicates gap clean up.

Among the dielectric materials with higher relative dielectric constants, distilled water and ethylene glycol appear quite attractive. Pulse breakdown tests conducted with the 2-Mv pulser indicated that the distilled water ($\epsilon_r = 78$) broke down with a repeatability of about 10 percent or better at about 2 million volt/inch, provided no bubbles were allowed to collect at the electrodes. Ethylene glycol ($\epsilon_r \cong 40$) broke down at 2.7 million volts/inch the first time, subsequently stabilizing at 2 million volts/inch. No long term deterioration was noted; however, the tests were limited.

A water-polyethylene interface was tested for creep breakdown since support of electrodes is a major engineering problem

when contemplating the use of liquid dielectric storage (if water and a low dielectric constant material such as polyethylene are laminated in a high voltage field, essentially all of the potential drop occurs on the low dielectric constant material). With 1/2-inch spacing between 1-inch-diameter balls in water, arcing occurred at the water-polyethylene interface at approximately 300 kv. Use of a wetting agent Kodak Photo Flow did not seem to give measurable improvement and gave sizable increases in observed pre-breakdown currents, presumably because of ion mobility.

3.c High Pressure Gas Breakdown Tests

The success of the UV trigger electrode gap discussed below stimulated a simple experimental investigation of the voltage breakdown characteristics of nitrogen and air under pressurized conditions, as well as some voltage creep studies important in trying to design gap chambers.

Figure 39 summarizes the results obtained for voltage breakdown at fairly high pressures and voltages. Stainless steel ball gaps were employed and, as indicated by other investigators, were found to be considerably more satisfactory than brass at higher pressures.

Of particular interest is the fact that nitrogen begins to show saturation effects above about 100 pounds/square inch while air is relatively free from this effect up to twice this pressure. In fact, at 200 pounds/square inch and at moderately high voltages, air is seen to have a dielectric strength in excess of 1 million volt/inch, which is of sufficient magnitude to be of interest in the case of field-reversal generator lines dc-charged in the 100 - 200 kv range. The somewhat lower dielectric strength of nitrogen, compared to air, as well as its erratic behavior may be a result of gap roughening, which in the case of air dielectric is minimized by oxidation of the projections. Surface voltage creep breakdown for four conditions is indicated in Figure 40, nylon being the dielectric material. It is apparent that increasing the surface distance (e.g., by machining threads) does result in an increase in voltage stand-off which is significant but not directly proportional to path length. Observing Figure 41, it is seen

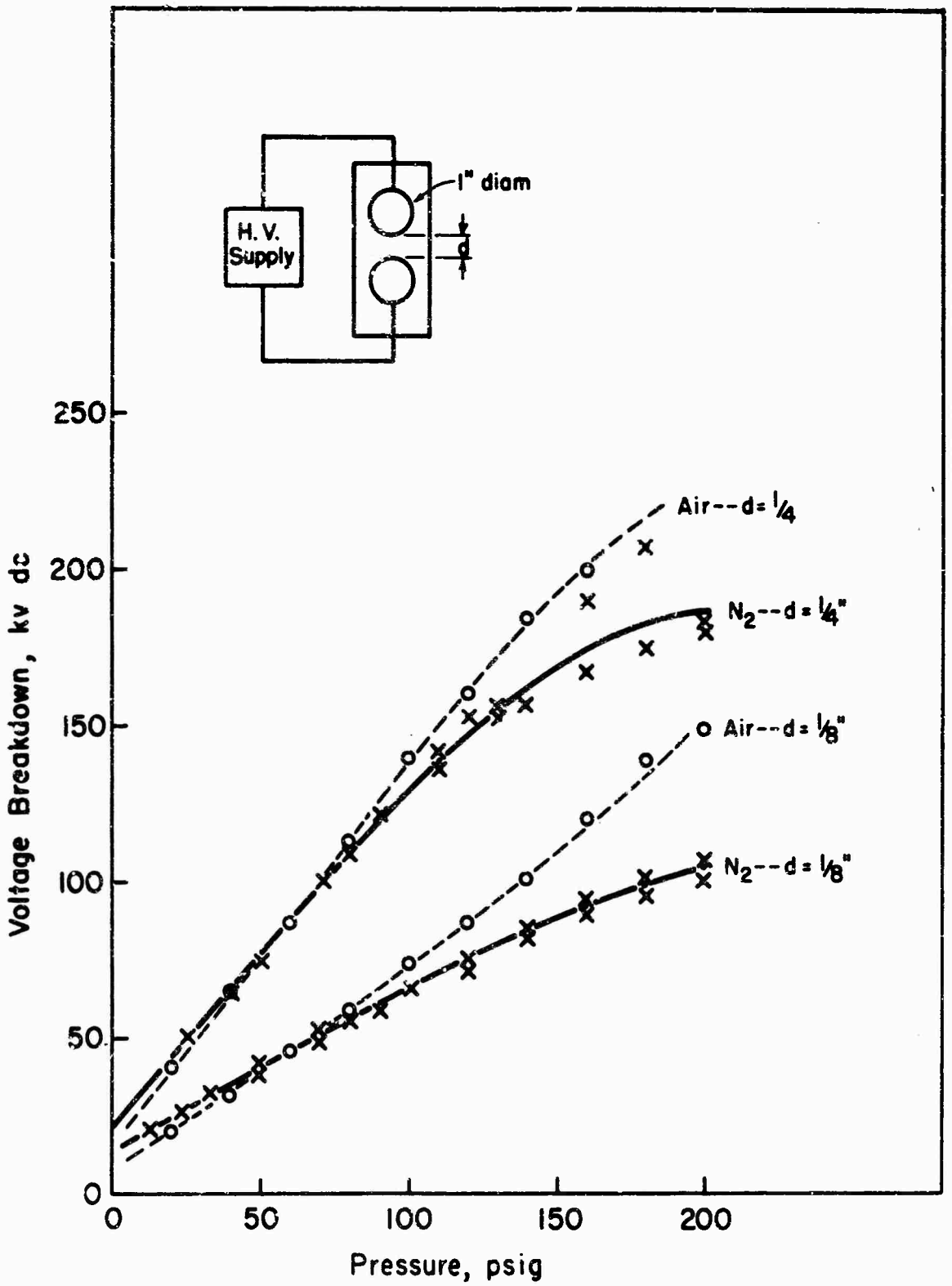

Figure 39 DC Voltage Breakdown as a Function of Pressure for Air and Nitrogen at 1/4 Inch and 1/8 Inch Spacing Between 1 Inch Diameter 304 Stainless Steel Ball Gaps.

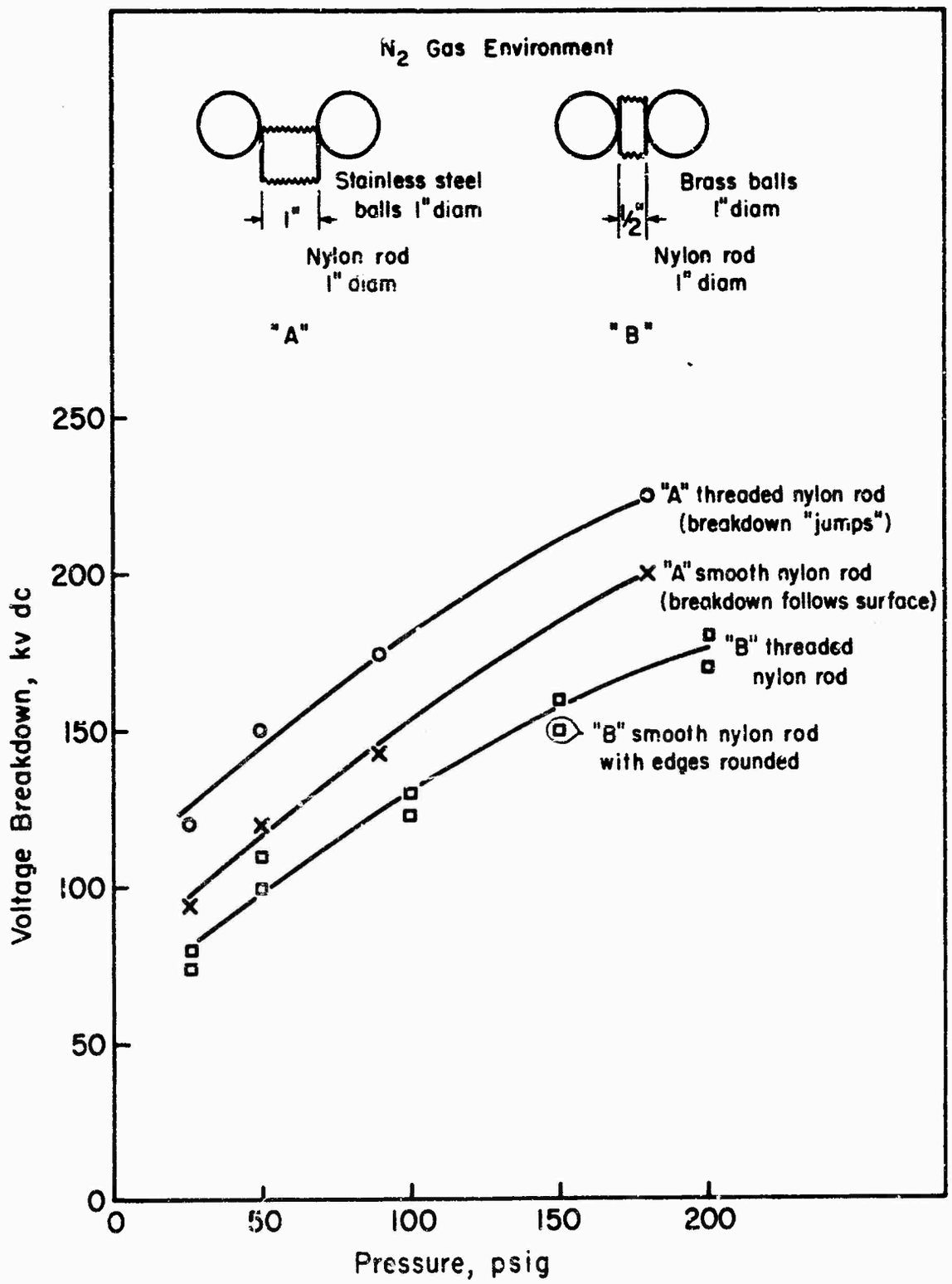

Figure 40 DC Voltage Creep Breakdown for Nylon in Nitrogen as a Function of Pressure for Various Geometries.

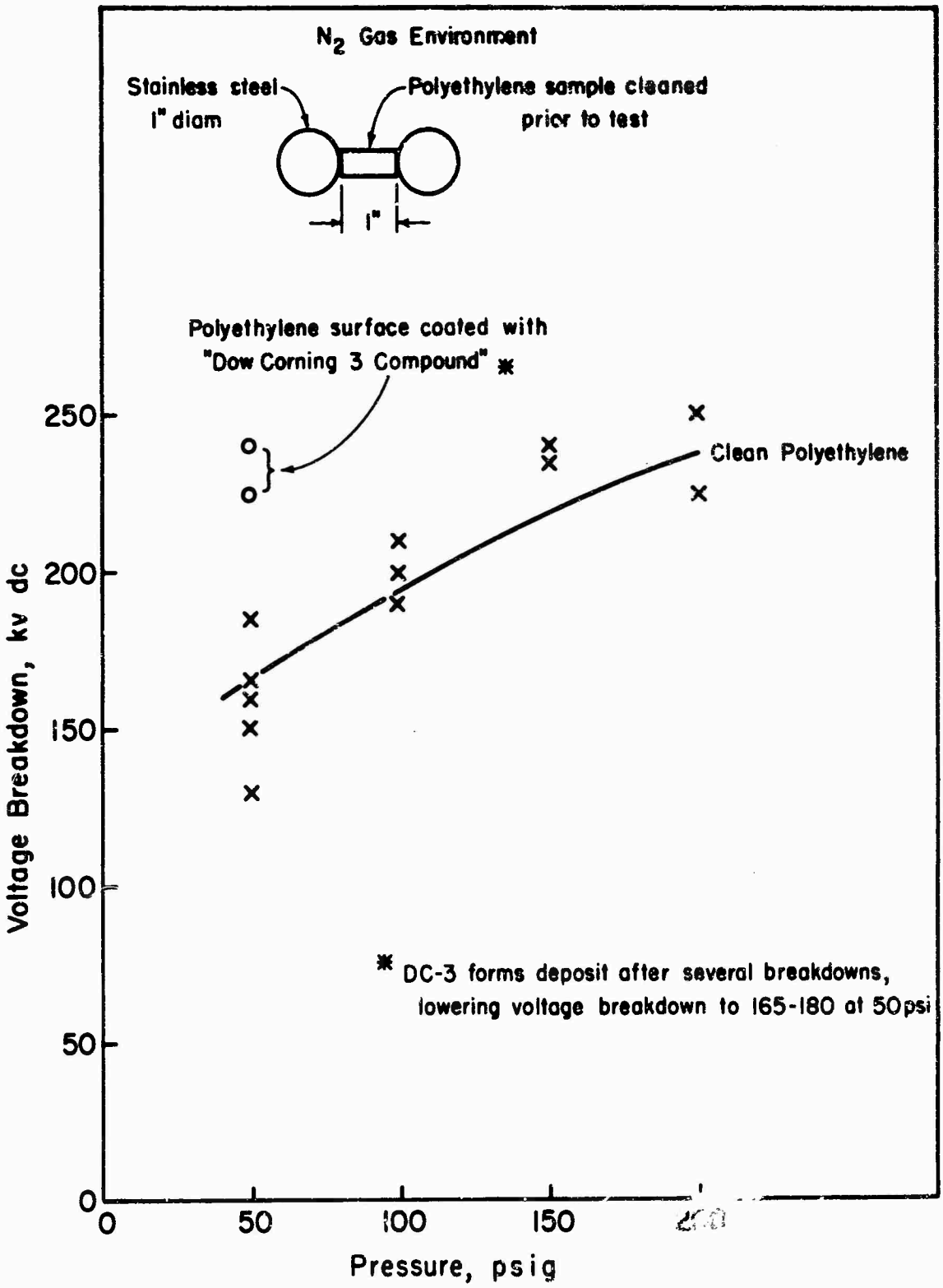

Figure 41 DC Voltage Creep Breakdown for Polyethylene in Nitrogen as a Function of Pressure for Various Surface Conditions.

that polyethylene gives somewhat similar performance to nylon with considerable initial improvement if the surface is first coated with a silicone compound. However, the disadvantage of this coating is its rapid deterioration after initial breakdown, the dielectric strength then becoming weaker than for the case of uncoated polyethylene.

Results for a particular creep breakdown study with teflon are shown in Figure 42. Performance at lower pressures is seen to be comparable with nylon and polyethylene, but much better operation is obtained at high pressures. It was also observed that teflon was able tc recover after breakdown, apparently by vaporization of surface deposits. Especially important, teflon appears to give the most reproducible operation of the various materials tested. However, when utilizing teflon with pressurized air, breakdown occurred at the highest test voltage through the volume of teflon, with combustion of the teflon and consequent production of possibly toxic residues. It would thus apparently be wise to allow an ample margin for safety when employing air as the dielectric gas.

4. Vacuum Breakdown Studies

In Section II-10, the importance of maintaining excellent vacuum insulation in an exploding wire system was discussed. The extreme variation in vacuum breakdown strength reported by various experimenters was indicated in Figure 22.

The mechanisms leading to vacuum breakdown are in general believed to initiate with field emission from microprojections on the negative or cathode electrode and/or ionization of the gas sheath formed on the introduction of energy into the wire transducer (Ref. 13). With the short pulse duration (50 nanoseconds) employed in the exploding wire system constructed by Field Emission Corp. and presently in use at Kirtland AFB (Ref. 1), vacuum breakdown may be dominated by these cathode emission processes. This also applies to the exploding wire system proposed in this present study, with an even shorter pulse duration of about 10 nanoseconds where energy deposition will hopefully occur before the shunting gas sheath can develop.

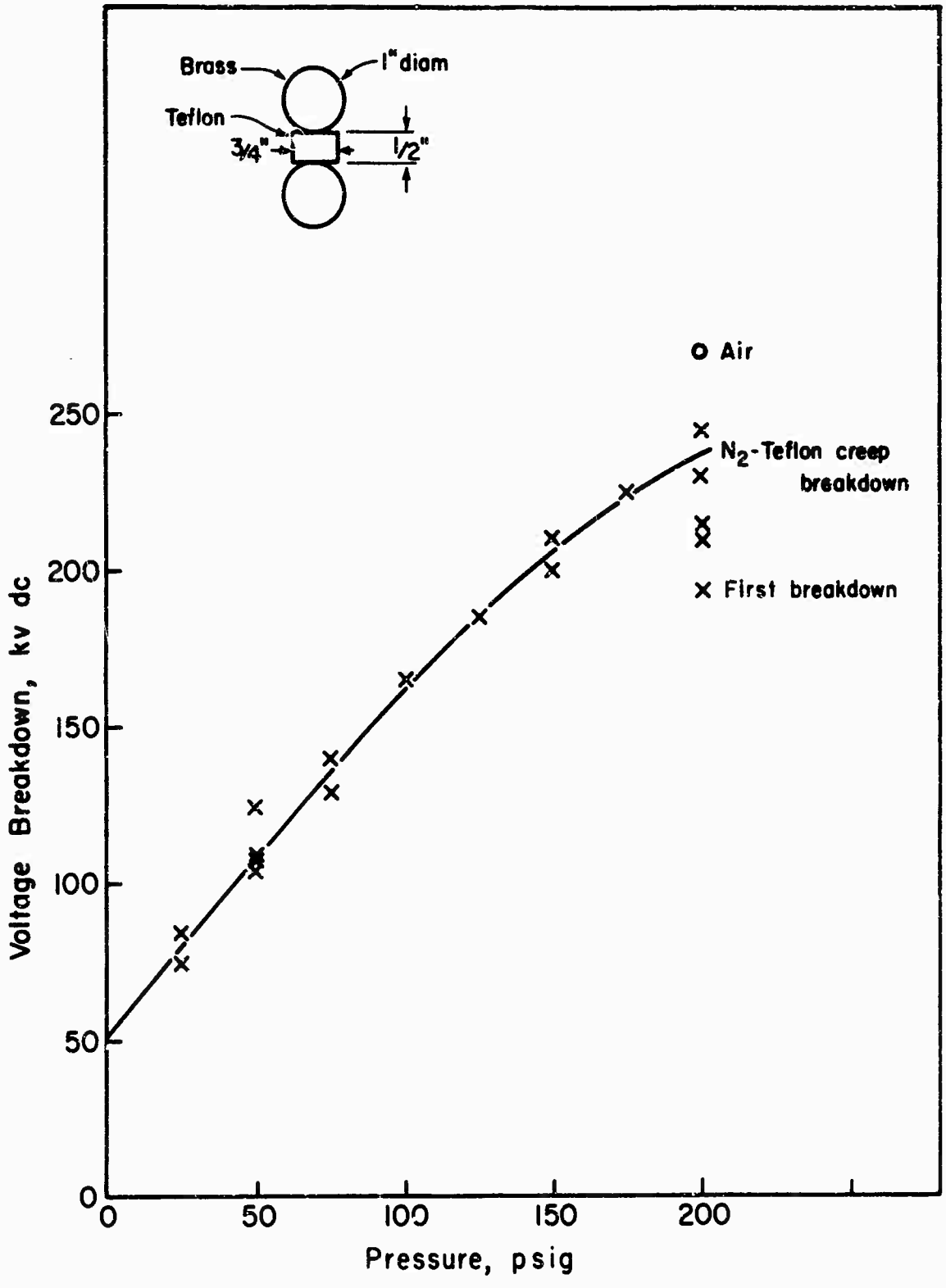

Figure 42 DC Voltage Creep Breakdown for Teflon as a Function of Nitrogen Pressure.

A portion of the effort under this design study program was therefore devoted to the evaluation of certain dielectric materials with the expectation that application of a coating to one or both of the transducer chamber surfaces would improve the voltage stand-off characteristics.

A small quantity of "glass resin", type 100, procured from the Owen-Illinois Glass Company was precured in accordance with the manufacturer's recommendations. Because of the highly viscous nature of the resin in this precured state, thinning was necessary before a substrate could be properly coated. In order to accomplish this thinning, the precured "glass resin" was mixed with one part by weight of resin to three parts by weight of acetone.

This mixture was then poured into a 1,000-milliliter flask which had a tubulation previously prepared for attaching to a vacuum system. The entire interior of the flask was coated with the resin and allowed to stand overnight at room temperature in air, to permit evaporation of the acetone.

The "glass resin" flask coating was then cured for 24 hours at $90^{\circ}C$ followed by heating to $130^{\circ}C$ for 24 hours and finally to $150^{\circ}C$ for an additional 24 hours.

The simple flask was then sealed to an ultra-high-vacuum system. This system, which after bake-out is capable of obtaining pressures of the order of 10^{-10} Torr or better, was equipped with an omegatron mass spectrometer and low-conductance gas admission valves for omegatron calibration.

The flask was pumped at room temperature for 24 hours with a pressure of 2×10^{-7} Torr being observed at this time. Residual gas analysis, by means of an omegatron, indicated a typical spectrum for this vacuum system consisting primarily of CO, H_2O, OH and methane traces, with the exception that an ethane cracking pattern had been added.

After baking for several hours at approximately $200^{\circ}C$, the vacuum system and flask reached a cold pressure of approximately 10^{-9} Torr, with no substantial change in the residual gas spectrum. However, moderate heating of the flask immediately (i.e., 30 seconds, $100^{\circ}C$)

evolved sufficient gas, apparently from the resin, so that operation of the omegatron was impossible due to an increase in pressure to approximately 10^{-4} Torr.

An ultimate cold vacuum pressure of better than 10^{-8} Torr was achieved with the flask on the vacuum system and continuous pumping. However, elevation of the flask temperature always resulted in considerable outgassing of the resin with the residual gas found to consist primarily of the ethane components.

After several days of operation at pressures better than 10^{-8} Torr the resin developed "crazing" and no longer adhered to the inside of the glass flask. This observed bonding problem probably does not preclude its usefulness for coating exploding-wire-system vacuum chamber electrodes since the resin manufacturer has indicated that the "glass resin" achieves substantially better surface bond with materials other than glass.

It has been reported that coated glass specimens have maintained static pressures of less than 10^{-6} Torr for weeks even under electron bombardment. Although the vacuum breakdown tests conducted by the manufacturer are somewhat inconclusive due to contaminants lodging in the coating during application and cure, the dielectric properties are reported to be roughly equivalent to Kel-F or the steatites. At one megacycle, the dielectric constant is 2.91 and the dissipation factor 0.0113. The volume resistivity is approximately 2×10^{16} ohm-cm. It appears that "glass resin" may be relatively easy to use and of interest for the proposed vacuum chamber application.

5. Experimental Switch Studies

All of the above proposed pulse generators are dependent upon successful low-impedance switching. For this reason a modest amount of effort under this study program was directed toward the design and evaluation of selected switch prototypes, aimed at obtaining preliminary operational data. These studies were mainly confined to either gaseous or liquid dielectric switching since a " self-healing" switch was considered highly desirable from the viewpoint of minimum system maintenance.

A limited survey of the literature, with respect to dielectric breakdown and high-speed switching devices, seemed to indicate that extreme over-voltage is the most effective means of rapid triggering. However, the dependence on ionization constitutes a practical problem in applying this technique to dielectric gases. In fact, preionazation by means of such techniques as ultraviolet illumination and isotope excitation has been employed successfully to "sensitize" the gap prior to breakdown.

The success obtained in gap synchronization with the AFWL multi-pulser exploding wire apparatus indicated the effectiveness of fast rise UV illumination. In the case of triggering by over-volting, extremely fast rise times are needed to achieve minimum jitter; such rise times have been obtained with very high pressure sharpening gaps, following a technique first employed by R. C. Fletcher (Ref. 18) and later by T. J. Tucker, (Ref. 19) at Sandia Corporation.

These two techniques were combined (Ref 20), employing a three-electrode "needle" gap in which the needle was located in the median plane and was floated at a potential midway between that of the other two electrodes. The schematic circuit employed and the resulting data are shown in Figures 43 and 44. The process is initiated by breakdown of a gap, G_1 discharging the energy from 20 feet of RG cable into the gap sharpening apparatus; this sharpening gap, G_2, also provides a UV source for preillumination of the trigger gap, G_3. A time delay between illumination and over-volting of the trigger gap is established by utilizing delay cable between the sharpening gap and the needle, as shown. Prior to application to the trigger electrode, the fast rise time is differentiated by the 6-picofarad coupling capacitance.

The crosses in Figure 44 correspond to operation with only ultraviolet triggering of the gap: a sizable increase in delay and jitter time is evident for a voltage drop of more than a few percent below self-fire voltage. With the needle electrode in place but not pulsed (however, connected at mid potential dc voltage), a noticeable change in operation is seen; this is perhaps attributed to perturbation of the space charge field by the presence of the needle, this space charge being produced by the ultraviolet illumination.

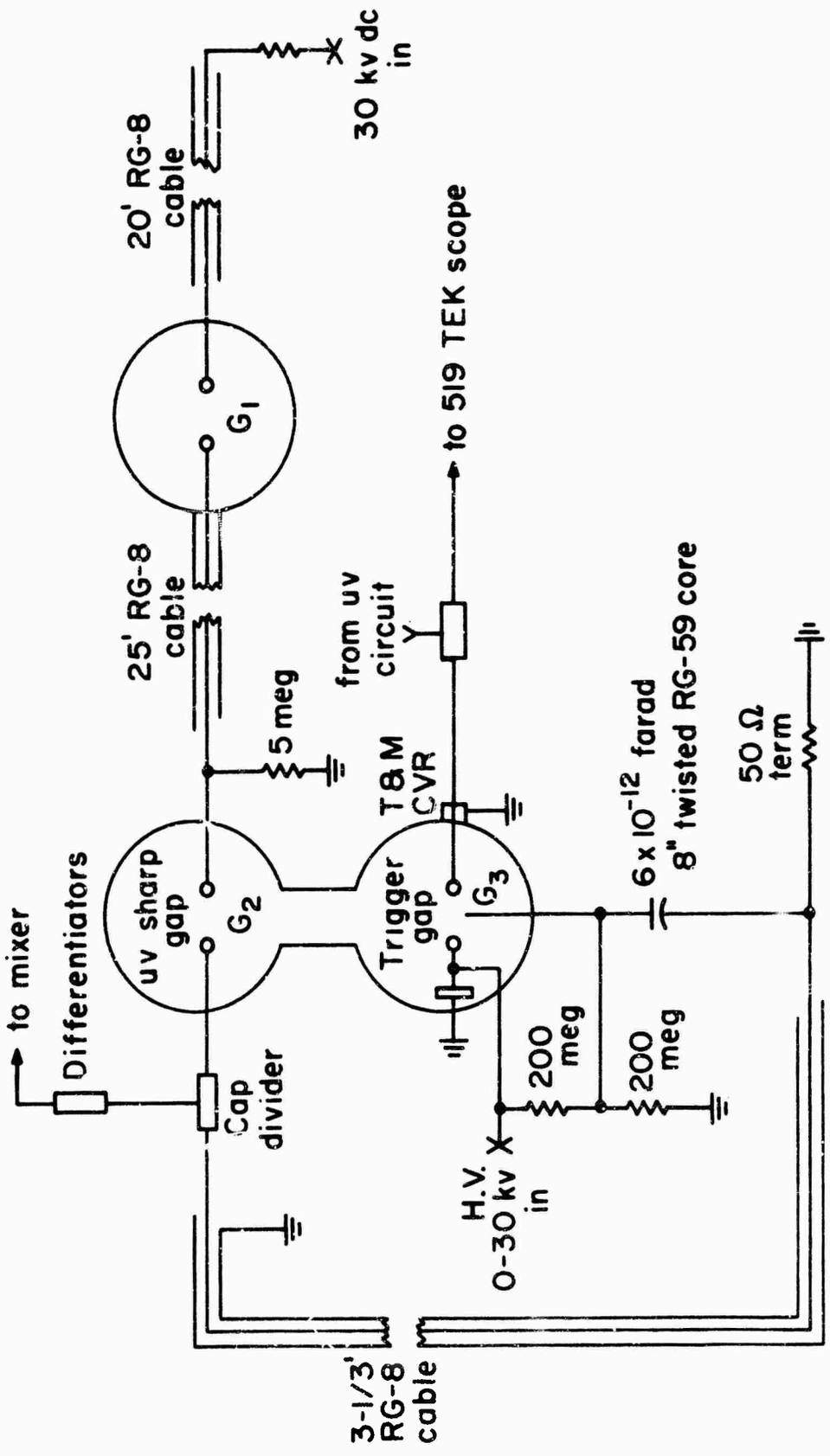

Figure 43 Schematic Circuit of 3-Electrode Needle Gap.

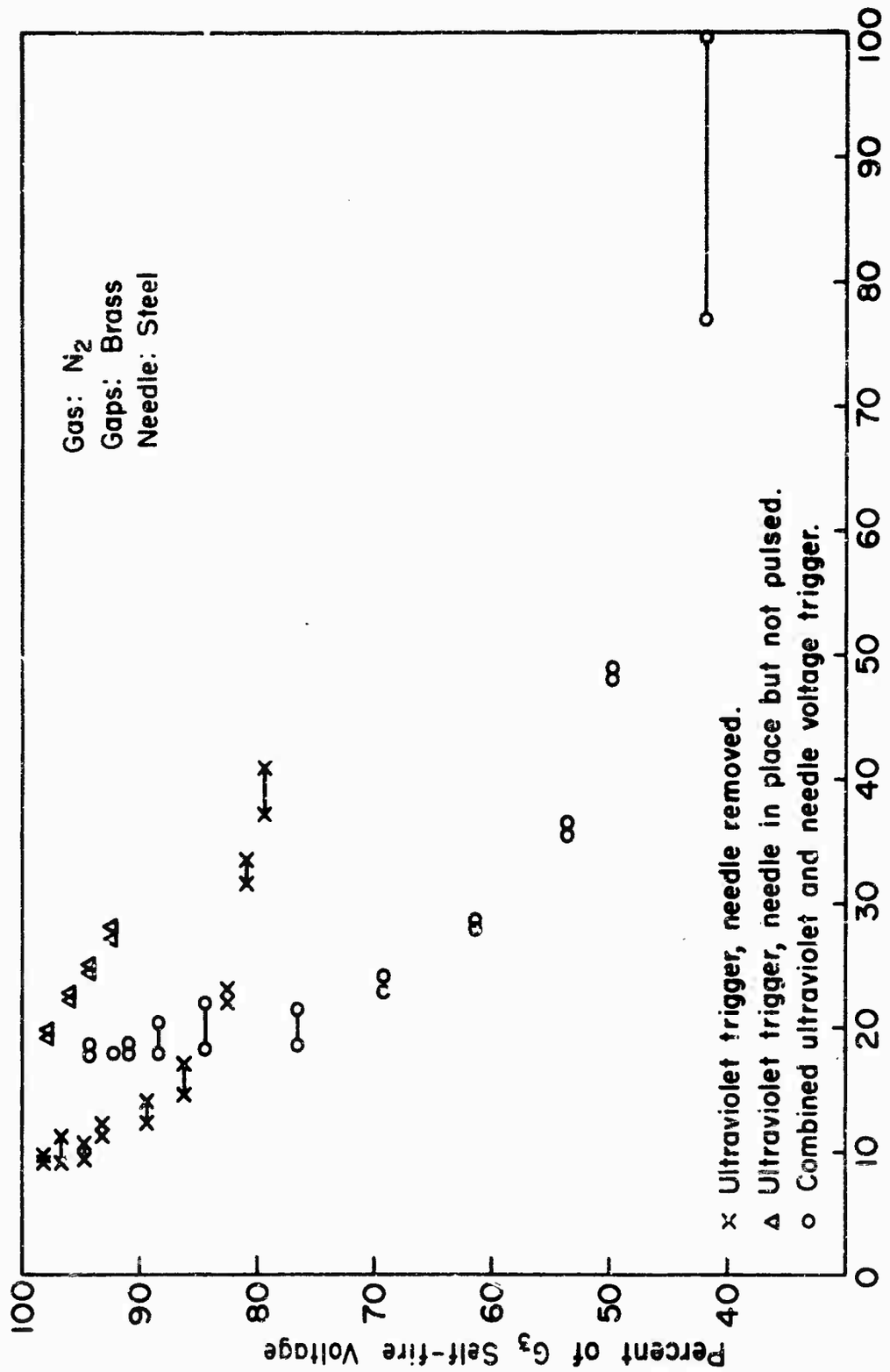

Figure 44 Delay Jitter is Indicated by Plotting Both Minimum and Maximum Delay Values.

With the combined use of ultraviolet preillumination and pulsed voltage applied to the needle, the trigger gap is seen to have a greatly increased latitude with only a modest increase in delay time and with little or no increase in jitter time down to about half of the self-fire voltage, thus exhibiting far superior overall performance to that obtained with other techniques of triggering. The apparent increase in jitter time, in the region from 75 to 90 percent of self-fire, is believed to result from some irregularity in the electrical hook-up and will probably disappear with more careful fabrication and circuitry.

In summary, this experiment demonstrates the feasibility of operating a gas dielectric trigger gap at 60 percent to 70 percent of self-fire voltage with minimum delay (20 to 30 ns) and with extremely low jitter ($\pm$ 1 ns maximum in this model). Operation at such a remote point from the self-fire affords considerable protection from possible breakdown due to gap roughening and/or corona effects. The extremely low jitter indicates that this technique should be applicable to multiple gap initiation which will prove useful either where separate pulsers are to be discharged into a common line (as in the case of the exploding wire system (Ref. 1), or where parallel gaps are attached to a common energy source such as a Blumlein to minimize the inductance and resistance inherent in individual switches.

The suitability of ultraviolet triggering of a pressurized spark gap would appear to imply that such a gap could also be triggered by an X-ray source. Such an experiment was performed, as indicated in Figure 45, utilizing a Model 845 FEXITRON Portable 150-kv flash X-ray system to illuminate the spark gap. The self-fire limit and lower X-ray trigger limit are shown in Figure 45 as a function of nitrogen pressure, the dose at the gap being adjusted to about 35 milliroentgens/pulse. The distance between the X-ray tube and the gap was then varied at a fixed pressure and the breakdown latitude evaluated as a function of X-ray dose, assuming attenuation inversely proportional to the spacing. These results are seen in Figure 46. The voltage latitude at the maximum dose is seen to be about 10 percent, or roughly what one obtains with ultraviolet illumination of

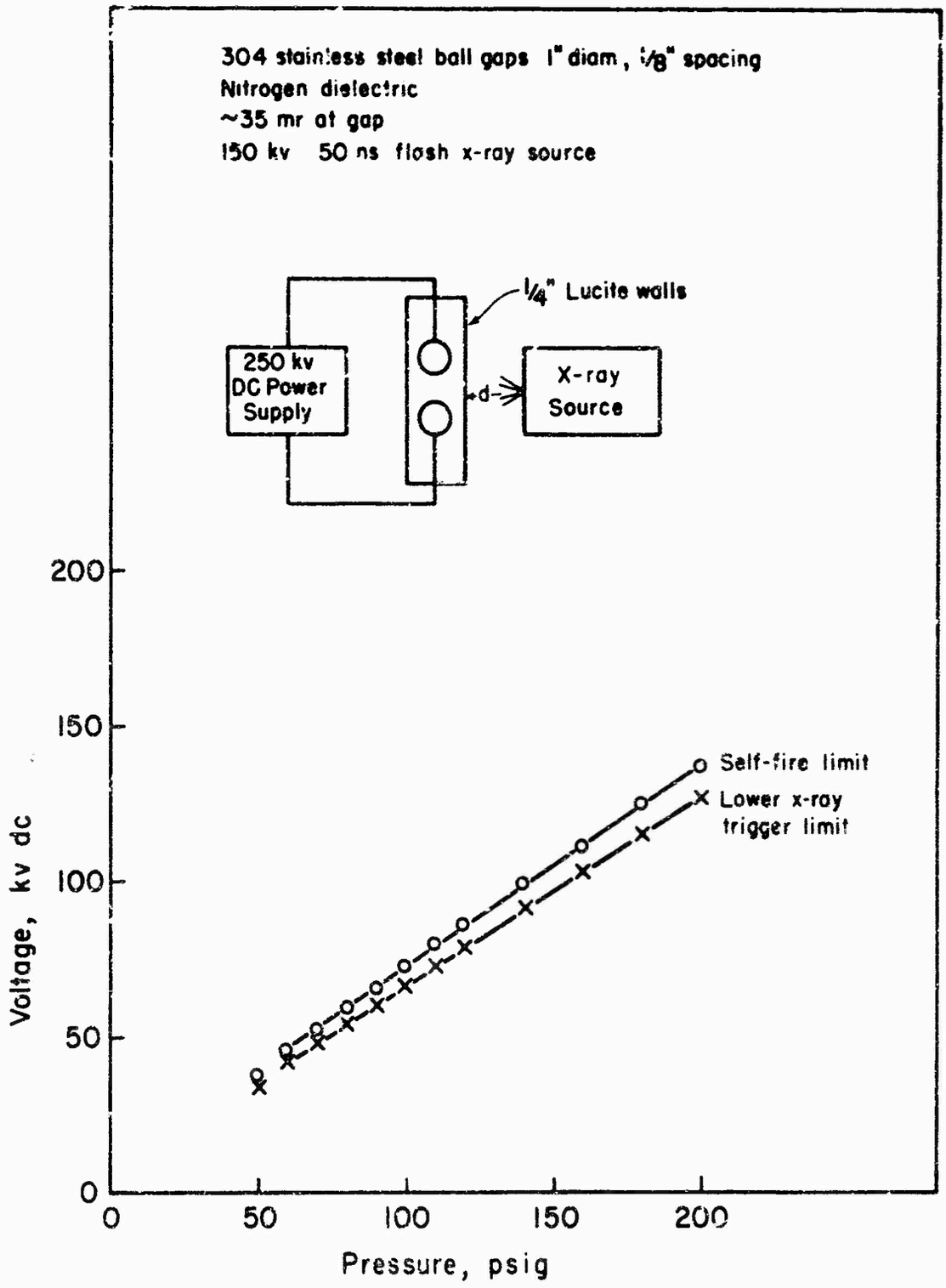

Figure 45 Voltage Breakdown as a Function of Pressure for a Nitrogen Spark Gap, With and Without X-Ray Gap Ionization. A Triggering Latitude of About 50 Percent is Seen to be Obtained Under the Conditions Indicated.

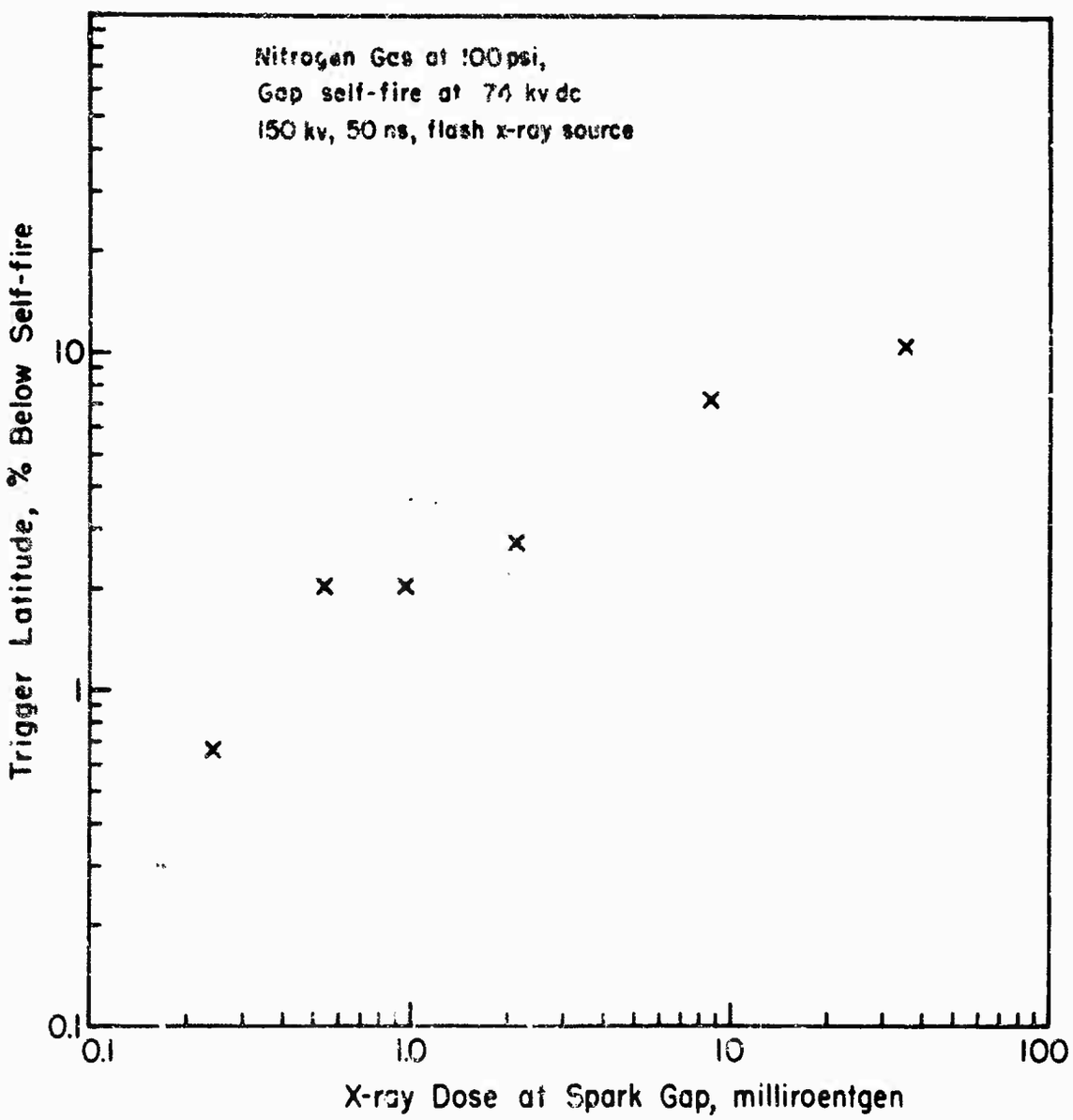

Figure 46 Effectiveness of X-Ray Triggering with the Apparatus of Figure 45 in Terms of Trigger Latitude (percent of self-fire) as a Function of Total X-Ray Dose per Pulse at the Spark Gap.

considerable intensity. A reduction in X-ray dose of about two orders of magnitude is found to cause a reduction in breakdown latitude of about one order of magnitude.

It should be noted that X-ray triggering does work with such gases as nitrogen, oxygen and air, but was found to be ineffective (within the accuracy of these breadboard experiments) with such strongly electronegative gases as Freon 12.

The above pressurized gas gaps are attractive for use with dc charging potentials. However, the literature survey (Refs. 21, 22) indicated that liquid gaps were attractive because of their greater electric strength, particularly for pulsed operation (see the following section of this report). It was therefore decided to experiment with two liquid switch gaps in parallel, employing the apparatus of Figure 47 to achieve simultaneous triggering by needle over-volting of the gaps. This apparatus was immersed in oil with one plate at ground potential and the other being pulsed with the 2-Mv Marx-surge generator. The needles were maintained at about mid-gap potential by means of capacity voltage division, the inner disc electrode serving this function. Breakdown was accomplished by adjusting the ball gap between the inner electrode and outer electrode such that breakdown of this gap occurred first, at a voltage level below the self-fire voltage of the two main gaps. This switching of the center gap rapidly changed the potential on the two-needle gaps, causing the needles to arc to the respective higher voltage balls of the external gaps. This is followed almost immediately by arcing across the gap to the other electrode because of the current limiting inductors.

This device was successfully tested for a number of pulses, down to 35 percent below the self-fire voltage of the outside gaps (the pulsed voltage being about 600 kv at this time). Firing of both gaps was repeatedly observed under these conditions, as verified by camera photographs. Assuming that gap resistance is modest, one can argue that discharge of one capacitor will rapidly drop the voltage between the two plates so that, in all cases where both gaps were observed to fire, the firing of the two gaps must

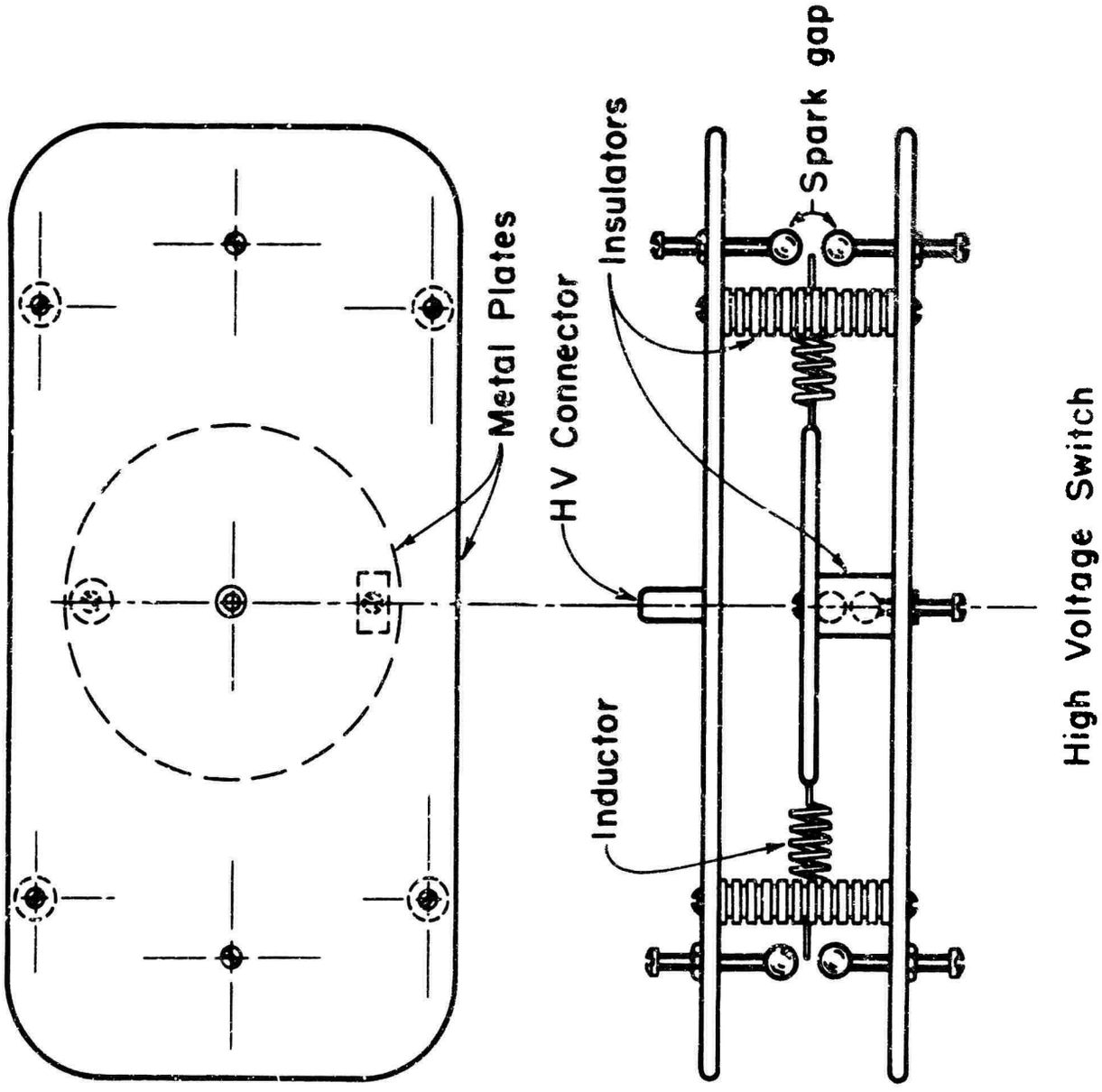

Figure 47 Experimental Oil High Voltage Switch Employed in Demonstrating Simultaneous Triggering of Gaps Connected in Parallel.

have been synchronized within 3 nsec or better. No attempt was made to verify precisely the degree of synchronization because of the rather elaborate instrumentation which would be required for that purpose.

This experiment appears to provide a method for the successful paralleling of high voltage pulsed switches which is required in certain applications to pulse-charged generators.

SECTION IV

PROPOSED PULSER DESIGNS

1. Flash X-Ray System

The general objective specifications for the X-ray system, as listed in the statement of work, are as follows:

a) Output energy per pulse	1,000 - 10,000 joules
b) Pulse duration	20 - 50 nanoseconds
c) Rise time (for a matched load)	1 - 10 nanoseconds
d) Pulser output impedance	80 ohms
e) Output voltage (into a matched resistive load)	2 - 4 Mv
f) Output peak current (into a matched load)	25,000 - 50,000 amperes
g) Output peak power (into a matched load)	5×10^{10} to 2×10^{11} watts

To illustrate the application of the general design techniques discussed in the previous report sections, a specific set of design parameters has been chosen:

a) Output energy per pulse	2,000 joules
b) Pulse duration	40 nanoseconds
c) Pulse output impedance	80 ohms
d) Output voltage (matched load)	2 Mv
e) Output peak current (matched load)	25,000 amperes
f) Output peak power (matched load)	5×10^{10} watts

A system layout is presented, including approximate dimensions, for these specific parameters. The system rise time is estimated for this specific

design, followed by comments concerning effects on system design of choosing certain other specifications within the listed range.

The system concept for the proposed flash X-ray system is based on the pulse-charged two-stage Blumlein circuit discussed in Section II-4. A schematic cross-sectional drawing of the charging circuit, Blumlein, switching and tube have been indicated in Figure 23. Oil dielectric is proposed both for general insulation and as the switch dielectric because of its relatively high pulse dielectric strength and proven self-healing characteristics.

The cross-section view of the proposed 2 Mv flash X-ray system is shown in Figure 48. The Blumlein outer diameter (electrical) of 40 inches is small compared to the length of 156 inches; hence, an approximately rectangular pulse shape is expected since the end capacity is moderate compared to the overall capacity. Apart from the switch geometry, the maximum voltage gradient during charging is estimated to be about 0.5 Mv/inch, a conservative figure. The inductor employed to connect the inner Blumlein conductor to ground during pulse charging is field graded to not exceed this gradient. The 6-inch-radius flare at the charging end of the Blumlein of Figure 48 can be eliminated by a variety of voltage grading techniques, permitting enclosure of the Blumlein in a tank only slightly larger than the 40-inch diameter.

It should be noted that the 80-ohm Blumlein impedance value was selected to conform with the amended study contract specifications. It is possible and may actually be desirable in some cases to operate at a considerably lower overall impedance level (e.g., 40 ohms) with only a modest increase (30 percent) in Blumlein diameter. This is apparent in examining Figure 16 above.

The flash X-ray tube should utilize a hollow beam, magnetically focused design for reasons, indicated in Section II-11, which are related primarily to improved X-ray spatial distributions and tube longevity through controlled target loading and prevention of glass bombardment.

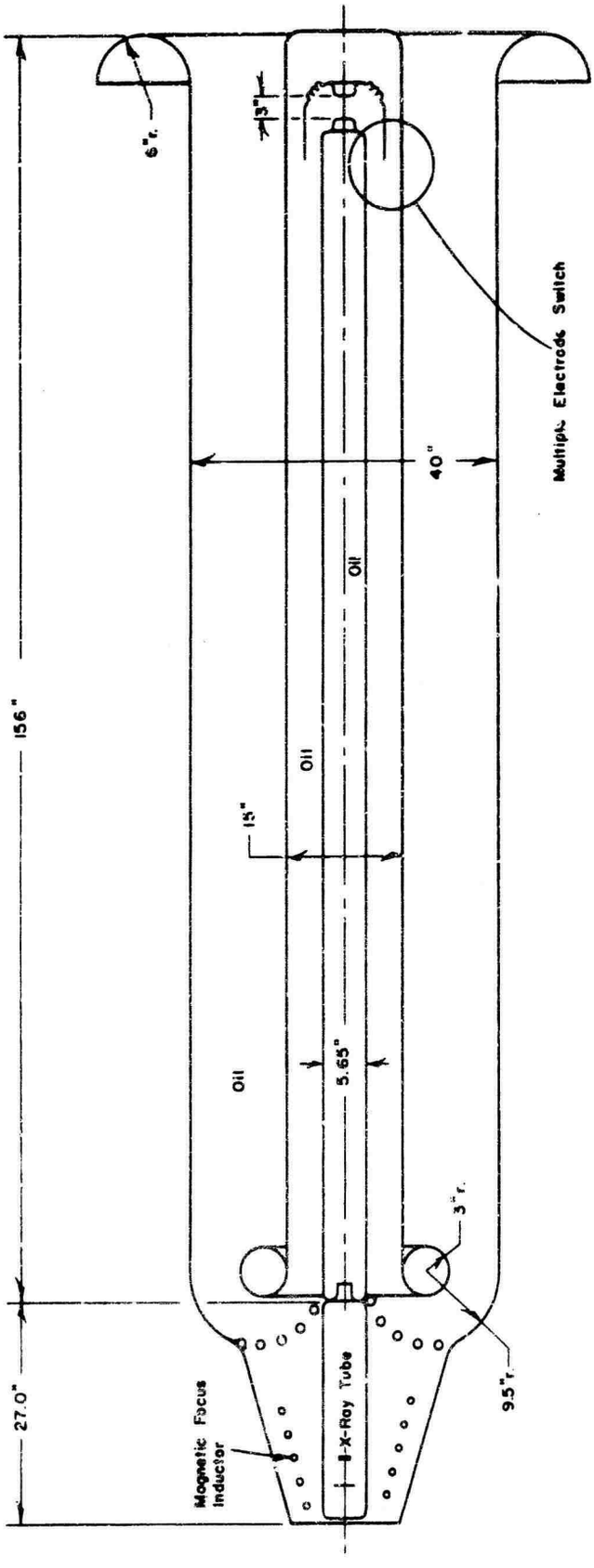

Figure 48 Cross Section of 80 ohm Coaxial Blumlein Pulse Generator Showing Location of Multiple Switch, Magnetic Focus Inductor, Charging Inductor and X-Ray Tube.

By utilizing pressurized gas (such as nitrogen) in a Marx-surge primary gap column switch configuration, this entire flash X-ray system should require an absolute minimum of maintenance. Multiple gapping reduces energy loading at the oil switches sufficiently to minimize gap roughening, and the oil can be filtered and recirculated to remove carbon particles produced during switching. Since magnetically focused flash X-ray tubes have been successfully utilized in the 1 to 2 Mv region at Field Emission Corporation during studies conducted for AFWL and for the Sandia Corporation with no unavoidable life-terminating mechanism out to at least 100 pulses, it should be possible to conduct radiation testing at a minimum cost and at a relatively high rate of usage (probably as high as 1 pulse/5 minutes with this proposed system). Such a design should therefore appear particularly attractive for intensive testing at relatively high and uniform dose rates and for moderate-size working volumes (1000 cubic inches or less).

A quantitative estimate of system rise time is not possible for the system of Figure 48, since detailed tube and switch geometries are not available. An estimate can be obtained, however, from the fact that the 5 nsec 50 ohm model, with a single Blumlein switch, had a rise time of about 5 nsec, as shown in Figure 37. With parallel switching and the relatively smooth pulser-to-tube transition of Figure 48, it should be possible to obtain a rise time of about 3 to 4 nsec with the 80 ohm 2 Mv system, provided a hollow beam tube design is employed to minimize tube inductance.

It is possible to estimate the dimension changes of Figure 48, for different output voltages and/or pulse durations. The several diameters are scaleable with output voltage, e.g., the inner diameter of the outer Blumlein conductor would be increased to 80 inches for a 4 Mv 80 ohm design, the center conductor to 30 inches and the inner conductor to 11.3 inches. The corona shield radii would also scale to 6 and 19 inches at 4 Mv. The length of the Blumlein assembly is affected by the pulse duration. The length of 156 inches in Figure 48, determined by the pulse duration of 40

nsec, would increase to 195 inches for a 50 nsec pulse length or decrease to 78 inches at 20 nsec.

A higher voltage lower impedance system (7 Mv, 30 ohm, 30 nsec generator) has been designed in more detail in a later study (Ref. 14), including a charging pulser and tube designs. Estimates are also provided for radiation yield and shielding.

2. Exploding Wire System

The general objective specifications for the exploding wire system, as listed in the statement of work, are as follows:

a) Output energy per pulse	1000 joules
b) Pulse duration	10 nanoseconds
c) Rise time (for a matched load)	0.1 - 1 nanoseconds
d) Pulser output impedance	1 - 2 ohms
e) Output voltage (into a matched resistive load)	300 - 500 kv
f) Output peak current (into a matched load)	200,000 - 300,000 amperes
g) Output peak power (into a matched load)	10^{11} watts

The higher voltage case will be employed as a design example, with the following parameters:

a) Output energy per pulse	1000 joules
b) Pulse duration	10 nanoseconds
c) Pulser output impedance	2.5 ohms
d) Output voltage (matched load)	500 kv
e) Output peak current (matched load)	200,000 amperes
f) Output peak power (matched load)	10^{11} watts

A system layout is presented, including approximate dimensions. The system rise time is estimated for certain conditions, followed by comments concerning specific design problems.

The design concepts and data presented in preceding sections have been applied to the evaluation of desirable design characteristics for

an advanced exploding wire pulser system. The basic concept is again that of a pulse-charged two-stage Blumlein circuit such as previously discussed in Section II-4. The Blumlein circuit, including the switch, transducer chamber and load was indicated schematically in Figure 21.

The primary limitation with respect to the rate of dumping energy in an exploding wire is the uncancelled system inductance. The general problems of switch design were discussed in Section II-6, and those related to the transducer chamber in Section II-10. In general, both chamber spacing and overall system dimensions must be kept to a minimum to achieve fast rise time.

A cross-section view of the proposed system is shown in Figure 49. The Blumlein outer diameter is about 27 inches and the overall length is about 90 inches. The thickness of the laminated polyethylene insulation in each section is 0.313 inch, corresponding to an electric gradient of 1.6 Mv/inch. It is estimated that this relatively high voltage gradient can be reconciled with useful system life provided that the pulse charging system is designed for sub-microsecond charging times and also that careful polyethylene grading techniques are used, particularly at the transducer chamber end of the center Blumlein conductor.

The maximum rise time obtainable can be estimated with the aid of Table I of Section II-10. With the gap spacing narrowed down to about 0.20 inch and the added capacity of the polyethylene, the switch inductance would be about 3 to 5 nanohenries, dependent upon the diameter of the breakdown channel across the gap. A generator (matched load) rise time of 1 to 2 nsec would thus be expected. One possible design for a replaceable solid dielectric switch is indicated in Figure 50, with the dielectric layers being overlapped at the replaceable section to avoid creep breakdown. Liquid dielectric wetting would probably be advisable to ensure reliability.

An alternate approach would involve liquid or solid switching by means of multiple switches situated around the periphery of the switch end of the system and initiated from a separate low impedance Blumlein circuit with a single trigger switch. If implemented, this alternate design (with

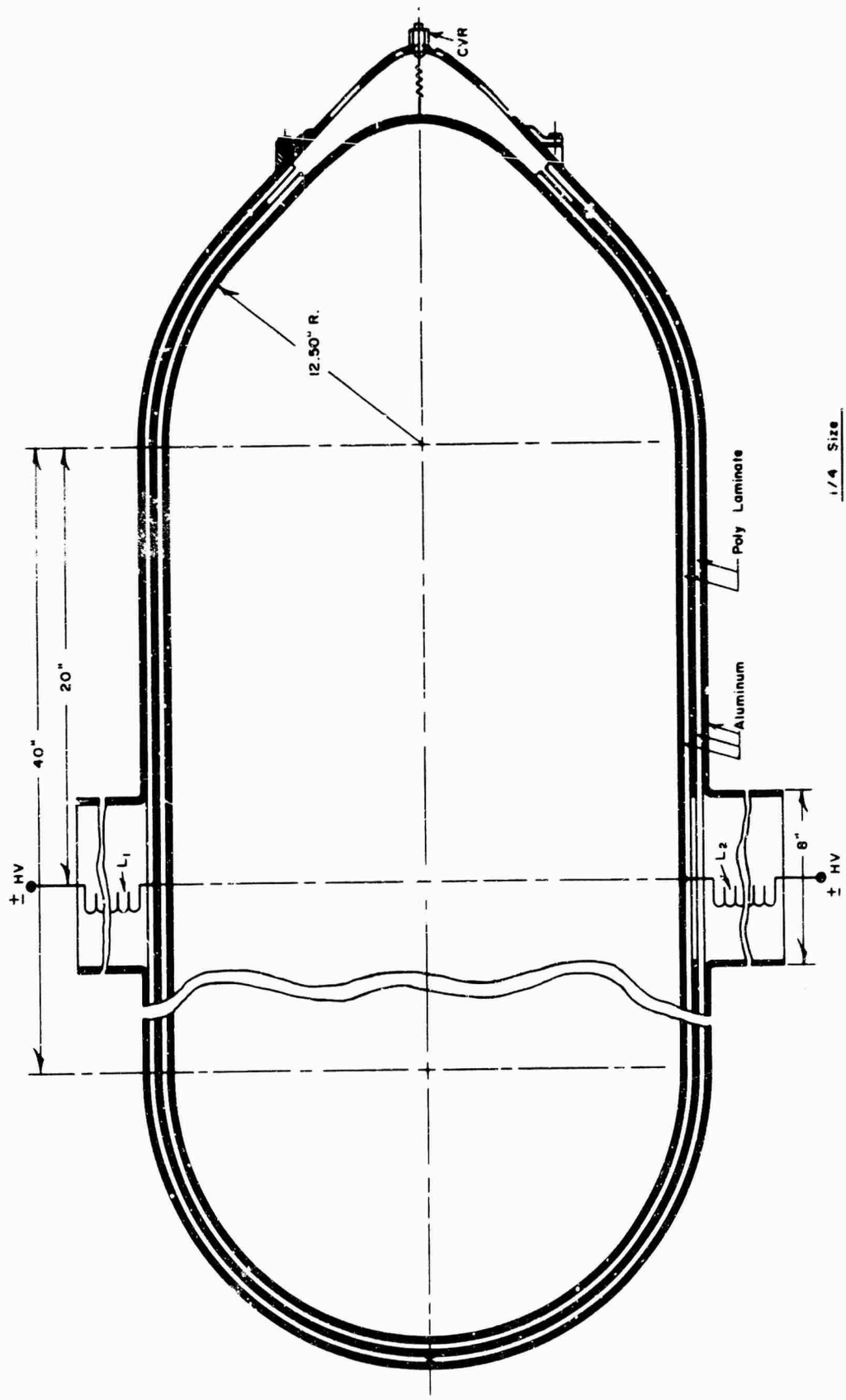

Figure 49 Cross Section of 2 ohm Coaxial Blumlein Pulser Showing Position of Charging Inductors and Load Chamber.

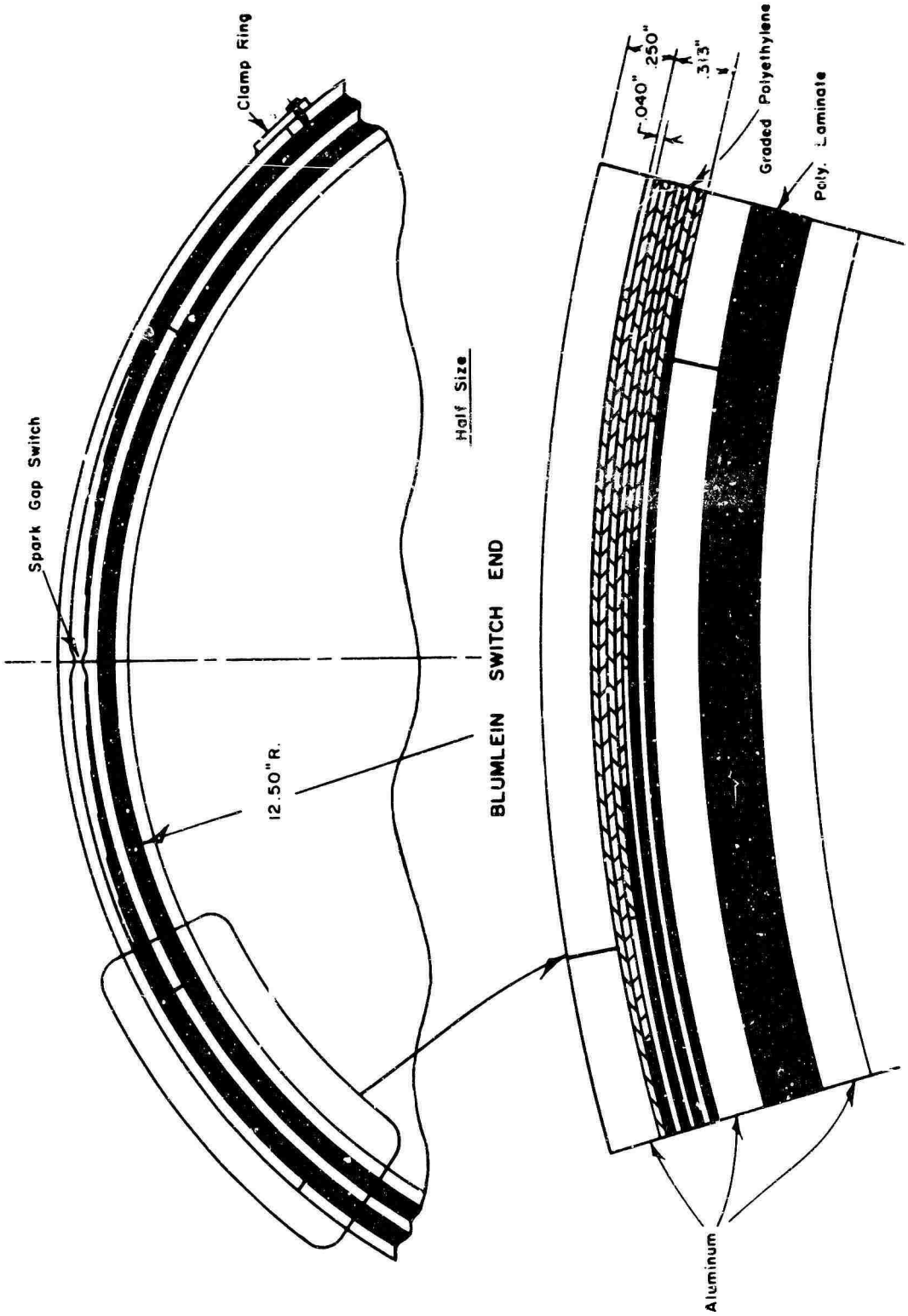

Figure 50 Cross Section of 2 ohm Coaxial Blumlein Pulser Spark Gap Switch Section Showing Voltage Grading Polyethylene Construction.

liquid dielectric switches and sufficiently low loading per switch to minimize roughening) would provide minimal system maintenance, and an arbitrarily low generator (matched load) rise time, if the switches are synchronized sufficiently accurately.

It is possible to reduce the impedance of the switches to an arbitrarily low value by employing a sufficient number of parallel switches. However, no such recourse appears available with respect to reduction of the transducer chamber inductance since the desired high energy deposition rates in the exploding wire require developing a high voltage across a very small diameter wire. Referring again to Table I (Section II-10) the wire chamber inductance is seen to depend critically upon the minimum permissible chamber spacing. However, conservative design should take into account the possibility that the pulser output voltage may initially approach the open circuit value of one megavolt, especially if the chamber and wire inductance values are sufficiently high to limit the rate of current build-up. In cases where it is permissible to surround the wire with liquid dielectrics, the chamber inductance may be held to a very low value. For example, referring to Table III in Section III-3, castor oil is seen to have a breakdown voltage of about 4 megavolts/inch and a dielectric constant of 4.67. The high dielectric constant would result in appreciable capacitive loading which, combined with the high breakdown strength and excellent wetting ability of castor oil, may allow reduction of the chamber impedance to the extent required to give di/dt values close to 10^{14} amp/sec (equivalent to a rise time of about 2 nsec) for wires a few mils in diameter, assuming negligible switch impedance.

Referring to the earlier gaseous breakdown data, it appears necessary to maintain a pressurized gas chamber spacing of at least 0.6 inch (for extremely high pressure nitrogen or quite high pressure electronegative gas such as SF_6). In such a chamber the maximum value of di/dt is approximately 2×10^{13} amp/sec for a 2-mil wire with the system rise time being greater than the system design pulse length of 10 nanoseconds.

The case for a high vacuum chamber is even less favorable as indicated in Figure 22 in Section II-10. With the anticipated high-inductance open-circuit voltage of 1 Mv, a major improvement in chamber design is required to achieve a spacing of one inch, corresponding to a di/dt value of less than 10^{13} amp/sec for the 2-mil wire.

It thus appears that the performance of this proposed exploding wire system is primarily limited by the required insulation spacing in the transducer chamber, especially for the case of vacuum studies. This latter problem will be discussed in more detail in the last report section.

SECTION V

CONCLUSIONS AND RECOMMENDATIONS

The foregoing report has identified promising approaches to improved pulser designs, indicating some general design considerations. Field reversal Blumlein generators seem to be the best suited to the proposed application. Various experimental and design studies have been conducted, leading to two proposed pulser designs for two specific cases: a 2-Mv flash X-ray system, employing a long-life hollow-beam tube, and a very low impedance exploding wire system.

1. Flash X-ray System

The design of the pulse-charged two-stage Blumlein flash X-ray system appears to be relatively straightforward, based on this study and on the system study (Ref. 14). As indicated above, anticipated key features include good tube life (potentially well in excess of 100 pulses), minimal maintenance through the use of self-healing switches, and relatively high and uniform dose rates for moderate-size working volumes. With such a pulser, it should be possible to conduct transient radiation effects testing at a minimum cost and a relatively high rate of usage. Such a design should therefore appear particularly attractive for research and development involving a large number of moderate-size (1000 cubic inches or less) to small objects.

2. Low Impedance Exploding Wire System

The Blumlein exploding wire system proposed above appears capable of meeting the specified system objectives of 500 kv at 2 ohms, at least insofar as the Blumlein circuit and switch portion of the system is concerned. However, as discussed in some detail, overall system rise time seems to be basically limited by the maximum transducer chamber

electrical strength of the dielectric (i.e., liquid, gas, vacuum) required for a particular series of tests. It was indicated that maximum di/dt values, for wires a few mils in diameter, would vary from 10^{14} amperes/second with optimum liquid chamber insulation to 1 to 2 x 10^{13} amperes/second for pressurized gas or vacuum insulation.

Since the vacuum dielectric strength actually demonstrated in the exploding wire system (Ref. 1) in use by the AFWL, Kirtland, has so far been considerably inferior to the 1 megavolt/inch strength assumed for a di/dt of about 10^{13} amperes/second, a further discussion of vacuum breakdown seems pertinent here.

3. Need for Further Work on Prevention of Vacuum Breakdown

As indicated in Section II-10, breakdown between clean surfaces in a high vacuum is generally believed to be initiated by field emission of electrons from microprojections on the negative electrode. Research by Dyke, et al., (Ref. 24) conducted with a single-needle tungsten cathode, proved that vacuum breakdown occurs when the emitted current density reaches a critical value for which emission-induced heating causes rapid vaporization of needle tip material. This form of vacuum breakdown was shown to be characterized by a sharp discontinuous increase in current accompanied by both melting and violent destruction of the needle point. It was established, however, that field strengths of the order of 5 x 10^{7} volts/cm or higher were always required at the tungsten needle tips to produce vacuum breakdown. Dyke's work was extended by Boyle, Kisluik and Germer(Ref. 25) to larger area electrodes, while still maintaining ultra-high vacuum and atomically clean surfaces. They showed that predischarged currents could still be attributed to field emission phenomena by assuming that the emission occurs from very small points on the supposedly smooth surface of the cathode. These points, though usually microscopically small, can be sharp enough to give rise to voltage enhancement factors as high as 30 over the electric field computed on the basis of smooth electrode geometry. More recent studies (Ref. 26) have indicated that in practice surface irregularities have been encountered with geometries capable of producing even

greater enhancement factors. The recent work of Alpert, Lyman and co-workers (Ref. 27) further supports the high probability of field emission from cathode projections as the initiating mechanism for vacuum breakdown.

Since the pulse durations of interest in the design of exploding wire chambers are sufficiently short to reduce the importance of anode contributions to vacuum breakdown phenomena, it appears desirable to investigate possible techniques for reducing the emission from surface microprojections on the cathode or negative transducer chamber electrode. Several people have reported a significant improvement in vacuum breakdown gradients after coating the cathode electrode with dielectric materials. Jedynak (Ref. 28) reports success in maintaining without discharge dc voltages as high as 340 kv across a 5-millimeter gap composed of 15-cm-diameter Rogowski electrodes. This was accomplished by use of a suitable thin insulating film. Similar studies have been conducted by Ion Physics Corporation (Ref. 29) with a thin coating of "Nucerite,"* a dc voltage of about 230 kv was obtained across a gap spacing of 2 mm in vacuum. It was stated, however, that difficulties in obtaining surface adhesion were to be anticipated unless surface radii of less than 1 inch were maintained (too small for the present application). The Ion Physics group also noted the difficulty in maintaining as good insulation properties for large area electrodes as for small electrodes. This "area effect" may result from the higher discharge currents which are associated with electrode "break-in" because of the larger capacitively stored energy for the large electrodes. Little and Whitney (Ref. 30) evaluated several surface treatment techniques, among them optical grinding and polishing, heat treatment, glow discharges, evaporation of metal layers on the cathode and use of thin dielectric coatings on the cathode. The thin dielectric layers produced the most significant improvements in electric fields, with teflon or nylon on 304 stainless

* Pfaudler, Co., Div. Pfaudler Permutit Inc., Rochester, N.Y.

steel and aluminum oxide on type 6061 aluminum giving increases of from 2 to 5.

Another factor of significant interest in transducer chamber design for vacuum conditions is the configuration of the dielectric-vacuum interface required. Smith (Ref. 31) has given design criteria for various insulators which indicate that a working gradient as high as 200 to 300 kv/cm can be expected with dielectrics such as epoxy resin or certain types of rubber, provided a dielectric angle of the correct sign and magnitude is employed to ensure that electrons released from the insulator are collected on a metal electrode rather than being driven back to the insulator surface and thus giving rise to electron multiplication along that surface.

It would thus appear that vacuum chamber voltage gradients of the order of 300 kv/cm or better are possible, provided a technique for cathode dielectric coating can be developed which is compatible with the relatively large area electrodes required and the wire holder geometry. Some development work with respect to the dielectric-vacuum interfaces also is advisable.

If such development can be undertaken and successfully completed, an immediate benefit could be gained by modification of the vacuum chamber for the exploding wire system (Ref. 1) presently in operation at Kirtland AFWL. The success of the combined ultraviolet and needle overvolting triggering technique, performed under the present contract and discussed in Section III-5 has led to a proposal for modification of the 15-pulser triggering system to give improved synchronization and ease of operation. With this modification, it is anticipated that di/dt values approaching 10^{13} amperes/second could be obtained for wire diameters of the order of a few mils, provided a transducer chamber spacing of 1 inch can be employed successfully (for the 300-kv matched load system output voltage), thus permitting operation of the present system at performance levels approaching those which appear feasible with faster system design proposed herein, in the case of vacuum chamber operation.

Thus, work specifically directed at improved design and surface processing of vacuum transducer chambers, to improve their voltage gradient stand-off capability, appears to be particularly desirable.

REFERENCES

1. Trolan, J. K., et al., Development of an Ultra-Fast Pulsed Power System, AFWL TR 65-1.

2. Stratton, J. A., Electromagnetic Theory, McGraw-Hill Book Co., N.Y. (1941), pp 110-111.

3. Kimbark, E. W., Electrical Transmission of Power and Signals, John Wiley (1949), p 165.

4. Goldman, S., Transformation Calculus and Electrical Transients, Prentice Hall (1949) p 304.

5. Glascoe, G. N., and Lebacqz, J.V., Pulse Generators, Mass. Institute of Tech. Radiation Lab. series, Vol 5, Boston Technical Publishers, Inc. (1964) pp 494-496.

6. Vorobyev, A. A. Vorobyev, G. A., et al., High Voltage Testing Equipment and Apparatus, Ch. IV, Tech. Documents Liaison Office MCL-1265/1 + 2, OTS 62-32532 (1960).

7. Dutton, J., Haydon, S. C., and Llewellyn-Jones, F., Brit. J. Appl. Phys., 4, 170 (1953).

8. Pendleton, W. K., Guenther, A. H., "Investigation of a Laser Triggered Spark Gap," paper presented to the American Nuclear Society, April 1964.

9. Fitch, R. A., Howell, V.T.S., Proc. Inst. Elec. Eng. 111, 849-855 (1964).

10. Schatz, E. R. and Williams, E.M., Proc. Inst. Radio Engrs. 38, 1209 (1950).

11. Williams, E. M., and Schatz, E.R., Proc. Inst. Radio Engrs., 39, 84, (1951).

12. Moreno, T., Microwave Transmission Design Data, Dover Publications Inc., New York, S459, 12 (1958).

13. Edelson, H. D. and Korueff, T., in Exploding Wires, Vol 3, Eds, Chace, W. C. and Moore, H. K., Plenum Press, New York, (1964), p 267.

14. Brewster, J. L., et al., AFWL TR 65-63. Field Emission Corporation (1965).

15. Brewster, J. L., Anderson, R. E., Smith, K. E., Charbonnier, F. M., Final Report, Sandia Corporation, Albuquerque, P. O. No. 74-8155, Field Emission Corporation (1964).

16. Burrill, E. A., and McGregor, M. H., Nucleonics 18, 64 (1960).

17. Bouwers, A., Gath, P. G., Philips Tech. Rev. 6, 270-278 (1941).

18. Fletcher, R. C., Rev. Sci. Inst. 20, 861 (1949).

19. Tucker, T. J., Rev. Sci. Inst. 31, 165 (1960).

20. Guenther, A. H., Personal correspondence.

21. Sharbaugh, A. H. and Watson, P. K., in Progress in Dielectrics, Vol 4, Eds. Birks, J. B., and Hart, J., Academic Press Inc., New York, 201-248 (1962).

22. Swan, D. W., Brit. J. Appl. Phys., 13 208 (1962).

23. Sletton, A. M. and Lewis, T. J., Brit. J. Appl. Phys. 14, 883 (1963).

24. Dyke, W. P., Trolan, J. K., Martin, E. E., and Barbour, J. P., Phys. Rev. 91, 1054 (1953).

25. Boyle, W. S., Kisluik, T. and Germer, L. H., J. Appl. Phys. 26, 720 (1955).

26. Little, R. P. and Smith, S. T., Proc. Inter. Symp. on Insulation of High Voltages in Vacuum, Oct. 19-20, 1964, Boston, p 171

27. Alpert, D. et al., Proc. Inter. Symp. on Insulation of High Voltages in Vacuum, 2 and 23, Oct. 19-20, 1964, Boston.

28. Jedynak, L., J. Appl. Phys. 35, 1727 (1964); Proc. Inter. Symp. on Insulation of High Voltages in Vacuum, Oct. 19-20. 1964, Boston; p 147.

29. Feasibility and Design Studies for Electrostatic Generators, Quarterly Tech. Prog. Report No. 4, 30 April 1963, prepared under Contract AF 33(616)-7230 for Flight Accessories Lab., Aeronautical Systems Div., Air Force System Command, Wright-Patterson AFB, Ohio.

30. Little, R. P. and Whitney, W. T., Studies of the Initiation of Electrical Breakdown in Vacuum, NRL Report 5944, U.S. Naval Research Lab., Washington, D.C., AD No. 408298.

31. Smith, I. D., "Pulse Breakdown of Insulator Surfaces in a Poor Vacuum," Proc. Inter. Symp. on Insulation of High Voltages in Vacuum, Oct. 19-21, 1964, Boston, p 261.

APPENDIX

SUMMARY OF INDUCTANCE DERIVATIONS AND CALCULATIONS FOR THE UNIFORM-GAP SPHERICAL CAVITY

A. Introduction

As in most cases in which the magnetic field is confined to a finite and well-defined region, the calculation of self-inductance due to currents in the conductors of the present configuration can be carried out more readily from the point of view of energy storage than flux linkages. The computed inductance, in either case, is based on a static or low-frequency field assumption. Solutions of the wave equation for the fields are required for the high-frequency or pulse applications, but these low-frequency or pulse applications, but these low-frequency values will serve as first-order approximations.

Initial assumptions of symmetry:

(1) Spherically symmetric surfaces except at input and load regions.

(2) Axial symmetry everywhere.

The hemispherical region under study will be broken up into four subregions for purposes of integration, as follows:

Region I. gap from input to base of load

Region II. gap from base of load to top of load

Region III. load (interior)

Region IV. interior of inner sphere plus region exterior to outer sphere.

These descriptions refer to the orientation shown in Figure 51, a cross section which does not show the azimuth coordinate.

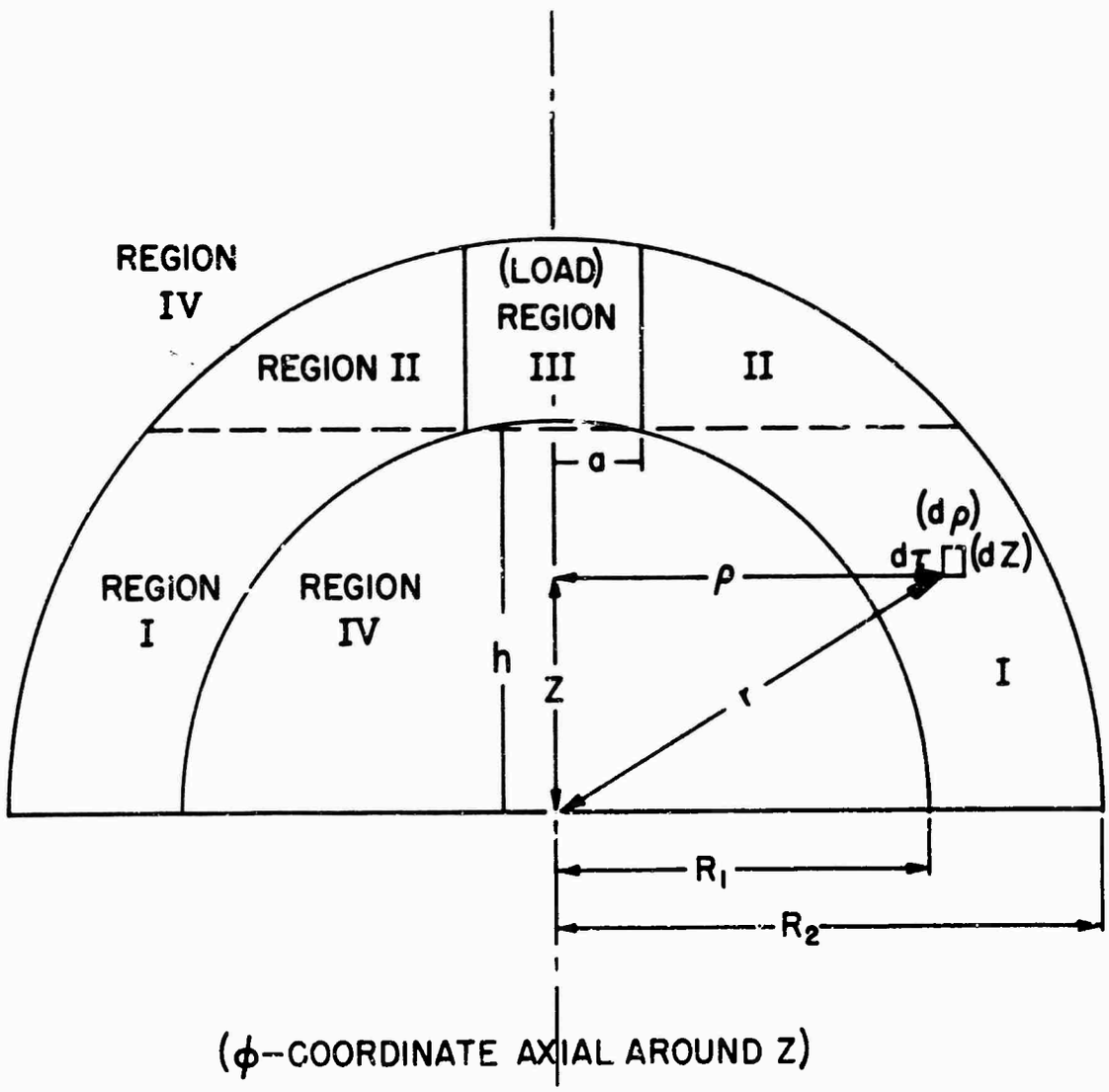

Figure 51 Hemispherical Region of Under Study Showing Breakdown of the Four Subregions

B. Region I

Equations of boundaries of Region I:

$$Z = 0, \quad Z = h \tag{34}$$

$$r = R_1, \quad r = R_2 \tag{35}$$

but $$\rho = \sqrt{r^2 - Z^2} \tag{36}$$

then the r-boundaries can be written

$$\rho = \sqrt{R_1^2 - Z^2} \tag{37}$$

$$\rho = \sqrt{R_2^2 - Z^2} \tag{38}$$

(note: $Z < R_1 < R_2$)

Ampere's Line Integral Law, applied to the circle about the z-axis passing through the element $d\tau$ is

$$\oint \overline{B} \cdot \overline{dl} = \mu I \tag{39}$$

Where B is the magnetic induction at points on the circle through $d\tau$ and I is the current cutting the area of the circle. From axial symmetry we have

$$B \cdot 2\pi\rho = \mu I \tag{40}$$

or

$$B(\rho, Z) = \frac{\mu I}{2\pi\rho} \tag{41}$$

Now the energy density in a magnetic field, due to the magnetic intensity, is

$$\frac{dW}{d\tau} = \int B dH = \frac{1}{\mu} \int B dB = B^2/2\mu \tag{42}$$

In this case, then

$$\frac{dW}{d\tau} = \frac{\mu I^2}{8\pi^2 \rho^2} \tag{43}$$

We can express $d\tau$ in the cylindrical coordinates indicated in Figure 51 as

$$d\tau = \rho \, d\phi \, d\rho \, dZ \tag{44}$$

where ϕ is the azimuthal coordinate. Then

$$dW = \frac{\mu I^2}{8\pi^2 \rho} \, d\phi \, d\rho \, dZ \tag{45}$$

or

$$W_I = \frac{\mu I^2}{8\pi^2} \int_0^{2\pi} d\phi \int_0^{h} \int_{\sqrt{R_1^2 - Z^2}}^{\sqrt{R_2^2 - Z^2}} \frac{i\rho}{\rho} \, dZ \tag{46}$$

$$W_I = \frac{\mu I^2}{4\pi} \left[\int_0^{h} \log \sqrt{R_2^2 - Z^2} \, dZ - \int_0^{h} \log \sqrt{R_1^2 - Z^2} \, dZ \right] \tag{47}$$

the energy stored in Region I. Let the indefinite integrals be J_2 and J_1, respectively. Then

$$W_I = \frac{\mu I^2}{4\pi} (J_2 - J_1) \Big|_0^{h} \tag{48}$$

where $J_2 = \int \log \sqrt{R_2^2 - Z^2} \, dZ = \frac{1}{2} \int \log (R_2^2 - Z^2) \, dZ$

$$J_2 = \frac{1}{2} \left[Z \log (R_2^2 - Z^2) - 2Z + R_2 \log \left(\frac{R_2 + Z}{R_2 - Z} \right) \right] \tag{49}$$

(Dwight 624)*, remembering $Z < R_2$. Similarly,

$$J_1 = \frac{1}{2} \left[Z \log R_1^2 - Z^2) - 2Z + R_1 \log \left(\frac{R_1 + Z}{R_1 - Z} \right) \right] \tag{50}$$

Then

$$(J_2 - J_1) = \frac{1}{2} \left[Z \log \left(\frac{R_2^2 - Z^2}{R_1^2 - Z^2} \right) + R_2 \log \left(\frac{R_2 + Z}{R_2 - Z} \right) - R_1 \log \left(\frac{R_1 + Z}{R_1 - Z} \right) \right] \tag{51}$$

and

$$W_I = \frac{\mu I^2}{8\pi} \left[h \log \left(\frac{R_2^2 - h^2}{R_1^2 - h^2} \right) + R_2 \log \left(\frac{R_2 + h}{R_2 - h} \right) - R_1 \log \frac{R_1 + h}{R_1 - h} \right] \tag{52}$$

C. Region II

For the energy W_{II}, stored in region II, we have

* Dwight, H. B., Tables of Integrals and other Mathematical Data, Revised Edition McMillan 1947 page 138.

$$W_{II} = \frac{\mu I^2}{8\pi^2} \int_0^{2\pi} d\phi \int_h^{R_2} \int_a^{\sqrt{R_2^2 - Z^2}} (d\rho/\rho) \, dZ \tag{53}$$

where a is the outer radius of the load.

$$W_{II} = \frac{\mu I^2}{4\pi} \int_h^{R_2} (\log \sqrt{R_2^2 - Z^2} - \log a) \, dZ = \frac{\mu I^2}{4\pi} \left[J_2 \Big|_h^{R^2} - (R_2 - h) \log a \right] \tag{54}$$
(55)

or

$$W_{II} = \frac{I^2}{4} \left\{ \frac{1}{2} \left[Z \log (R_2^2 - Z^2) - 2Z + R_2 \log \left(\frac{R_2 + Z}{R_2 - Z} \right) \right]_h^{R_2} - R_2 - h) \log a \right\} \tag{56}$$

As $Z \rightarrow R_2$ both the first and third terms in the square bracket become infinite. However, their sum is finite and can be shown to be

$$\lim_{Z \rightarrow R_2} \left[A \log (R_2^2 - Z^2) + R_2 \log \left(\frac{R_2 + Z}{R_2 - Z} \right) \right] = 2R_2 \log (2R_2) \tag{57}$$

Then,

$$W_{II} = \frac{I^2}{4} \left\{ \frac{1}{2} \left[2 R_2 \log (2 R_2) - 2 R_2 - h \log (R_2^2 - h^2) + 2 h - R_2 \log \left(\frac{R_2 + h}{R_2 - h} \right) \right] - (R_2 - h) \log a \right\} \tag{58}$$

D. Region III

Magnetic energy storage in the load itself depends largely on the current distribution within it and this, in turn, depends on the mechanisms of conduction, pinching, expansion, melting, vaporization, etc. Two cases, representing likely limits of the current distribution are (1) uniform distribution and (2) skin conduction with negligible penetration.

The case of uniform current distribution over a solid cylinder of radius a and length $(R_2 - h)$ (see Figure 1) yields a self inductance of

$$L_{III} = \frac{\mu}{8\pi} (R_2 - h) \tag{59}$$

while a skin current of infinitesimal penetration has no internal field and hence no contribution to the self-inductance.

The cylindrical-shell water load used in this project represents an intermediate case between these two limits. However, as it will be shown that Equation (26) produces a result negligible in comparison with other contributions, the water-load case need not be separately computed.

E. Region IV

In view of the physical configuration proposed, penetration of the current into the conductors of the inner and outer spherical shells would not be excessive in any case and will certainly be negligible for the high-frequency current components contemplated. Therefore, it is reasonable to assume zero magnetic field in Region IV.

F. Inductance -- small-wire case

The energy stored in Regions I and II, combined, may be written

$$W_{I,II} = \frac{\mu I^2}{8\pi}\left[2R_2(\log 2R_2 - 1) - h\log(R_1^2 - h^2) + 2h - R_1\log\left(\frac{R_1 + h}{R_1 - h}\right) - 2(R_2 - h)\log a\right] \quad (60)$$

Since $a^2 = R_1^2 - h^2$ this may be further simplified:

$$W_{I,II} = \frac{\mu I^2}{8\pi}\left[2R_2\log\frac{2R_2}{a} - 2(R_2 - h) - R_1\log\left(\frac{R_1 + h}{R_1 - h}\right)\right] \quad (61)$$

Self-inductance can be identified as a parameter of energy storage and the relationship is

$$W = \frac{1}{2}LI^2$$

or

$$L = \frac{2W}{I^2} \quad (62)$$

Then the expression for self-inductance of the circuit due to the magnetic field in Regions I and II is

$$L_{I,II} = \frac{\mu}{4\pi}\left[2R_2\log\frac{2R_2}{a} - 2(R_2 - h) - R_1\log\left(\frac{R_1 + h}{R_1 - h}\right)\right] \quad (63)$$

Now consider the special case in which the wire is small and/or the gap is small; that is, $a \ll R_1$. Then

$$h = \sqrt{R_1^2 - a^2} = R_1\sqrt{1 - a^2/R_1 2} \tag{64}$$

or

$$h \cong R_1 - \frac{1}{2}\, a^2/R_1$$

so that the last term of Equation (30) becomes

$$-R_1 \log \frac{2R_1}{\frac{1}{2}\frac{a^2}{R_1}}$$

and, letting

$$\Delta R = R_2 - R_1 \cong R_2 - h$$

$$L_{I,II} \cong \frac{\mu}{4\pi} \; 2\left[R_2 \log \frac{2R_2}{a} - R_1 \log \frac{2R_1}{a} - \Delta R \right] \tag{65}$$

or

$$L_{I,II} \cong \frac{\mu}{4\pi}\left[2\,(\log \frac{R_2}{a} + \log 2 - 1)\,\Delta R + R_1 \log\left(\frac{R_2}{R_1}\right)\right] \tag{66}$$

$$= 2 \times 10^{-7}\left[(\log\frac{R_2}{a} - .307)\,\Delta R + R_1 \log\left(\frac{R_2}{R_1}\right)\right] \tag{67}$$

henries when R_1 and ΔR are given in meters.

We can obtain a direct-application engineering formula for the specific case of the 12-3/4 - inch sphere and 1-inch gap. After putting in the known quantities (R_1, R_2 and R) and converting to common logarithms, we have

$$L = 51.1 - 11.7 \log_{10} D_w \text{ nanohenries} \tag{68}$$

where D_w is the wire diameter in mils. Similarly, for the 12-3/4-inch sphere and the 3.3-inch gap,

$$L = 165 - 38 \log_{10} D_w \text{ nanohenries} \tag{69}$$

Formulas (35) and (36) are strictly only for inductance due to the field in Regions I and II. To these may be added the expression (26) for the internal self inductance of the load, assuming uniform current distribution. However, a quick calculation shows that the latter amounts to only 0.5 nanohenry per centimeter of load length of 1.3 for the small gap and 4.2 for the large gap case, which are almost negligible in comparison with the magnitude of the major contribution in each case, and which certainly become negligible when the current distribution is nonuniform but is concentrated in the outer layers.

G. Water Load

In the case of the 2-inch (diameter) water shell load, Equation (37) may be used for the inductance due to the field external to the load.

$$L_{I,II} = \frac{M}{4\pi}\left[2 R_2 \log \frac{2R_2}{a} - 2(R_2 - h) - R_1 \log\left(\frac{R_1 + h}{R_1 - h}\right)\right] \qquad (70)$$

where $R_2 = 6.375$ in $= .1620$ m

$R_1 = 3.075$ in $= .0780$ m

$a = 1$ in $= .0254$ m

$h\sqrt{R_1^2 - a^2} = .0737$ m

The result:

$$L_{I,II} = 37.2 \text{ nh}$$

The contribution due to the internal field will be less than 4.2 nh (see Section F); if a uniform current distribution is assumed in the 1/4-inch thick cylindrical shell, this contribution will be only 1.4 nh. Therefore, 38 nh is a reasonable figure for the total self inductance of the proposed water load.

It is interesting to note that the approximate formula (36) yields a value of 40 nh for a "wire" diameter of 2000 mils.

H. Summary

Formulas (35) and (36) may be used for most wires, probably up to several hundred mils, perhaps more. Representative values computed

from them are tabulated below. All inductances are in nanohenries.

D_w (mils)	1.0-inch gap	3.3-inch gap
1	51	165
2	48	154
5	43	138
10	39	127
20	36	115

(water load) (71)

Figure 52 is a semilog plot of the same two relationships.

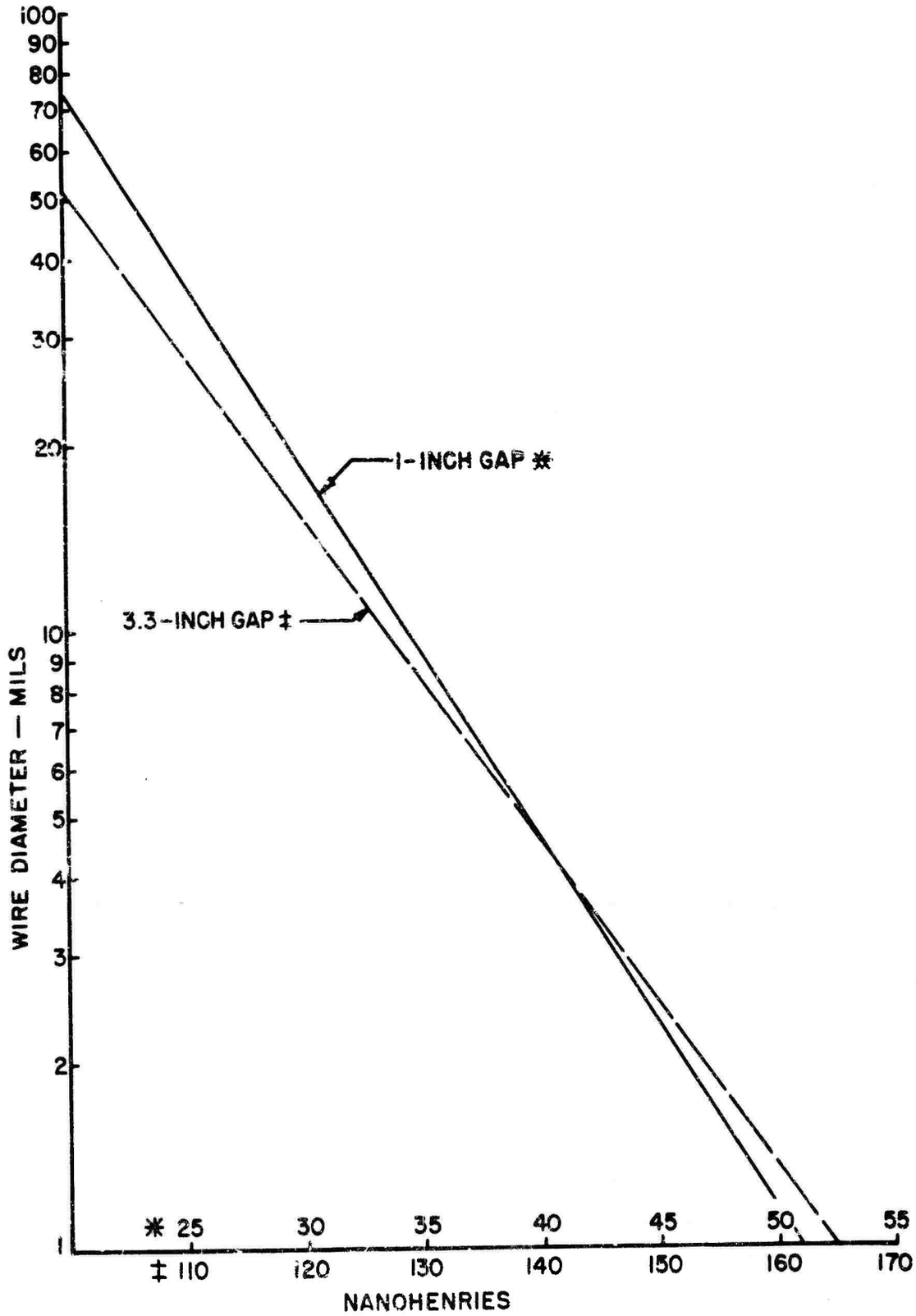

Figure 52 Semi-log Plot of Inductance as a Function of Wire Diameter

Unclassified

Security Classification

DOCUMENT CONTROL DATA - R&D

(Security classification of title, body of abstract and indexing annotation must be entered when the overall report is classified)

1. ORIGINATING ACTIVITY (Corporate author)	2a. REPORT SECURITY CLASSIFICATION
Field Emission Corporation McMinnville, Oregon	Unclassified 2b. GROUP

3. REPORT TITLE

DESIGN STUDIES FOR ULTRA-FAST, LOW-IMPEDANCE, HIGH PEAK-POWER PULSED SYSTEMS

4. DESCRIPTIVE NOTES (Type of report and inclusive dates)

April 1962 through November 1964

5. AUTHOR(S) (Last name, first name, initial)

Brewster, J. L.; Charbonnier, F. M.; Garrett, L. F.; Riegelmann, K. W.; Trolan, J. K.

6. REPORT DATE	7a. TOTAL NO. OF PAGES	7b. NO. OF REFS
November 1965	152	31

8a. CONTRACT OR GRANT NO.	9a. ORIGINATOR'S REPORT NUMBER(S)
AF29(601)-5380 b. PROJECT NO. 5710 c. Subtask 07.002 d.	AFWL-TR-65-21 9b. OTHER REPORT NO(S) (Any other numbers that may be assigned this report)

10. AVAILABILITY/LIMITATION NOTICES

Qualified users may obtain copies of this report from DDC. Distribution is limited because of the technology discussed in the report.

11. SUPPLEMENTARY NOTES	12. SPONSORING MILITARY ACTIVITY
	Air Force Weapons Laboratory (WLRE) Kirtland Air Force Base, New Mexico

13. ABSTRACT Ultrafast pulsed power systems have proved to be effective energy sources for transducers to produce intense X rays, dense electron beams, and very high temperature plasmas. The principal function of a single shot or low repetition rate pulsed power system is to accept energy at low power levels and subsequently to deliver such energy at extremely high power levels, with maximum efficiency, to a suitable transducer. This objective can best be met by use of either distributed or lumped-constant pulse forming networks where optimum performance is realized by maintaining the proper impedance match between the power source and transducer throughout the energy delivery process. Attainment of the proper impedance match can impose stringent and sometimes contra-indicating requirements upon the dielectric storage media, the switching mechanism, and the transducer chamber. The most promising approach to such power sources appears to be a pulse-charged two-stage coaxial Blumlein system. Such a system can deliver 25 kiloamperes at 2 megavolts in a pulse width of 40 nanoseconds to a suitably matched flash X-ray tube to produce relatively high dose rates with long tube life and minimal maintenance. The performance of a Blumlein exploding wire system, with respect to the rate of energy transfer, is primarily limited by the uncancelled transducer chamber impedance to the extent required to give di/dt values close to 10^{14} amp/sec for wires a few mils in diameter. Attainment of transducer chamber voltage gradients of 300 kv/cm or better in vacuum will result in di/dt values of 1 to 2 x 10^{13} amp/sec.

DD FORM 1 JAN 64 1473

Unclassified

Security Classification

14 KEY WORDS	LINK A		LINK B		LINK C	
	ROLE	WT	ROLE	WT	ROLE	WT
Blumlein						
Coaxial transmission systems						
Dielectric material						
Electric discharge						
Electricity - storage						
Exploding wires						
Field reversal						
Gas breakdown						
Inductance calculations						
Neutron generation						
Pulse power						
Pulse-Forming Networks						
Vacuum breakdown						
X Ray - Generation						

INSTRUCTIONS

1. ORIGINATING ACTIVITY: Enter the name and address of the contractor, subcontractor, grantee, Department of Defense activity or other organization *(corporate author)* issuing the report.

2a. REPORT SECURITY CLASSIFICATION: Enter the overall security classification of the report. Indicate whether "Restricted Data" is included. Marking is to be in accordance with appropriate security regulations.

2b. GROUP: Automatic downgrading is specified in DoD Directive 5200.10 and Armed Forces Industrial Manual. Enter the group number. Also, when applicable, show that optional markings have been used for Group 3 and Group 4 as authorized.

3. REPORT TITLE: Enter the complete report title in all capital letters. Titles in all cases should be unclassified. If a meaningful title cannot be selected without classification, show title classification in all capitals in parenthesis immediately following the title.

4. DESCRIPTIVE NOTES: If appropriate, enter the type of report, e.g., interim, progress, summary, annual, or final. Give the inclusive dates when a specific reporting period is covered.

5. AUTHOR(S): Enter the name(s) of author(s) as shown on or in the report. Enter last name, first name, middle initial. If military, show rank and branch of service. The name of the principal author is an absolute minimum requirement.

6. REPORT DATE: Enter the date of the report as day, month, year, or month, year. If more than one date appears on the report, use date of publication.

7a. TOTAL NUMBER OF PAGES: The total page count should follow normal pagination procedures, i.e., enter the number of pages containing information.

7b. NUMBER OF REFERENCES: Enter the total number of references cited in the report.

8a. CONTRACT OR GRANT NUMBER: If appropriate, enter the applicable number of the contract or grant under which the report was written.

8b, 8c, & 8d. PROJECT NUMBER: Enter the appropriate military department identification, such as project number, subproject number, system numbers, task number, etc.

9a. ORIGINATOR'S REPORT NUMBER(S): Enter the official report number by which the document will be identified and controlled by the originating activity. This number must be unique to this report.

9b. OTHER REPORT NUMBER(S): If the report has been assigned any other report numbers *(either by the originator or by the sponsor)*, also enter this number(s).

10. AVAILABILITY/LIMITATION NOTICES: Enter any limitations on further dissemination of the report, other than those imposed by security classification, using standard statements such as:

(1) "Qualified requesters may obtain copies of this report from DDC."

(2) "Foreign announcement and dissemination of this report by DDC is not authorized."

(3) "U. S. Government agencies may obtain copies of this report directly from DDC. Other qualified DDC users shall request through _____."

(4) "U. S. Military agencies may obtain copies of this report directly from DDC. Other qualified users shall request through _____."

(5) "All distribution of this report is controlled. Qualified DDC users shall request through _____."

If the report has been furnished to the Office of Technical Services, Department of Commerce, for sale to the public, indicate this fact and enter the price, if known.

11. SUPPLEMENTARY NOTES: Use for additional explanatory notes.

12. SPONSORING MILITARY ACTIVITY: Enter the name of the departmental project office or laboratory sponsoring *(paying for)* the research and development. Include address.

13. ABSTRACT: Enter an abstract giving a brief and factual summary of the document indicative of the report, even though it may also appear elsewhere in the body of the technical report. If additional space is required, a continuation sheet shall be attached.

It is highly desirable that the abstract of classified reports be unclassified. Each paragraph of the abstract shall end with an indication of the military security classification of the information in the paragraph, represented as *(TS), (S), (C), or (U)*.

There is no limitation on the length of the abstract. However, the suggested length is from 150 to 225 words.

14. KEY WORDS: Key words are technically meaningful terms or short phrases that characterize a report and may be used as index entries for cataloging the report. Key words must be selected so that no security classification is required. Identifiers, such as equipment model designation, trade name, military project code name, geographic location, may be used as key words but will be followed by an indication of technical context. The assignment of links, rules, and weights is optional.